Persoonia 54, 2025: 147–195
https://www.persoonia.org

RESEARCH ARTICLE

ISSN (Online) 1878-9080
https://doi.org/10.3114/persoonia.2025.54.05

A taxonomic revision of *Aureobasidium* (*Saccotheciaceae, Dothideales*) with new species, new names, and typifications

B. Jumbam[1,2], I.A. Zasada[3], K. Bensch[4], P.W. Crous[4,5,6], M.C. Aime[1*]

[1]Department of Botany and Plant Pathology, Purdue University, West Lafayette, IN 47907, USA
[2]Current address: Department of Plant Sciences and Plant Pathology, Montana State University, Bozeman, MT 59717, USA
[3]USDA-ARS Horticultural Crops Research Unit, Corvallis, Oregon 97330, USA
[4]Westerdijk Fungal Biodiversity Institute, Uppsalalaan 8, 3584 CT Utrecht, The Netherlands
[5]Department of Biochemistry, Genetics and Microbiology, Forestry and Agricultural Biotechnology Institute (FABI), University of Pretoria, Pretoria, South Africa
[6]Microbiology, Department of Biology, Utrecht University, Padualaan 8, Utrecht, 3584 CH, The Netherlands

*Corresponding author: maime@purdue.edu

Key words:
Aureobasidium pullulans
black yeasts
Dothideomycetes
GCPSR species recognition criteria
new taxa

Abstract: *Aureobasidium* comprises dimorphic yeast-like fungi that usually produce melanised cells at maturity. Species are globally distributed and ubiquitous, colonizing a variety of habitats. At present, ca 40 species are accepted, with the type, *A. pullulans*, representing a complex of unresolved cryptic species. In this study, we isolated 128 *Aureobasidium* from multiple temperate and tropical regions. We performed multigene analyses using eight loci (ITS, 28S, *EF1a*, *ELO2*, *RPB2*, *BTUB*, mtLSU and mtSSU) on new isolates and including sequences from type material for all available *Aureobasidium* species. Data on growth, physiological profiles, micro- and macromorphological attributes were also collected and analysed. Several DNA-based species delimitation methods were evaluated for their ability to delimit species. We found that assimilation of D-quinic acid, L-sorbose, D-mannitol, gluconolactone, erythritol, L-arabinose, and sodium succinate dibasic hexahydrate were important in delineating species of *Aureobasidium* and note that production of pigmentation in culture often takes longer than the 14 d standard for carbon assimilations. Genealogical concordance phylogenetic species recognition criteria (GCPSR) provided the most consistent results for species delimitation. We describe nine new species of *Aureobasidium (A. albui*, *A. cavalettoi*, *A. diazvalderramae*, *A. ellingtonae*, *A. essambei*, *A. peruvianum*, *A. rubi*, *A. toomeae*, and *A. vanuatuense*), make new combinations for *A. aubasidani* (≡ *A. pullulans* var. *aubasidani*), *A. fermentans* (≡ *Pullularia fermentans*), and *A. mahoniae* (≡ *Selenophoma mahoniae*), validate and provide descriptions for *A. musti* and *A. uvarum*, and provide lecto- and epitypes for *Dematium pullulans,* the basionym of *A. pullulans.* Finally, we resolved the phylogeny for *Aureobasidium*, reduce *Kabatiella* (based on *K. microsticta*) to synonymy, and provide an updated list of species to facilitate future studies.

Citation: Jumbam B, Zasada IA, Bensch K, Crous PW, Aime MC (2025). A taxonomic revision of *Aureobasidium* (*Saccotheciaceae*, *Dothideales*) with new species, new names, and typifications. *Persoonia* **54**: 147–195. doi: 10.3114/persoonia.2025.54.05
Received: 24 July 2023; **Accepted:** 14 March 2025; **Effectively published online:** 14 May 2025
Corresponding editor: J. Houbraken

INTRODUCTION

Aureobasidium is genus of dimorphic yeast-like ascomycetes (*Saccotheciaceae*, *Dothideales*) (Schoch *et al.* 2006, Humphries *et al.* 2017, Nasr *et al.* 2018). Sporulating conidiophores can be reminiscent of basidia, leading some earlier workers to classify *Aureobasidium* within the basidiomycetes (Clements & Shear 1931). The genus is widespread throughout temperate, tropical and polar regions (Gostinčar *et al.* 2014) with saprotrophic, endophytic, epiphytic, and plant pathogenic species (Singh *et al.* 2015). Known members of the genus grow as yeasts or as filamentous fungi, depending on environmental conditions (Gaur *et al.* 2010). *Aureobasidium* species are variable in their production of melanised chlamydospores (Wang *et al.* 2019), which, when produced, impart a blackened aspect to cultures as they mature and from which the common name “black yeasts” derives. Sister genera include *Hormonema*, *Kabatiella,* and *Saccothecium* (Yurlova *et al.* 1996, Schoch *et al.* 2006, Humphries *et al.* 2017, Nasr *et al.* 2018). Sexual morphs are not known for *Aureobasidium* although a hypothesis that the sexual morph of *A. pullulans* is *Columnosphaeria fagi* cannot be discarded (Zalar *et al.* 2008, Humphries *et al.* 2017).

Aureobasidium species can thrive in or tolerate a wide range of habitats. They have been isolated from various

environments including damp indoor walls and floors, food, feeds, hypersaline waters, and rocks (Sharma *et al.* 2009, Singh *et al.* 2015, Nasr *et al.* 2018, Al-Araimi *et al.* 2019, Diguța *et al.* 2019) and from substrates such as honey, romaine lettuce, and dogs (Bakonyi *et al.* 2003, Loncaric *et al.* 2009, Haelewaters *et al.* 2021). *Aureobasidium pullulans*, in particular, has been isolated from the surfaces of multiple plant species and outdoor environments (Hogg & Hudson 1966, van Nieuwenhuijzen *et al.* 2015). *Aureobasidium pullulans* is also frequently found as a contaminant in hospital laboratories (Loncaric *et al.* 2009).

Aureobasidium species have been reported to cause opportunistic diseases in humans although these are not considered as important as infections caused by black yeasts in the genus *Exophiala* (de Hoog *et al.* 2000). However, *Aureobasidium* infection may be life threatening especially in immunocompromised individuals. For example, fungal meningitis, commonly caused by fungi such as *Cryptococcus neoformans* and species of *Coccidioides* and *Candida* in HIV patients, is now associated with the black yeast *A. proteae* (Kutleša *et al.* 2012). *Aureobasidium* species have been isolated from the skin surfaces of healthy individuals and from neonates as opportunistic pathogens (Wang *et al.* 2019). They have been identified as causal agents in respiratory tract infections (Taylor *et al.* 2006, Pikazis *et al.* 2009) and pneumonias (Singh *et al.* 2015). Plant parasitic species cause disease symptoms in a variety of plants including species of *Leucospermum*, *Pinus*, *Tilia*, and *Zea* (Friend 1965, Flett & Nowell 1995, Crous *et al.* 2011, Jiang *et al.* 2019).

The widespread distribution and ease of culturing makes *Aureobasidium* species readily available for biotechnological studies. Recent studies have reported *Aureobasidium* species to be valuable for bio-based economies. *Aureobasidium pullulans* as well as other members produce a biodegradable extracellular polysaccharide (EPS) known as pullulan. This EPS has been demonstrated to be valuable in enhancing the recovery of crude oil (Al-Araimi *et al.* 2021). It is also important as a biosurfactant and source of single-cell oil production (Kim *et al.* 2015, van Nieuwenhuijzen *et al.* 2016). For instance, *A. pullulans* var. *aubasidani* produces single cell oils, which are a rich source of unsaturated fatty acids, biodiesel, and fumaric acid (Wang *et al.* 2018a). The biotechnological application of these single cell oils is not limited to the food and biofuel industries but have also been applied in the textile industry for the improvement of cotton fabrics (Li *et al.* 2014, Bettencourt *et al.* 2020). *Aureobasidium pullulans* is commercially important because of its demonstrated potential to produce antifungal and antibacterial chemicals as well as different hydrolytic enzymes (Chi *et al.* 2009, Kim *et al.* 2015, Singh *et al.* 2015, Mulay & Deopurkar 2017). *Aureobasidium melanogenum* can be used in the production of alcohol from low-cost substrates (Zeng *et al.* 2019).

Aureobasidium species have also been tested for application as biocontrol agents of fungal plant pathogens or of food spoilage fungi (Lima *et al.* 1997, Castoria *et al.* 2001, Schena *et al.* 2003, Singh *et al.* 2008, Prasongsuk *et al.* 2018, Wang *et al.* 2018b, Zajc *et al.* 2020). *Aureobasidium pullulans* has been shown to be effective against *Penicillium expansum*, *Botrytis cinerea,* and *Rhizopus stolonifer* that cause postharvest rot in fruits like pears, berries, apples, kiwifruits, sweet cherries, and table grapes (Lima *et al.* 1997, Ippolito *et al.* 2000, Schena *et al.* 2003, Robiglio *et al.* 2011, Mari *et al.* 2012, de Jong *et al.* 2019). Control of *Diplodia seriata*, the grapevine trunk disease pathogen (Pinto *et al.* 2018), and brown rot of stone fruits (di Francesco *et al.* 2020) has been achieved using *A. pullulans*. Finally, root and foliar application of *A. pullulans* was found to induce host resistance against Verticillium wilt in *Olea europaea* (López-Moral *et al.* 2022).

Species now classified in *Aureobasidium* have been previously placed in multiple different genera. *Aureobasidium pullulans*, the type species, was originally described in *Dematium* (De Bary 1866), now regarded as a synonym of *Periconia*. Later, Viala & Boyer (1891) established the name *Aureobasidium*. Cooke (1959) provides an account of synonyms placed in more than 30 different genera, including *Aureobasis*, *Dematium*, *Hormonema*, *Kabatiella*, *Pullularia,* and *Torula*, that have been applied to members of *Aureobasidium*. Familial placement has also varied. Schoch *et al.* (2009) classified *Aureobasidium* in the *Dothioraceae.* Using a three-locus analysis, Thambugala *et al.* (2014) considered *Dothioraceae* a later synonym of *Dothideaceae* that did not include *Aureobasidium*, placing the latter in a new family, *Aureobasidiaceae* as the sister to *Dothideaceae* in *Dothideales*. *Aureobasidiaceae* is now treated as a synonym for *Saccotheciaceae* which is the family that now contains *Aureobasidium*, *Saccothecium*, and their allies (Hongsanan *et al.* 2020).

Roughly 40 species of *Aureobasidium* are currently accepted (www.indexfungorum.org, www.mycobank.org; Table 1), excluding varieties and formae speciales. Of these, sequence data are available for 28. Among some of the recently described species of *Aureobasidium* are *A. aerium* (Wang *et al.* 2022), *A. tremulum* (Crous *et al.* 2019), *A. pini* (Jiang *et al.* 2019), *A. microtermitis* (Crous *et al.* 2021), and others (Crous *et al.* 2023, Hyde *et al.* 2023, Tan *et al. 2024,* Wu *et al.* 2023). The type species, *A. pullulan,* part of a species complex (Schoch *et al.* 2006) that has been particularly recalcitrant to resolve in part because variability in interspecies morphology can be subtle and thus difficult to apply to species delimitation. Zalar *et al.* (2008) used molecular, morphological, and growth data to describe four new varieties of *A. pullulans* (*A. pullulans* var. *pullulans*, *A. pullulans* var. *melanogenum*, *A. pullulans* var. *subglaciale,* and *A. pullulans* var. *namibiae*) now regarded as species. While growth type, growth rate, colony colour, and physiological tests can provide useful characters for species delimitation within *Aureobasidium* (de Hoog & Yurlova 1994, Loncaric *et al.* 2009), there is also the need to sequence additional DNA loci for this purpose.

Combinations of species recognition criteria (SRC) have been applied to delimit species in fungal groups. For instance, Bhunjun *et al.* (2021) used phylogenetic, evolutionary, and coalescent-based species recognition (CBSR) methods such as multi-rate Poisson tree processes (mPTP) and the generalized mixed Yule-coalescent (GMYC) methods (Fujisawa & Barraclough 2013) to establish species boundaries in *Colletotrichum*. Liu *et al.* (2016) applied genealogical concordance phylogenetic species recognition criteria (GCPSR), Poisson tree processes (PTP) (Zhang *et al*. 2013), and GMYC to establish the status of *C. siamense*. Species boundaries were determined in the entomopathogenic genus *Beauveria* and a new species (*B. peruviensis*) was described using coalescent-based, GCPSR,

Table 1. *Aureobasidium* names and their status. Data are compiled from MycoBank, Index Fungorum, Species Fungorum and NCBI databases.

***Aureobasidium* name**	**Name status**	**Basionym**	**Current name[1]**	**MycoBank #**	**Reference[2]**
Aureobasidium slovacum	Legitimate	—	*Alternaria slovaca*	MB 803699	Woudenberg *et al.* (2013)
Aureobasidium aerium	Legitimate	—	***Aureobasidium aerium***	MB 843527	Wang *et al.* (2022)
Aureobasidium aleuritis	Legitimate	*Kabatiella aleuritis*	***Aureobasidium aleuritis***	MB 309377	Hermanides-Nijhof (1977)
Aureobasidium albui	Legitimate	—	***Aureobasidium albui***	MB 848255	This study
Aureobasidium apocryptum	Legitimate	*Gloeosporium apocryptum*	***Aureobasidium apocryptum***	MB 309378	Hermanides-Nijhof (1977)
Aureobasidium pullulans var. *aubasidani*	Legitimate	—	***Aureobasidium aubasidani***	MB 848279	This study
Aureobasidium aurantiacum	Legitimate	—	***Aureobasidium aurantiacum***	MB 902111	Tan *et al.* (2024)
Aureobasidium bupleuri	Legitimate	*Kabatiella bupleuri*	***Aureobasidium bupleuri***	MB 835676	Haelewaters *et al.* (2021)
Aureobasidium castaneae	Legitimate	—	***Aureobasidium castaneae***	MB 838314	Jiang *et al.* (2021)
Aureobasidium caulivorum	Legitimate	*Gloeosporium caulivorum*	***Aureobasidium caulivorum***	MB 326817	Simon *et al.* (2009)
Aureobasidium cavalettoi	Legitimate	—	***Aureobasidium cavalettoi***	MB 848256	This study
Aureobasidium dalgeri	Legitimate	*Kabatiella dalgeri*	***Aureobasidium dalgeri***	MB 309379	Hermanides-Nijhof (1977)
Aureobasidium diazvalderramae	Legitimate	—	***Aureobasidium diazvalderramae***	MB 848257	This study
Aureobasidium ellingtonae	Legitimate	—	***Aureobasidium ellingtonae***	MB 848258	This study
Aureobasidium essambei	Legitimate	—	***Aureobasidium essambei***	MB 848259	This study
Aureobasidium faidherbiae	Legitimate	—	***Aureobasidium faidherbiae***	MB 848079	Crous *et al.* (2023)
Aureobasidium fermentans	Legitimate	*Pullularia fermentans*	***Aureobasidium fermentans***	MB 848272	This study
Aureobasidium harposporum	Legitimate	*Gloeosporium harposporum*	***Aureobasidium harposporum***	MB 309380	Hermanides-Nijhof (1977)
Aureobasidium indicum	Legitimate	—	***Aureobasidium indicum****	MB 103074	Pande & Ghate (1985)
Aureobasidium insectorum	Legitimate	—	***Aureobasidium insectorum***	MB 571251	Wu *et al.* (2023)
Aureobasidium intercalariosporum	Legitimate	—	***Aureobasidium intercalariosporum***	MB 571252	Wu *et al.* (2023)
Aureobasidium iranianum	Legitimate	—	***Aureobasidium iranianum***	MB 800705	Arzanlou (2012)
Aureobasidium khasianum	Legitimate	—	***Aureobasidium khasianum***	MB 828278	Prabhugaonkar & Pratibha (2018)
Aureobasidium leucospermi	Legitimate	—	***Aureobasidium leucospermi***	MB 560556	van Nieuwenhuijzen *et al.* (2016)
Aureobasidium lilii	Legitimate	—	***Aureobasidium lilii***	MB 326819	Crişan & Hodişan (1964)
Aureobasidium lini	Legitimate	*Polyspora lini*	***Aureobasidium lini***	MB 283371	Hermanides-Nijhof (1977)
Aureobasidium mahoniae	Legitimate	*Selenophoma mahoniae*	***Aureobasidium mahoniae***	MB 848273	This study
Aureobasidium mangrovei	Legitimate	—	***Aureobasidium mangrovei***	MB 823444	Nasr *et al.* (2018)
Aureobasidium acericola	Invalid		*Aureobasidium melanogenum*	MB 836925	This study
Aureobasidium melanogenum	Legitimate	*A. pullulans var. melanogenum*	***Aureobasidium melanogenum***	MB 807698	Gostinčar *et al.* (2014)
Aureobasidium microstictum	Legitimate	*Kabatiella microsticta*	***Aureobasidium microstictum***	MB 326821	Cooke (1962)
Aureobasidium microtermitis	Legitimate	—	***Aureobasidium microtermitis***	MB 839078	Crous *et al.* (2021)

Table 1. (Continued).

***Aureobasidium* name**	**Name status**	**Basionym**	**Current name[1]**	**MycoBank #**	**Reference[2]**
Aureobasidium motuoense	Legitimate	—	***Aureobasidium motuoense***	MB 571263	Wu *et al.* (2023)
Aureobasidium mustum	Legitimate	—	***Aureobasidium mustum***	MB 836845	This study
Aureobasidium namibiae	Legitimate	*A. pullulans var. namibiae*	***Aureobasidium namibiae***	MB 807701	Gostinčar *et al.* (2014)
Aureobasidium peruvianum	Legitimate	—	***Aureobasidium peruvianum***	MB 848261	This study
Aureobasidium pini	Legitimate	—	***Aureobasidium pini***	MB 828664	Jiang *et al.* (2019)
Aureobasidium planticola	Legitimate	—	***Aureobasidium planticola***	MB 571262	Wu *et al.* (2023)
Aureobasidium proteae	Legitimate	*Kabatiella proteae*	***Aureobasidium proteae***	MB 560557	Crous *et al.* (2011)
Aureobasidium prunicola	Legitimate	*Gloeosporium prunicola*	***Aureobasidium prunicola***	MB 309382	Hermanides-Nijhof (1977)
Aureobasidium australiense	Invalid	—	*Aureobasidium pullulans*	MB 501787	This paper.
Aureobasidium nigricans	Legitimate	*Protocoronospora nigricans*	*Aureobasidium pullulans*	MB 272280	Cooke (1962)
Aureobasidium oleae	Legitimate	*Torula oleae*	*Aureobasidium pullulans*	MB 309381	Hermanides-Nijhof (1977)
Aureobasidium pullulans	Legitimate	*Dematium pullulans*	***Aureobasidium pullulans***	MB 508998	Arnaud (1918)
Aureobasidium vitis	Legitimate	—	*Aureobasidium pullulans*	MB 101771	Hermanides-Nijhof (1977)
Aureobasidium vitis var. *album*	Legitimate	—	*Aureobasidium pullulans*	MB 169013	Montemartini (1899)
Aureobasidium vitis var. *tuberculatum*	Legitimate	—	*Aureobasidium pullulans*	MB 168866	Arnaud (1918)
Aureobasidium ribis	Legitimate	*Kabatiella ribis*	***Aureobasidium ribis***	MB 309384	Hermanides-Nijhof (1977)
Aureobasidium rubi	Legitimate	—	***Aureobasidium rubi***	MB 848262	This study
Aureobasidium sanguinariae	Legitimate	*Gloeosporium sanguinariae*	***Aureobasidium sanguinariae***	MB 309386	Hermanides-Nijhof (1977)
Aureobasidium subglaciale	Legitimate	*A. pullulans var. subglaciale*	***Aureobasidium subglaciale***	MB 807700	Gostinčar *et al.* (2014)
Aureobasidium thailandense	Legitimate	—	***Aureobasidium thailandense***	MB 801148	Peterson *et al.* (2013)
Aureobasidium thujae-plicatae	Legitimate	—	***Aureobasidium thujae-plicatae***	MB 309387	Morelet (1978)
Aureobasidium toomeae	Legitimate	—	***Aureobasidium toomeae***	MB 848263	This study
Aureobasidium tremulum	Legitimate	—	***Aureobasidium tremulum***	MB 829941	Crous *et al.* (2019)
Aureobasidium umbellulariae	Legitimate	*Kabatiella phoradendri f. umbellulariae*	***Aureobasidium umbellulariae***	MB 309388	Hermanides-Nijhof (1977)
Aureobasidium uvarum	Legitimate	—	***Aureobasidium uvarum***	MB 836846	This study
Aureobasidium vineae	Invalid	—	*Aureobasidium uvarum*	MB 836849	This study
Aureobasidium vaccinii	Legitimate	—	***Aureobasidium vaccinii***	MB 126507	Richiteanu & Teodorescu (1989)
Aureobasidium vanuatuense	Legitimate	—	***Aureobasidium vanuatuense***	MB 848260	This study
Aureobasidium welwitschiae	Legitimate	—	***Aureobasidium welwitschiae***	MB 848078	Crous *et al.* (2023)
Aureobasidium xishuangbannaensis	Legitimate	—	***Aureobasidium xishuangbannaense***	MB 849254	Hyde *et al.* (2023)
Aureobasidium zeae	Legitimate	*Kabatiella zeae*	***Aureobasidium zeae***	MB 283372	Sun & Xue (2014)

Table 1. (Continued).

***Aureobasidium* name**	**Name status**	**Basionym**	**Current name[1]**	**MycoBank #**	**Reference[2]**
Aureobasidium foliicola	Invalid	*Sporotrichum foliicola*	*Coniochaeta hoffmannii*	MB 803421	Khan *et al.* (2013)
Aureobasidium prunorum	Legitimate	—	*Dothiora prunorum*	MB 816142	Crous & Gorenewald (2016)
Aureobasidium mansonii	Legitimate	*Microsporum mansonii*	*Exophiala castellanii*	MB 106813	Hermanides-Nijhof (1977)
Aureobasidium salmonis	invalid	—	*Exophiala salmonis*	MB 119468	Hermanides-Nijhof (1977)
Aureobasidium microstromoides	Legitimate	*Gloeosporium microstromoides*	*Gloeosporium microstromoides*	MB 299139	Cooke (1962)
Aureobasidium bolleyi	Legitimate	*Gloeosporium bolleyi*	*Microdochium bolleyi*	MB 317661	Hermanides-Nijhof (1977)
Aureobasidium nigrum	Legitimate	*Saccharomyces niger*	*Torula dematia*	MB 326824	Torre (1963)

[1] *Aureobasidium* names in **bold** represent the name associated with the holotype for accepted species; * denotes doubtful name (see text).

[2] = sequence data available and referenced in Supplementary Table S1

and distance-based species recognition (DBSR) approaches such as the automatic barcode gap detection (ABGD) method (Bustamante *et al.* 2019). Quaedvlieg *et al*. (2014) applied the consolidated species concept to resolve species in the *Teratosphaeriaceae*. Finally, GCPSR, PTP, and GMYC were applied to study lineages within the *Diaporthe amygdali* species complex (Hilário *et al*. 2021).

For this study, we: 1) isolated 128 *Aureobasidium* strains from multiple locales and substrates and characterized these with physiological and morphological data; 2) generated an eight-locus dataset (ITS, 28S, *EF1a*, *ELO2*, *RPB2*, *BTUB*, mtLSU, and mtSSU) for as many species and isolates as possible; 3) applied and compared GMYC, PTP and its Bayesian implementation (bPTP), GCPSR, ABGD, and ASAP for delimiting species, including within the *A. pullulans* complex; 4) describe and fully characterized nine new species, and provide three new combinations, validate two names, and provide lecto- and epitypification for the basionym of *A. pullulans*; and, 5) provide a compilation of all currently accepted names in *Aureobasidium*.

MATERIALS AND METHODS

Sample isolation and storage

Our study materials were isolated from a variety of substrates across different geographical regions including Africa, Europe, North America, South America, and Oceania (Table S1); information on collecting permits is provided in acknowledgements. Isolates were obtained by several methods: 1) the ballistosporic drop method detailed in Toome *et al.* (2013); 2) by exposing 10 % NaCl or 20–50 % glucose amended potato dextrose agar (PDA) plates to air as described in Díaz-Valderrama *et al.* (2017); 3) by directly swabbing substrates with a sterile swab moistened in sterile H2O, then serially diluted and plated on PDA amended with chloramphenicol (0.1 g/L); or 4) from cysts of the potato cyst nematode, *Globodera ellingtonae*, following a procedure similar to that of Morgan-Jones & Rodriguez-Kabana (1986). Briefly, cysts were disinfected by washing with 0.5 % NaOCl and rinsed six times in sterile distilled water. They were then transferred in a 1.5 mL Eppendorf tube and crushed with a melted pipette tip. Eighty microliters of the inoculum were then plated on PDA, MEA and Rose Bengal agar amended with chloramphenicol. Plates were incubated at 25 °C for 4–7 d. Colonies were isolated as they appeared and subcultured on PDA until axenic isolates were obtained. All isolates used in this study were preserved on PDA slants stored at 4 °C and in cryovials containing 40 % glycerol stored at -80 °C and housed in the Purdue University Kriebel Herbarium (PUL) culture collection, Department of Botany and Plant Pathology at Purdue University, West Lafayette, IN. Holotype specimens for new species were deposited in PUL as dried, inert preparations; ex-type cultures are deposited in the United States Department of Agriculture ARS culture collection (NRRL) and the Westerdijk Fungal Biodiversity Centre (CBS) in the Netherlands.

Macromorphological and physiological tests

Growth rates and pigmentation development were scored on yeast nitrogen base (YNB: Difco; Dickinson and Company, Sparks, MD 21152 USA), malt extract agar (MEA: Oxoid Ltd (CM0059); Wade Road, Basingstoke, Hants, RG24 8PW, UK), PDA (Difco (CM0139); Dickinson and Company, Sparks, MD 21152 USA), Czapek yeast extract agar (CZYA), Czapek yeast extract agar with 20 % sucrose (CZYA20S) (Pitt & Hocking 2009), malt extract agar with four salt concentrations (5 %, 10 %, 15 %, and 20 % NaCl), and Harrold's malt yeast extract with 40 % and 60 % sucrose (M40Y and M60Y) at 7 dpi. The inoculum was prepared by mixing a small number of cells with distilled water and 10 µL were carefully pipetted at the centre of each media plate. Plates were incubated in the dark and morpho- and physiological data were collected at 3 dpi, 7 dpi, and 15 dpi at 4, 15, 25, 28, 30, and 37 °C. For species represented by more than one isolate, data were collected for all representative isolates (Table S2). Plates that were incubated at 4 °C, wrapped in a black plastic bag to prevent light penetration resulting from frequent opening and closing of the refrigerator door. Culture colours were compared with plates in the Online Auction Color Chart (Kramer 2004).

Assimilation and fermentation tests were done following the protocols in *Manual for Yeast Work* (Suh *et al.* 2005). Briefly, for nitrogen assimilation, a 2× yeast carbon base solution was prepared (23.4 g/L) and 250 mL were aliquoted into glass beakers. One-fifth of each nitrogen compound (N0–N10 and NP) was added individually into each beaker and the pH was adjusted to 5.5–6.5. We then added 10 g of agar and 250 mL of sterile distilled water in each beaker to bring the volume to 500 mL. Each solution was autoclaved at 121 °C for 20 min and poured into Petri plates. The plates were inoculated with each *Aureobasidium* isolate as described above, incubated at 25 °C and observations were made at 3, 7, and 14 d. For carbon assimilation, 4.5 mL deionized water (DIW) were added into each test tube (16 × 125 mm) and autoclaved as above. A 10× stock solution (6.7 g yeast nitrogen base and 5 g carbon compound in 100 mL) was prepared and filter-sterilized and 0.5 mL was aseptically added into each test tube containing sterilized DIW. The test tubes were inoculated with 100 µL of each *Aureobasidium* isolate and incubated at 25 °C for 21 d. Carbon assimilation was recorded for up to 28 d at 7 d intervals. Finally, for fermentation tests, 14 (F1–F14) compounds were tested including a negative control (F15). Each carbon source was mixed with yeast extract in the ratio 2:1 (w/w; in 100 mL) and 6 mL of the solution was dispensed into test tubes (12 × 150 mm) containing inverted Durham tubes (6 × 50 mm). The mixture was autoclaved for 15 min and inoculated with 100 µL of each *Aureobasidium* isolate. The setup was incubated at 25 °C, with periodic shaking, and the amount of displaced gas was recorded every 7 d for 3 wk.

Microscopic morphology

Microscopic analyses were made from cultures grown on MEA and PDA. Mounts of cultures grown 7–14 d were either prepared in 5 % KOH, lactophenol, lactic acid or water. Photomicrographs were taken with an Olympus SC30 camera mounted on an Olympus BH2 bright field compound microscope (Olympus Co., Tokyo, Japan) using cellSens v. 1.18 imaging software (https://www.olympus-lifescience.com/en/software/cellsens/). At least 20 individual dimensions of each conidia and chlamydospore type were recorded. Images were processed using Gimp v. 2.10.12 (http://gimp.org) and photographic plates were prepared in Inkscape v. 1.1 (https://inkscape.org) and Adobe Illustrator (Adobe Inc. 2019).

DNA extraction and PCR amplification

DNA extraction of the isolates was done by transferring a small quantity of cells to a 1.5 mL microcentrifuge tube containing either 80 mL of 1× TAE buffer or milliQ water. The mixture was microwaved for 2 min and centrifuged at top speed for 1 min and the DNA-containing supernatant was transferred to a new tube used as template for polymerase chain reaction (PCR). Both the internal transcribed spacer (ITS) barcode region and the large subunit (28S) of the nrDNA repeat were amplified using the primer pairs ITS1F/ITS4 for the ITS (White *et al.* 1990, Gardes & Bruns 1993) and LR0R/LR5 for the 28S (Vilgalys & Hester 1990, Rehner & Samuels 1994). The translation elongation factor 1-α (*EF1a*) and the RNA polymerase II second largest subunit (*RPB2*) regions were amplified and sequenced with the primer pairs EF1-983/EF1-2218 (Rehner & Buckley 2005) and fRPB2-5F/fRPB2-7cR (Liu *et al.* 1999) (Table 2). The primer pairs YTEF-CF/YTEF-CR, YTEF-PF/YTEF-PR, and RPB-PenR1/RPB-PenR2, RPB-PenR3/RPB-PenR4 (Manitchotpisit *et al.* 2009) were also used to amplify the *EF1a* and *RPB2* genes respectively. The latter primer pairs were used only in cases where we encountered difficulties amplifying the targeted regions with the initial primer pair. For amplification and sequencing of the mitochondrial large (mtLSU) and small (mtSSU) subunits the primer pairs ML1/ML2 and MS1/MS2 (White *et al.* 1990) were used, respectively. The primer pairs ELO2-F/ELO2-R (Zalar *et al.* 2008) and Bt2a/Bt2b (Glass & Donaldson 1995) were used for the amplification and sequencing of portions of the elongase-encoding (*ELO2*) and beta-tubulin (*BTUB*) genes, respectively.

Amplification reactions consisted of 12.5 µL of Promega 2× or MyTaq 2× PCR Master Mix, 1.25 µL of each 10 µm primer, 8.0 µL of H2O, and 2.0 µL of template DNA. All amplifications were done in an Eppendorf Mastercycler® EP Thermal Cycler (Hauppauge, New York, USA). The PCR procedure for ITS and 28S follow Jumbam *et al.* (2019); cycling conditions of the other six loci are provided in Table 2. Amplified nrDNA fragments were subjected to electrophoresis in a 1 % agarose gel in 1× TAE buffer and was run at 110 V cm^{-1} for 30 min with a 1 kbp ladder and detected by staining with GelRed. The PCR products were sent to Genewiz (South Plainfield, New Jersey, USA) for purification and sequencing. Single isolate ex-type strains were re-sequenced at each locus to confirm the sequences. Raw sequence reads were assembled and manually edited using Sequencher v. 5.2.3 (Gene Codes Co., Ann Arbor, Michigan, USA) software. Edited sequences are deposited at the National Center for Biotechnology Information (NCBI) GenBank (Table S1).

Table 2. List of primers and the cycling conditions used for polymerase chain reactions in this study.

Target locus	Primers[1]	Sequence 5'-3'	Cycling conditions	Length (bp)	Reference
ITS	ITS1F[a]	CTTGGTCATTTAGAGGAAGTAA	94 °C, 1 min; 50 °C, 45 s; 72 °C, 90 s	600	Gardes & Bruns (1993)
	ITS4[b]	TCCTCCGCTTATTGATATGC			White *et al*. (1990)
28S	LROR[a]	GTACCCGCTGAACTTAAGC	94 °C, 1 min; 50 °C, 45 s; 72 °C, 90 s	600	Rehner & Samuels (1994)
	LR5[b]	ATCCTGAGGGAAACTTC			Vilgalys & Hester (1990)
ELO2	ELO2-F[a]	CACTCTTGACCGTCCCTTCGG	94 °C, 2 min; 58 °C, 15 s; 72 °C, 45 s	700	Zalar *et al.* (2008)
	ELO2-R[b]	GCGGTGATGTACTTCTTCCACCAG			
BTUB	Bt2[a]	GGTAACCAAATCGGTGCTGCTTTC	94 o°C, 5 min; 53 °C, 1 min; 72 °C, 1 min	450	Glass & Donaldson (1995)
	Bt2[b]	ACCCTCAGTGTAGTGACCCTTGGC			
mtLSU	ML1[a]	GTACTTTTGCATAATGGGTCAGC	94 °C, 3 min; 50 °C, 50 s; 72 °C, 90 s	250	White *et al.* (1990)
	ML2[b]	TATGTTTCGTAGAAAACCAGC			
mtSSU	MS1[a]	CAGCAGTCAAGAATATTAGTCAATG	95 °C, 3 min; 45 °C, 1 min; 72 °C, 1 min	725	White *et al.* (1990)
	MS2[b]	GCGGATTATCGAATTAAATAAC			
EF1α	EF-983F[a]	GCYCCYGGHCAYCGTGAYTTYAT	95 °C, 30 s; 54 °C, 1 min; 72 °C, 1 min	750	Rehner & Buckley (2005); Manitchoptpisit *et al*. (2009)
	EF-2218R[b]	ATGACACCRA-CRGCRACRGTYTG			
	YTEF-CF[a]	TCCAAAGTACATGGTCACCG			
	YTEF-CR[b]	CAGACGTTACCTCGACGGATC			
	YTEF-PF[a]	GGTCACCGTGATTTCATCAAG			
	YTEF-PR[b]	CTTGACGGAGACGTTCTTGAC			
RPB2	fRPB2-5F[a]	GAYGAYMGWGATCAYTTYGG	95 °C, 30 s; 54 °C, 1 min; 72 °C, 1 min	1100	Liu *et al.* (1999); Manitchoptpisit *et al*. (2009)
	fRPB2-7cR[b]	CCCATRGCTTGYTTRCCCAT			
	RPB-PenR1[a]	GTTCACTCAACTYGTGCGYGA			
	RPB-PenR2[b]	GGCAGGGTGAATYTCGCAATG			
	RPB-PenR3[a]	GACTTCAAYCTYACYCTTGCTG			
	RPB-PenR4[b]	GAGACATGACCATCATGGCAG			

[1] a and b refer respectively to the forward and reverse primers used for amplification of each locus.

Sequence alignment and molecular phylogenetic inference

The generated sequences for each of the different loci were subjected to a blast search against the NCBI GenBank standard nucleotide database (http://blast.ncbi.nlm.nih.gov/Blast.cgi). The query parameters were optimized to search for the closest relatives and the resulting sequences of previously described *Aureobasidium* spp. were downloaded. A total of 20 species of *Aureobasidium* had associated sequence data; where possible, we chose exemplars from ex-type sequences and where this was not available, a proxy sequence best representing the type was used. *Delphinella strobiligena*, *Sydowia polyspora*, and/or *Hormonema prunorum* were added to the single locus datasets as outgroups. Multiple sequence alignments (MSA) were performed using Muscle v. 3.8.31 (Edgar 2004). The MSA were used to construct single locus trees of the ITS, 28S, mtLSU, mtSSU, *BTUB*, *ELO2*, *EF1a,* and *RPB2* loci (Fig. S1A–I). Phylogenetic analyses of sequence data were done using IQ-TREE v. 2.0 (Kalyaanamoorthy *et al.* 2017) for Maximum Likelihood (ML) and Maximum Parsimony (MP) analyses with UFBoot and MPBoot, respectively (Minh *et al.* 2013, Hoang *et al.* 2018), and MrBayes v. 3.0b4 (Ronquist & Huelsenbeck 2003) for Bayesian Inference (BI) analyses. We performed a genealogical concordance test (Taylor *et al.* 2000) prior to concatenation to generate a combined eight-locus dataset (8-LDS). The single locus datasets were reordered in BioEdit (Hall 1999) and concatenated with MEGA v. 11 (Tamura *et al.* 2021). To resolve the *A. pullulans* species complex (ApC) we used a 6-locus concatenated dataset (6-LDS) comprising ITS, mtSSU, *BTUB*, *ELO2, EF1a*, and *RPB2* with *A. lini* and *A. toomeae* as outgroups.

The best fit evolutionary model for each of the single locus datasets was selected using the in-built Model Finder package of IQ-TREE. The selected model was used to infer ML by ultrafast bootstrap approximation and BI of the single locus phylogenies. The models selected by corrected Akaike information criterion (AIC) were GTR+F+I+G4, TIM+F+I+G4, TIM2e+I+G4, TN+F+I+G4, F81+F+I, TIM3+F+I, TIM2e+I+G4, and TIM2+F+I+G4 for *EF1a*, *ELO2*, ITS, 28S, mtLSU, mtSSU, *RPB2* and *BTUB* respectively. Bootstrap values (BS) were calculated after 1000 replicates in the ML analysis. The concatenated datasets containing eight (or six for the *A. pullulans* dataset) sub-alignments, each corresponding to the above substitution models was subjected to a gene-partitioned analysis. Phylogenetic trees were inferred from ML and BI in IQ-TREE and MrBayes respectively, following the gene-partitioned analysis. A ghost analysis was also performed in IQ-TREE (Crotty *et al.* 2019) to verify the final topology of the concatenated trees. For the BI analysis, four Markov chains were run for 2 runs initiated from random starting trees for 2 M generations for all single-locus datasets and 4 M generations for the concatenated datasets. Trees were sampled every 100 generations, and the first 25 % of the generations were discarded as burn-in. Bayesian posterior probabilities (BPP) were calculated for the remaining trees. For MP analyses, a heuristic search was performed with 100 random taxon additions and the subtree pruning regrafting (SPR) method as the branch-swapping algorithm. Characters were of equal weight, unordered, while gaps were treated as missing data. A bootstrap analysis was performed with 1000 replicates to assess clade stability, and the number of distinct locally optimal trees were set to 100. Trees were visualized using FigTree v. 1.4.3 (http://tree.bio.ed.ac.uk/software/figtreel). The naming conventions of Zalar *et al.* (2008) were followed with modifications to group names — PullG, MelaG, NamiG, SubgG, and ThaiG for pullulans, melanogenum, namibiae, subglaciale, and thailandense groups, respectively.

Phylogenetic Species Recognition (PSR)

Genealogical concordance phylogenetic species recognition analysis (GCPSR)

The concordance of gene trees is a valuable criterion for the evaluation of gene flow between groups of taxa within an evolutionary timescale (Quaedvlieg *et al.* 2014). The GCPSR analysis with a pairwise homoplasy index (PHI) was used to assess the level of genetic recombination between every pair of clades for new species and their neighbours. The PHI test was conducted using the GCPSR model in SplitsTree v. 6.3.10 (Huson 1998, Huson & Bryant 2006). A PHI below a 0.05 threshold ($\Phi w < 0.05$) indicated significant recombination between clades in the dataset. This was done for each of the single-locus datasets, the 8-LDS and the 6-LDS used to resolve the ApC.

Coalescent-Based Species Recognition (CBSR)

The GMYC method requires a fully resolved ultrametric tree of each single-locus gene as input for analysis. The xml-formatted input files for BEAST v. 2.7.6 (Drummond *et al.* 2012, Bouckaert *et al.* 2014) were prepared in BEAUTi v. 2.7.6 (part of BEAST) using two priors including the Yule and coalescent constant population models. The substitution models selected earlier were specified for the site model parameter and the gamma category count was set to four for both priors. Bayesian Markov chain Monte Carlo (MCMC) was run for 2×10^7 generations. Trees were sampled every 2×10^3 generations for a total of 1×10^4 trees. The posteriors (loglikelihood curves, estimate-effective sample size ≥ 200, and the burn-in state) were confirmed by visualizing trace files in Tracer v. 1.7.2 (Rambaut *et al.* 2018). The first 25 % of trees were removed as burn-in and the remaining trees were used to generate an ultrametric tree in TreeAnnotator v. 2.7.6 from BEAST v. 2.7.6 as an input file for GMYC analyses. The GMYC with single and multiple threshold methods was performed in R under the splits package v. 1.0-19 (Ezard *et al.* 2015), using the "gmyc" function. The single threshold method uses a single transition model with the assumption that all species have the same coalescent branching rate whereas the multiple threshold method uses variable transition models from coalescent to speciation across different clades (Monaghan *et al.* 2009) For each single- and multi-locus dataset, we considered one single and one multiple threshold model that delimited the highest number of species.

The Poisson tree processes (PTP) and its Bayesian implementation (bPTP) use different levels of intraspecific genetic divergences for each species (Zhang *et al.* 2013)

. A simple heuristic search was performed with 1 M MCMC generations. In addition to the simple heuristic search, bPTP also estimates species numbers using a maximum likelihood approach. Thinning was set to 1000 with a burn-in frequency

Table 3. Colony diam (mm) of *Aureobasidium* strains at 7 dpi on various media. Plates were incubated at 25 °C unless otherwise noted.

Growth condition	**Species**[1]									
	A. albui NRRL 64182	*A. cavalettoi* NRRL 64177	*A. diazvalderramae* NRRL 64175	*A. ellingtonae* NRRL 64185	*A. essambei* NRRL 64172	*A. musti* NRRL 64173	*A. peruvianum* NRRL 64183	*A. rubi* NRRL 64179	*A. toomeae* NRRL 64186	*A. vanuatuense* NRRL 64180
M40Y	21	23	22	37	16	36	36	35	23	21
M60Y	20	17	21	17	14	27	22	21	19	18
PDA	20	23	27	32	13	38	34	29	23	19
CZYA	16	15	—	15	11	24	31	15	9	13
CZYA20S	17	18	—	21	14	27	28	15	8	16
YNB	20	21	—	16	13	27	27	24	17	17
MEA + 5 % NaCl	16	12	11	16	15	15	13	11	21	14
MEA + 10 % NaCl	8	8	7	9	11	12	8	8	14	8
MEA + 15 % NaCl	0	7	0	6	6	0	0	7	0	7
MEA + 20 % NaCl	0	0	0	0	0	0	0	0	0	0
MEA at 4 °C	9	13	7	12	9	11	10	11	10	9
MEA at 15 °C	11	17	17	—	9	—	13	14	—	10
MEA at 25 °C	20	23	25	43	12	47	38	18	23	18
MEA at 28 °C	25	27	29	11	17	45	25	28	17	21
MEA at 30 °C	23	15	12	13	15	45	39	18	14	14
MEA at 37 °C	0	0	0	13	0	13	25	0	19	0

[1] — = no data; 0 = no growth was observed.

Table 4. Colony characteristics of studied *Aureobasidium* strains at 7 dpi on different media and on MEA under different incubation temperatures and osmotic conditions.

Conditions	Species and colony characteristics[1]	
Strain/medium	***A. albui* SA46**	***A. cavalettoi* INDP41**
MEA 4 °C	dark brown, filamentous	brown, filamentous
MEA at 25 °C	dark greenish brown, yellow, filamentous	pinkish, filamentous
MEA at 28 °C	brown, black, yellow, filamentous	cream, yeast
MEA at 30 °C	yellow, greenish black, filamentous	pinkish, yeast, lobed
MEA at 37 °C	no growth	no growth
M40Y	pale yellow, filamentous	greenish, cream, filamentous
M60Y	orangish, filamentous	greenish, cream, filamentous
PDA	cream, orangish, filamentous	white, dark grey, filamentous
MEA + 5 % NaCl	greenish brown, yellowish, filamentous	greenish brown, filamentous
MEA + 10 % NaCl	cream, yeast	greenish, filamentous
MEA + 15 % NaCl	no growth	pale pink
MEA + 20 % NaCl	no growth	no growth
Strain/medium	***A. diazvalderramae* MCA7096**	***A. ellingtonae* JB68**
MEA 4 °C	greenish, filamentous	cream, filamentous
MEA at 25 °C	pinkish, filamentous	cream, filamentous
MEA at 28 °C	pinkish, filamentous	cream, filamentous
MEA at 30 °C	brownish, cream, filamentous	pinkish, yeast
MEA at 37 °C	no growth	cream, filamentous
M40Y	cream, filamentous	pinkish, filamentous
M60Y	pinkish, filamentous	pinkish, filamentous
PDA	cream, dark brown, filamentous	cream, filamentous
MEA + 5 % NaCl	cream, filamentous	cream, filamentous
MEA + 10 % NaCl	cream, yeast	cream, yeast
MEA + 15 % NaCl	no growth	n/a
MEA + 20 % NaCl	no growth	no growth
Strain/medium	***A. essambei* MCA7731**	***A. peruvianum* MCA7097**
MEA 4 °C	black, yeast	blackish, filamentous
MEA at 25 °C	black, filamentous	greenish, black, filamentous
MEA at 28 °C	black, filamentous	greenish, black, filamentous
MEA at 30 °C	black, cream, filamentous	greenish, black, filamentous
MEA at 37 °C	no growth	black, yellowish, filamentous
M40Y	greenish brown, filamentous	brown, cream, filamentous
M60Y	dark green, filamentous	brown, cream, filamentous
PDA	cream, filamentous	black-dark green, filamentous
MEA + 5 % NaCl	black, filamentous	dark green, filamentous
MEA + 10 % NaCl	greenish brown, filamentous	black, greenish, filamentous
MEA + 15 % NaCl	no growth	n/a
MEA + 20 % NaCl	no growth	no growth
Strain/medium	***A. rubi* MCA3890**	***A. toomeae* MT159**
MEA 4 °C	pinkish, filamentous	cream, filamentous
MEA at 25 °C	pinkish, filamentous	golden-black, filamentous
MEA at 28 °C	cream, greenish, filamentous	pinkish, filamentous
MEA at 30 °C	cream, filamentous	black, golden, lobed
MEA at 37 °C	no growth	pinkish, filamentous
M40Y	pinkish, filamentous	cream, filamentous
M60Y	pinkish, filamentous	cream, yellowish, filamentous
PDA	white, black, filamentous	greenish, cream, filamentous
MEA + 5 % NaCl	pinkish, filamentous	cream, brownish, filamentous

Table 4. (Continued).

Conditions	Species and colony characteristics[1]	
MEA + 10 % NaCl	pinkish, yeast	greenish brown, filamentous
MEA + 15 % NaCl	creamy	n/a
MEA + 20 % NaCl	no growth	no growth
Strain/medium	***A. musti* TAR230**	***A. vanuatuense* MCA7387**
MEA 4 °C	yellow, yeast	black, yeast
MEA at 25 °C	orange, yellow, black, filamentous	greenish-brown, pale yellow, filamentous
MEA at 28 °C	black, yellow, filamentous	brownish, yellow, filamentous
MEA at 30 °C	brick red, pink, cream, filamentous	pinkish, yeast
MEA at 37 °C	black, lobed	no growth
M40Y	yellow, orange, filamentous	purplish, filamentous
M60Y	yellow, orange, filamentous	orangish, filamentous
PDA	purple-brown-light red, cream, filamentous	cream, greenish, filamentous
MEA + 5 % NaCl	deep orange, filamentous	yellowish, filamentous
MEA + 10 % NaCl	cream, filamentous	cream, yeast
MEA + 15 % NaCl	n/a	cream, yeast
MEA + 20 % NaCl	no growth	no growth

[1] n/a = not available; where colony colour is uniform, one color is given; colonies with different color zones are indicated as centre color [comma] middle zone color [comma] outer zone color (if different from middle); the last item refers to margin features.

of 10 % and the dataset had no outgroups. The analysis was performed for each single-locus and concatenated dataset in the PTP standalone software using an unrooted nexus tree file from IQ-TREE.

Distance-Based Species Recognition (DBSR)

The automatic barcode gap delimitation (ABGD) was used to sort each of the single- and multi-locus alignments into hypothetical species. ABGD detects a barcode gap within a distribution of pairwise genetic distances and determines the number of species hypotheses in a dataset (Puillandre *et al.* 2012). For each of the tested priors on the x-axis, there is a corresponding number of species hypothesis detected on the y-axis. Two types of partitions are produced by ABGD once a barcode gap is computed. Sequences are initially divided into species hypothesis based on a barcode gap inferred statistically in the initial partition. Then, each of the species hypotheses delimited in the initial partition independently undergoes rounds of splitting in the recursive partition until no more split is made, and no additional barcode gaps are found (Puillandre *et al.* 2012, Kekkonen *et al.* 2015). The recursive partition tends to detect divergent populations within species, leading to an overestimation of the total number of species (Puillandre *et al.* 2012). Prior to analysis, the model criteria were set as follows: minimum gap width (X) of 1.0, distance metric was computed for Jukes-Cantor and Kimura using the Kimura-2-parameter, intraspecific divergence (P) values were set to 0.001 (Pmin) and 0.1 (Pmax), and 20 screening steps. The analysis was performed with the standalone ABGD software using multiple sequence alignments without outgroups.

Like ABGD, assemble species by automatic partitioning (ASAP) proposes primary species hypothesis based on DNA sequences (Puillandre *et al.* 2021) Sequences are grouped based on their genetic distances into partitions until the point where all sequences are grouped into one species hypothesis. At each merging step, the newly defined partition is characterized in two complementary ways. First, it is assigned a probability that quantifies the chances that each of its new subset is a single species. Then, the width of the barcode gap between the previous and current partition is computed. The probability and barcode gap width are merged into a metric called the ASAP score which is then applied to rank each partition. Settings were: 1000 replicates, P = 0.001, and distance = K2P. The analysis was done with the ASAP desktop software or on web-based platform at http://galaxy.itaxotoolsweb.org/, using multiple sequence alignment files of the single- and multi-locus datasets. The lower the ASAP score, the stronger the partition.

RESULTS

Morphology

The growth parameters of strains on media with varying salt or sugar concentrations at different temperatures are shown in Table 3. Only a few strains tolerated salt concentrations of up to 15 % NaCl, while most strains grew at concentrations of 10 % and below. Colour pigmentation of colonies ranged from cream or white to deep shades of yellow, orange, purple, and red, to greenish, brownish, dark green, dark brown and finally to black (Table 4). Growth rates were tested between 4–37 °C for all species (Table 3). All strains exhibited growth when incubated at 4–30 °C, but the most luxuriant growth was observed at 25 °C or 28 °C depending on the strain. A few strains grew at 37 °C, primarily in the filamentous form, although the growth was slower compared to that at lower temperatures (Table 3). Growth of *A. musti* was lobed and twisted at 37 °C. All isolates grew in filamentous form on MEA at 28 °C except for *A. cavalettoi* (NRRL 64177).

Table 5. Assimilation profiles of carbon and nitrogen sources and fermentation ability of the *Aureobasidium* strains studied.

Compound	Species1									
	A. albui NRRL 64182	*A. cavalettoi* NRRL 64177	*A. diazvalderramae* NRRL 64175	*A. ellingtonae* NRRL 64185	*A. essambei* NRRL 64172	*A. mustum* NRRL 64173	*A. peruvianum* NRRL 64183	*A. rubi* NRRL 64179	*A. toomeae* NRRL 64186	*A. vanuatuense* NRRL 64180
Carbon assimilation										
D-glucose	+++	++	++	++	+++	++	+	++	+	+++
L-sorbose	+	+	—	—	+++	—	—	—	—	—
D-glucosamine	—	—	—	—	—	—	—	—	—	—
L-arabinose	+++	+	++	+	+++	++	+	++	+	++
D-arabinose	—	—	—	—	—	—	—	—	—	—
a-rhamnose monohydrate	—	—	+	—	—	—	+	—	—	—
D-salicin	—	+	+	—	—	—	+	+	—	—
Soluble starch	—	—	—	—	—	—	—	—	—	—
Glycerol	—	—	—	—	—	—	—	—	—	—
Erythritol	—	—	+	—	—	—	+	—	+	+
Ribitol (Adonitol)	—	+	—	—	—	—	—	—	—	—
Xylitol	—	—	—	—	—	—	+	—	—	—
D-manitol	+	+	+	—	—	—	+	++	+	+
Dulcitol (Galactitol)	++	—	—	—	—	—	+	—	—	—
Myo-inositol	—	—	+	—	—	—	—	—	—	—
Gluconic acid lactone	+	—	—	—	—	—	+	—	—	—
Gluconic acid sodium salt	++	+++	—	+	++	+++	+	++	++	++
Sodium succinate dibasic hexahydrate	+++	+	++	—	—	+	—	—	—	+++
Ethanol	—	—	—	—	—	—	—	—	—	—
Propane-1,2-diol	—	—	—	—	—	—	+	—	—	—
D-quinic acid	+++	—	+	—	+++	+	—	—	++	+++
Fermentation										
D-glucose	—	—	—	—	+	—	+	—	—	+
D-galactose	—	—	—	—	—	—	—	—	—	—
Maltose	—	—	—	—	—	—	+	—	—	—
α-methyl-D-glucoside	—	—	—	—	—	—	—	—	—	—
Sucrose	+	—	—	—	+	—	+	—	—	+
Trehalose	—	—	—	—	—	—	+	—	—	—
Melibiose	+	—	—	—	—	—	++	—	—	—

Table 5. (Continued).

Compound	Species1									
	A. albui NRRL 64182	*A. cavalettoi* NRRL 64177	*A. diazvalderramae* NRRL 64175	*A. ellingtonae* NRRL 64185	*A. essambei* NRRL 64172	*A. mustum* NRRL 64173	*A. peruvianum* NRRL 64183	*A. rubi* NRRL 64179	*A. toomeae* NRRL 64186	*A. vanuatuense* NRRL 64180
Lactose	—	—	—	—	—	—	—	—	—	—
Cellobiose	—	—	—	—	—	—	+	—	—	—
Melezitose	—	—	—	—	+	—	+	—	—	+
Raffinose	—	—	—	—	+	—	+	—	—	+
Inulin	—	—	—	—	—	—	w	—	—	—
Starch	—	—	—	—	—	—	—	—	—	—
D-xylose	—	—	—	—	—	—	—	—	—	—
Nitrogen assimilation										
KNO3	+++	+++	++	++	+++	+	+++	+++	—	++
NaNO2	+++	—	—	+++	—	+	++	—	—	+
Ethylamine-HCl	++	—	++	+++	+++	+	—	++	+	+++
L-lysine-HCl	+++	+++	++	+++	+++	++	+++	+++	+	+++
Cadaverine-HCl	+	+	++	++	++	+	+	++	++	+
Creatine	—	—	—	—	—	—	—	—	—	—
Creatinine	—	—	—	—	—	—	—	—	—	—
D-glucosamine	++	+	—	+	+++	+	+++	—	—	+
Imidazole	—	—	—	—	—	—	—	—	—	—
D-tryptophan	—	+	—	—	+	+	+++	—	—	+

[1] Strong assimilation (**+++**); moderate assimilation/fermentation (**++**); weak assimilation/fermentation (**+**); very weak assimilation/fermentation (**w**); no growth (—).

Aureobasidium musti (NRRL 64173), *A. vanuatuense* (NRRL 64180) and *A. essambei* (NRRL 64172) were unable to produce hyphae on MEA at 4 °C. Results on physiological tests are summarized in Table 5 and presented for each new species in the taxonomic section.

Phylogenetic inference

The BI analysis stopped at average standard deviation of split frequencies of 0.006358, 0.005154, 0.027540, 0.013512, 0.006725, 0.004472, 0.009258 and 0.004961 for *EF1a*, *ELO2*, ITS, 28S, mtLSU, mtSSU, *RPB2* and *BTUB*, respectively. The ITS dataset (Table S1) consisted of 208 isolates with 542 nucleotide positions including gaps, of which 73 % were constant and 132 were parsimony-informative. There were 103 isolates in the 28S dataset containing a total of 773 nucleotide positions. Of these, 84 % were constant and 85 were parsimony-informative. The mtLSU dataset had 35 isolates with a total of 248 nucleotide positions, of which 83 % were constant and 33 were parsimony-informative. There were 24 isolates and 573 nucleotide positions in the mtSSU dataset. Of these, 83 % were constant and 30 were parsimony-informative. The *BTUB* dataset had 37 isolates and 453 nucleotide positions of which 82 % were constant and 59 parsimony-informative. The *EF1a* dataset had 50 isolates and 880 nucleotide positions, of which 80 % were constant sites and 122 were parsimony-informative. In the *ELO2* dataset, there were 50 isolates and 698 nucleotide positions, of which 64 % were constant and 187 were parsimony-informative. Finally, the *RPB2* dataset had 82 isolates and 753 nucleotide positions of which 55 % were constant and 301 were parsimony-informative.

Prior to concatenation, we assessed individual locus trees for conflicts using the GCPSR as detailed in that section, below, and pruned the number of isolates to those that represented types or type proxies and additional isolates with available multi-locus data. After aligning, trimming, and concatenating the pruned single locus datasets, the final 8-LDS and 6-LDS were used for phylogenetic analyses. The final concatenated 8-LDS comprised 77 isolates and 4748 characters (525 characters for ITS, 572 for 28S, 754 for *RPB2*, 699 for *ELO2*, 921 for *EF1a*, 454 for *BTUB*, 250 for mtLSU, and 573 for mtSSU) and 890 parsimony-informative sites (131 sites for ITS, 73 for 28S, 288 for *RPB2*, 179 for *ELO2*, 113 for *EF1a*, 48 for *BTUB*, 36 for mtLSU, and 22 for mtSSU). The gene boundaries in the concatenated tree (Fig. 1A) were 1–525 for ITS, 526–1097 for 28S, 1098–1851 for *RPB2*, 1852–2550 for *ELO2*, 2551–3471 for *EF1a*, 3472–3925 for *BTUB*, 3926–4175 for mtLSU, and 4176–4748 for mtSSU. Topology of the final 8-LDS tree (Fig. 1) did not conflict with any of the single locus phylogenies and recovered most of the *Aureobasidium* groups of Zalar *et al.* (2008).

The pullulans group (PullG) correspons to the *Aureobasidium pullulans* clade sensu Zalar *et al.* (2008). This group was strongly supported (BS and BPP) in all phylogenies except for *RPB2*, *BTUB*, and mtSSU. The support values were 94/100 for ITS, 94/100 for 28S, 98/100 for ELO2,100/100 for *EF1a*, 70/- for mtLSU, and 100/100 for the 8-LDS phylogeny. Five species of the ApC are resolved in the 6-LDS analyses of PullG (Fig. 1B) that include the ex-epitype of *A. pullulans* (CBS 584.75), the ex-epitype of *A. proteae* (CBS 114273), the ex-type of *A. pullulans* var. *aubasidani* (CBS 100524), the ex-type of *A. lini* (CBS 125.21), and *A. microstictum* (CBS 342.66). Also resolved in PullG are sequences from *Columnosphaeria fagi* (CBS 171.93) suspected to be the sexual morph of *A. pullulans* (Zalar *et al.* 2008), and two new species; *A. ellingtonae* (NRRL 64185) and *A. toomeae* (NRRL 64186).

The namibiae (NamiG) (group 4 of Zalar *et al.* 2008) was well supported in *ELO2* (100/100), *EF1a* (96/98), *BTUB* (87/98), mtLSU (98/99), mtSSU (89/-), *RPB2* (95/98), and the 8-LDS phylogeny (97/100). It contains the ex-type or ex-epitype strains of *A. namibiae* (CBS 147.97), *A. pini* (CFCC 52778), *A. leucospermi* (CBS 130593), *A. khasianum* (NFCCI-4275), *A. insectorum* (KCL139), *A. intercalariosporum* (MGL11-3), *A. xishuangbannaense* (KUMCC 21-0703), and *Pullularia fermentans* var. *fermentans* (CBS 298.56) as well as the new species *A. cavalettoi* (NRRL 64177), *A. diazvalderramae* (NRRL 64175), and *A. rubi* (NRRL 64179). Sequences from three unidentified strains (DTO 302-F1, DTO 285-E2, and DTO 296-F9) (van Nieuwenhuijzen *et al.* 2016) are conspecific with *A. insectorum* in our analyses (Fig. S1A). The subglaciale group (SubgG) (Group 3 of Zalar *et al.* 2008) was resolved within the NamiG group in the *EF1a* phylogeny (Figs 4B, S1C) but was otherwise strongly supported in all analyses except for mtLSU and mtSSU. Support values were 95/- for ITS, 93/100 for 28S, -/94 for *RPB2*, 100/100 for *ELO2*, 98/100 for *BTUB*, and 100/100 for the 8-LDS phylogeny. SubgG contains the ex-type (CBS 123387) and other isolates of *A. subglaciale*.

The melanogenum group (MelaG) (group 2 of Zalar *et al.* 2008) was well supported in all phylogenies except for mtLSU. Support values were 92/98 for the ITS phylogeny, 95/100 for 28S, 100/98 for *RPB2*, 99/100 for *ELO2*, 89/97 for *EF1a*, 95/100 for mtSSU, and 94/90 for the 8-LDS phylogeny. MelaG contains the ex-types of *A. acericola* (KACC 49605), *A. melanogenum* (CBS 105.22), *A. motuoense* (XZY411-4), and *A. musti* (NRRL 64173). One new group, the thailandense group (ThaiG) is resolved with our data and strongly supported in the ITS (76/94), *RPB2* (99/100), *ELO2* (92/100), *EF1a* (87/-), *BTUB* (79/-), mtLSU (99/100), mtSSU (78/100), and 8-locus ML (100/100) analyses. It comprised the ex-types of *A. castaneae* (JJ73), *A. thailandense* (NRRL 58539), and *A. microtermitis* (NFCCI 4901) as well as three new species: *A. albui* (NRRL 64182), *A. vanuatuense* (NRRL 64180), and *A. essambei* (NRRL 64172).

Species delimitation

We tested several different in silico species recognition approaches, including GPCSR, distance-based species recognition (ABGD and ASAP), and coalescence-based species recognition (PTP, bPTP, GMYC) with inconsistent results (Table 6, Figs 2–5) as detailed below.

Genealogical Concordance Phylogenetic Species Recognition (GCPSR)

In the GCPSR analysis, all the single-locus and concatenated datasets had a PHI > 0.05 (Table 6). The PHI test did not find statistically significant evidence for recombination between *Aureobasidium* species (as delimited in Fig. 1A) in the single-locus and 8-LDS datasets (PHI > 0.05). There was also no significant evidence of recombination events between the

Table 6. Species predicted by different species recognition criteria in *Aureobasidium* in single-locus and concatenated datasets. A GCPSR index (PHI; pairwise homoplasy index) was used to assess recombination in the input data sets. PHI < 0.05 indicates significant recombination in the dataset. The numbers under DBSR and CBSR indicate the number of species detected by each algorithm. For ASAP the number after the slash (/) indicates the confidence score and the smaller the score (smallest score is 1), the more accurate the partition. For CBSR, the numbers after the / symbol indicate the confidence interval for correct determination of number of species from the input data set.

SRC	**Method**[1]	**Loci**[2]									
		BTUB	*EF1a*	*ELO2*	ITS	28S	mtLSU	mtSSU	*RPB2*	MLT	ApC
GCPSR	*PHI*	0.89	0.85	0.99	0.82	0.30	0.76	0.06	0.50	1.00	0.92
Species detected by GCPSR		12	16	20	38	41	10	10	24	44	7
DBSR	*ABGD(KIP)*	13	15	14	44	32	7	9	17	20	5
	ABGD(JKIP)	13	15	14	44	32	7	9	17	20	5
	ASAP/score	13 / 2.0	16 / 1.5	13 / 2.5	2 / 1.0	17 / 3.0	7 / 3.0	9 / 2.0	24 / 2.0	34 / 3.5	2 / 1.0
CBSR	*PTP*	4	16	15	5	17	3	6	17	26	3
	bPTP[1]	4	18	16	7	17	3	6	17	26	3
	bPTP	14	18	17	39	49	11	12	17	34	7
	YSC/CI	5 / 1–6	7 / 1–7	7 / 1–7	3 / 3–3	8 / 8–10	2 / 1–5	3 / 1–4	5 / 4–5	20 / 16–22	1 / 1–7
	YSE/CI	12 / 1–17	10 / 1–20	15 / 9–23**	3 / 3–3	15 / 14–19**	2 / 1–15	4 / 1–13	24 / 11–26**	34 / 27–39*	3 / 1–11
	CSC/CI	5 / 1–6	7 / 1–7	7 / 4–7	3 / 1–20	8 / 8–11	2 / 1–5	4 / 1–4	5 / 4–5	20 / 8–24	1 / 1–7
	CSE/CI	12 / 1–17	10 / 1–20	15 / 8–23**	3 / 1–71	15 / 14–22**	2 / 1–15	8 / 1–13	24 / 11–26**	34 / 12–49*	3 / 1–18
	YMC/CI	4 / 1–5	5 / 1–7	6 / 5–6	3 / 3–19	9 / 8–10	2 / 1–5	3 / 3–4	6 / 5–6	20 / 17–22	4 / 1–7
	YME/CI	13 / 1–13	14 / 1–15	17 / 8–18***	3 / 3–32	18 / 15–18***	4 / 1–8	5 / 3–8	22 / 10–22**	41 / 29–42*	8 / 1–10
	CMC/CI	6 / 2–6	5 / 1–7	6 / 5–6	8 / 4–18	10 / 8–10	4 / 1–5	3 / 1–4	6 / 5–6	21 / 15–24	3 / 1–7
	CME/CI	8 / 2–12	14 / 1–15	17 / 8–18***	10 / 5–33	18 / 16–18**	7 / 1–9	5 / 1–9	22 / 10–22**	40 / 21–41*	7 / 1–10
Total no. of sequences		18	21	29	72	62	16	14	31	74	19

[1] ABGD = automatic barcode gap detection, ApC = A. pullulans species complex, ASAP = assemble species by automatic partitioning, bPTP[1] = poisson tree processes by maximum likelihood search, (b) PTP = poisson tree processes by simple heuristic search, CI = confidence interval, Clusters = OTUs delineated by GMYC with more than one sequence, CMC = coalescent multiple threshold clusters, CME = coalescent multiple threshold entities, CSC = coalescent single threshold clusters, CSE = coalescent single threshold entities, Entities = singleton OTUs delineated by GMYC, GCPSR = genealogical concordance phylogenetic species recognition, JKIP = jukes-cantor initial partition, KIP = kimura initial partition, MLT = multi-locus tree, PHI = pairwise homoplasy index, SRC = species recognition criteria, YSC = yule single threshold clusters, YSE = yule single threshold entities, YMC = yule multiple threshold clusters, YME = yule multiple threshold entities.

[2] * = indicates significant results of the likelihood ratio test (the more the stars, the smaller the p-value).

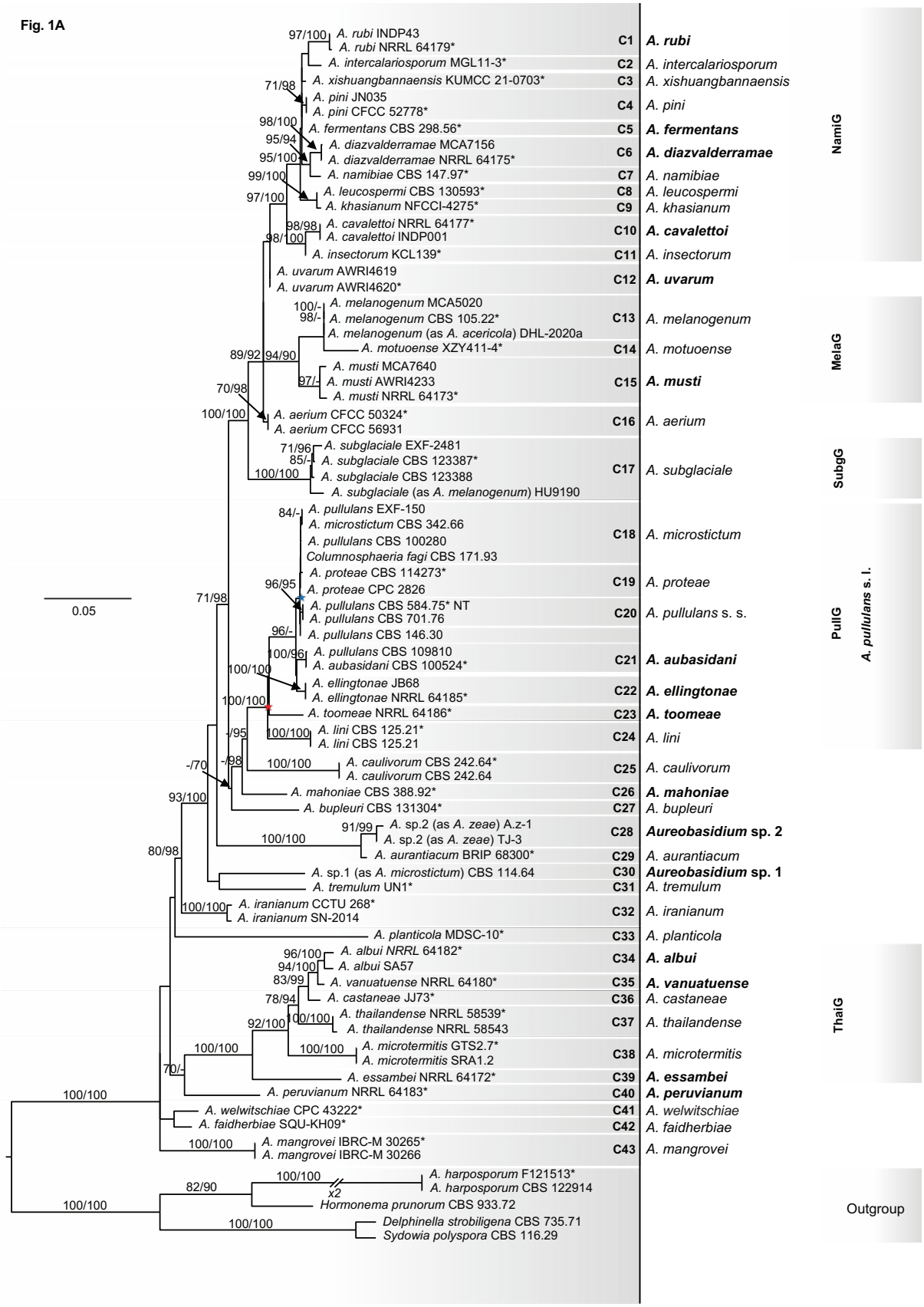

Fig. 1. Phylogenetic reconstruction of *Aureobasidium* species based on Bayesian inference (BI) and maximum likelihood (ML) analyses. The bootstrap percentages of the ML ≥ 70 % and BI posterior probability (pp) values ≥ 0.95 are presented at the nodes as ML/BI. Only values > 70 % bootstrap support or > 0.95 posterior probability are indicated. Scale bar = number of nucleotide substitutions per site. Sequences derived from ex-types strains are indicated with an asterisk (*) and species names in **bold** represent new descriptions, new combinations, or new names from this study. **A.** Results from 8-LDS concatenated dataset (ITS, 28S, *RPB2*, *EF1a*, *ELO2*, mtSSU, mtLSU, *BTUB*) showing the relationship between 68 *Aureobasidium* sequences. The tree is rooted to *Delphinella strobiligena* (CBS 735.71), *Sydowia polyspora* (AFTOL-ID 1300), and *Hormonema prunorum* (CBS 933.72). *Aureobasidium* species are indicated as C1–C43. The five groups also identified in the single locus phylogenies are indicated as PullG, NamiG, MelaG, SubgG and ThaiG (see text for explanation). **B.** Concatenated phylogeny resulting from the 6-LDS (ITS, RPB2, *EF1a*, *ELO2*, mtSSU, *BTUB*) showing the relationship between 19 *Aureobasidium* sequences from the *A. pullulans* complex, PullG, sensu Zalar *et al*. (2008). The tree is rooted to *A. lini* (CBS 125.25) and *A. toomeae* (NRRL 64186) based on the analyses shown in Fig. 1A.

species of the ApC (as delimited in Fig. 1B) in the 6-LDS of the PullG (PHI = 0.92). All newly proposed species were congruent and non-discordant following GCPSR analysis of the single-locus datasets (Figs 2–5). The exception was with four previously described species – *A. motuoense, A. planticola, A. tremulum,* and *A. welwitschiae* – represented only by ITS and 28S data that had incongruent placements in the individual locus analyses but were significantly supported in the eight-locus concatenated phylogeny (Figs 1A, 2A, B).

Distance-Based Species Recognition (DBSR)

The genetic distance-based method based on ABGD was performed using both the Kimura-2P and Jukes-Cantor distances. We found similar results with these two methods. ABGD found diverse numbers of species in the different single-locus datasets probably because these datasets had missing data for some species. It detected barcode gaps in all datasets except for the 8-LDS and 28S datasets and therefore was unable to accurately propose primary partitions and correctly delineate species in these datasets. Initial partitions have been considered close to the hypothetical number of species in other studies (Puillandre *et al.* 2012, Bhunjun *et al.* 2020). ABGD detected 44 species in the ITS dataset (Table 6, Fig. 2A) and 32 species in 28S (Fig. 2B). For the mitochondrial genes, it detected seven species in mtLSU (Fig. 3A) and nine in mtSSU (Fig. 3B). Meanwhile, in the protein-coding genes, ABGD found 13 species in *BTUB*, 15 in *EF1a*, 14 in *ELO2*, and 17 in *RPB2* (Table 6 and Fig. 4A–D, respectively). When using recursion, ABGD proposed one species each in *BTUB* and *EF1a*, nine (mtLSU), 11 (ITS), 18 (*ELO2*), 21 (*RPB2*), and 34 species in MLT (Fig. 5A). Furthermore, ABGD delimited five and 20 species, respectively, in the ApC and multi-locus tree (MLT) datasets (Table 6, Fig. 5B). It was unable to detect any species recursively in the 28S, ApC, and mtSSU datasets (Table 6). Detected species in the protein-coding and mitochondrial genes coincided with clades recovered with the 8-LDS (Fig. 1A) except that *A. diazvalderramae* and *A. cavalettoi* were grouped as the same species in the mtLSU while *A. diazvalderramae* and *A. rubi* were conspecific in 28S and mtSSU (Figs 2B, 3A, B). Another slight difference was that A. *diazvalderramae* and *A. namibiae* were grouped as one species in *EF1a* while *A. vanuatuense* and *A. albui* were grouped together in the mtLSU, mtSSU, *ELO2*, and *RPB2* gene genealogies (Figs 3A, B, 4C, D).

Assemble Species by Automatic Partitioning (ASAP) detected two species hypotheses each from *ApC* and ITS datasets, 7 from mtLSU, 9 from mtSSU, 13 each from *BTUB* and *ELO2*, 16 from *EF1a*, 17 from 28S, 24 from *RPB2*, and 34 from the MLT dataset (Table 6). Species hypotheses inferred from *BTUB*, *EF1a*, *ELO2*, and *RPB2* genes largely coincided with monophyletic clades inferred from MLT topology of the 8-LDS phylogeny (Figs 4A–D, 5A, Table 6). However, there were slight differences in the groupings in these four datasets. For instance, *A. vanuatuense* and *A. albui* were grouped in the same clade in *BTUB* and *ELO2* datasets. In addition to grouping *A. ellingtonae* with the ApC in *ELO2* (Fig. 4C), ASAP also grouped *A. diazvalderramae, A. namibiae,* and *A. rubi* as a single species. In the MLT phylogeny, ASAP detected 34 species, grouping *A. diazvalderramae, A. fermentans, A. intercalariosporum, A. pini, A. rubi, and A. xishuangbannaense* as one species (Fig. 5A). Assemble Species by Automatic Partitioning only detected *A. lini* as a species and the remainder of the sequences as another species in the ApC phylogeny (Fig. 5B).

Coalescent-Based Species Recognition (CBSR)

Among the CBSR methods the highest number of hypothetical species was delimited by bPTP for ITS (38 species), 28S (49), mtLSU (11), mtSSU (12), *BTUB* (14), and *EF1a* (18 species) using a simple heuristic search (Tabel 6). In *ELO2*, bPTP and the multiple threshold Yule and coalescent priors of the of GMYC all detected 17 species hypotheses. Meanwhile, 24 hypothetical species were detected in the *RPB2* dataset by GMYC using the single threshold Yule and coalescent constant population priors. GMYC also delimited 41 and 8 species hypotheses in the MLT and ApC datasets respectively using the multiple threshold Yule prior (Table 6).

Species delimitation by PTP simple heuristic search and bPTP maximum likelihood search (bPTP[1]) was weak for most of the gene trees except for *EF1a*, *ELO2*, *RPB2*, and MLT (Figs 4B–D, 5A). PTP and bPTP[1] found and delimited a similar number of species in most gene trees except for *EF1a*, *ELO2*, and ITS. For instance, in the ITS gene tree (Fig. 2A), PTP considered everything from *A. pullulans* CBS 584.75 to *A. mangrovei* as a single species as well as the two sequences of *A. harposporum*. Meanwhile, bPTP[1] separated *A. mangrovei* from the species group above and also delimited the two sequences in *A. harposporum* as separate species. In the 28S gene tree, both PTP and bPTP[1] delimited the same species. In this gene phylogeny, the two models delimited everything from *A. cavalettoi* to *A. melanogenum* (as *A. acericola*) as a single species. All sequences from *A. pullulans* to *A. toomeae* were also considered conspecific as well as those from *A. albui* to *A. thailandense* (Fig. 2B). In the

Fig. 1B

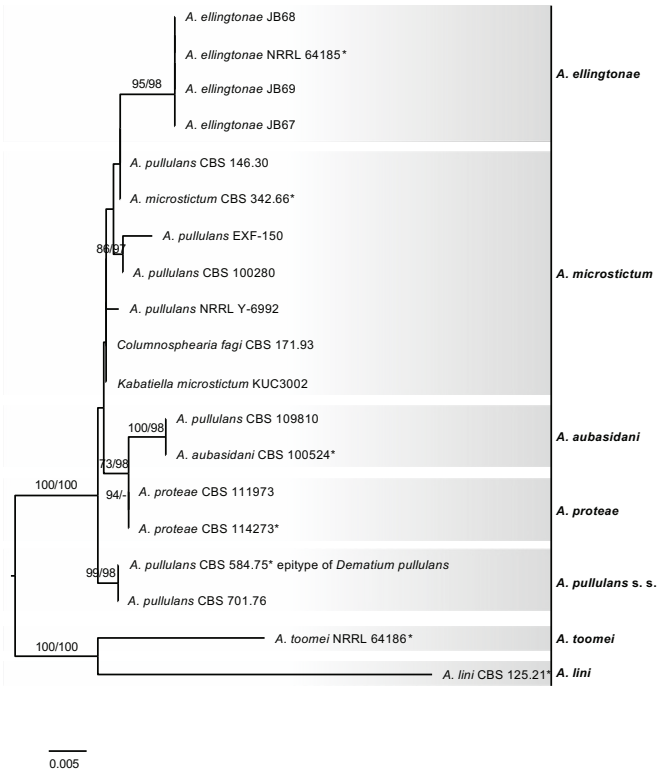

Fig. 1. (Continued).

Fig. 2A

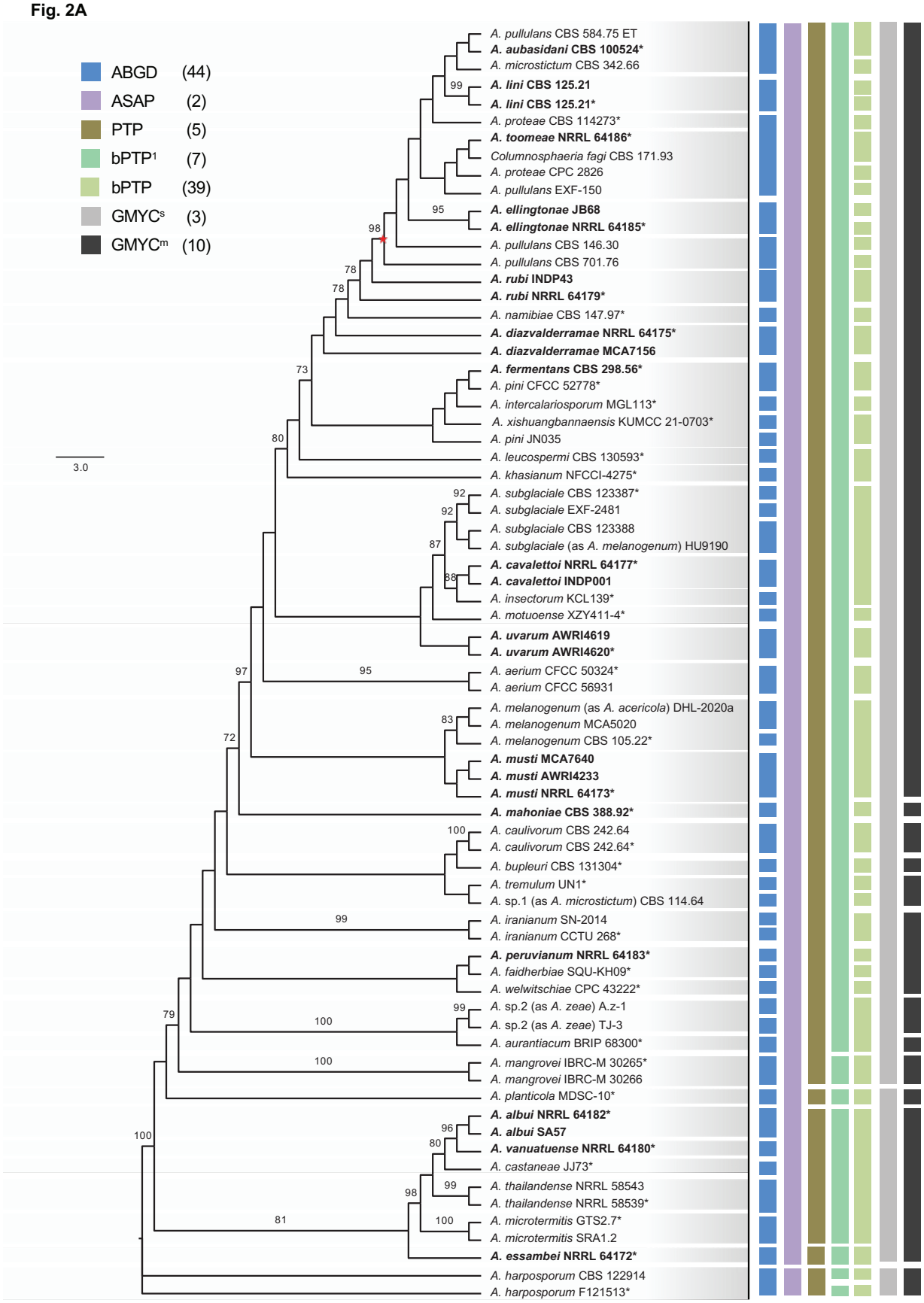

Fig. 2. Phylogenetic trees inferred by maximum parsimony (MP) analyses, trees showing species detection by different recognition criteria. Single locus analyses of all sequences used in the concatenated analyses of: **A.** ITS sequences of 72 *Aureobasidium* isolates, and **B.** 28S sequences of 62 isolates. The bootstrap percentages of the MP ≥ 70 % are presented at the nodes. Scale bar = the number of nucleotide substitutions per site. The tree is midpoint rooted. Sequences from ex-types are indicated with an asterisk (*). **Bold** names = new species, combinations, or names from this study. The red star indicates the node containing PullG, the *A. pullulans* species complex. Colored vertical blocks represent the species detected by: blue = Automatic Barcode Gap Delimitation (ABGD); lavender = Assemble Species by Automatic Partitioning (ASAP); khaki = Poisson Tree Processes (PTP); green = Bayesian PTP maximum likelihood (bPTP¹); yellow-green = Bayesian PTP (bPTP); grey = General Mixed Yule Coalescent by single threshold (GMYCˢ); black = General Mixed Yule Coalescent by multiple threshold (GMYCᵐ). Numbers in parentheses in key refer to total number of species delimited by that method.

Fig. 2B

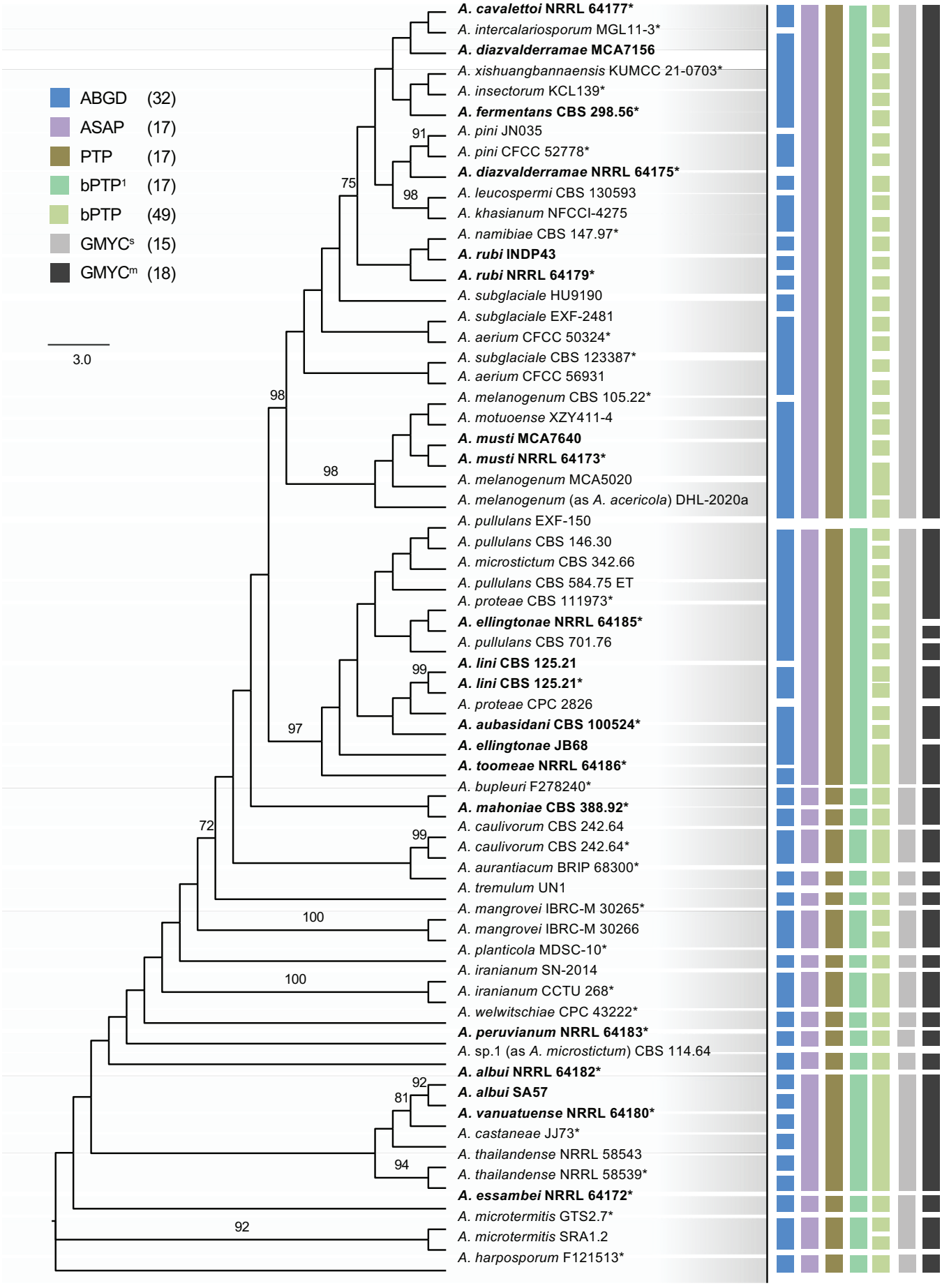

Fig. 2. (Continued).

mtLSU gene tree, these models considered all sequences from *A. melanogenum* to *A. peruvianum* as conspecific while sequences from *A. vanuatuense* to *A. essambei* were also grouped as a single species (Fig. 3A). PTP and bPTP[1] grouped *A. diazvalderramae, A. rubi, A. peruvianum,* and *A. musti* as one species and *A. vanuatuense* and *A. albui* as another species in the mtSSU phylogeny (Fig. 3B). In the *BTUB* phylogeny, PTP and bPTP[1] grouped *A. cavalettoi*, *A. diazvalderramae*, *A. ellingtonae*, *A. namibiae*, *A. pullulans* (EXF-150), *A. rubi*, *A. subglaciale,* and *A. toomeae* as one species and *A. albui and A. vanuatuense* as conspecific (Fig. 4A). PTP accurately delimited NRRL 64175 and MCA7156 as a species (*A. diazvalderramae*) as well as NRRL 64182 and SA57 (*A. albui*) in *EF1a*, while bPTP[1] delineated these four sequences as four separate species (Fig. 4B). The main difference in species delimitation in *ELO2* was that PTP delimited CBS 105.22 and MCA5020 as a single species (*A. melanogenum*) while bPTP[1] separated them as individual species (Fig. 4C). In the *ELO2* and *RPB2* phylogenies, PTP and bPTP grouped *A. diazvalderramae* and *A. namibiae* together. Additionally, in *RPB2*, *A. leucospermi* and *A. rubi* were also grouped together with *A. diazvalderramae* and *A. namibiae* (Fig. 4D). *Aureobasidium ellingtonae* was also grouped in the ApC by PTP and bPTP[1] in the *ELO2* and *RPB2* gene trees (Fig. 4C, D). bPTP by simple heuristic search consistently delimited more than the expected number of species in most gene trees except for *ELO2*, *RPB2*, MLT, and ApC (Table 6, Figs 4C, D, 5A, B).

The GMYC analysis was performed using two ultrametric trees, one based on the coalescent constant population prior and the other on the Yule prior. Both the single and multiple threshold models were used in the analysis and resulted in a better fit to the ultrametric tree than the null model. These two models had higher loglikelihood values compared to the null model. The analysis was performed for all single- and multi-locus datasets, and the multiple threshold model performed better than the single threshold model for most of the gene trees under the Yule and coalescent priors (Table 6). Overall, for the GMYC analysis, the multiple threshold model under the coalescent constant population prior performed better than all tested models as it delimited more species with higher loglikelihood values. GMYC under the multiple threshold coalescent prior estimated the highest number of species in ITS (10 species), 28S (18), mtLSU (7), *EF1a* (14), *ELO2* (17), MLP (41), and ApC (8). The coalescent constant population single threshold model delimited 8 and 24 species in mtSSU and *RPB2*, respectively, while 13 species were delimited by the Yule multiple threshold model in the *BTUB* dataset. We found statistically significant results in the likelihood ratio test of the GMYC species delineation in the *ELO2*, 28S, *RPB2*, and MLT datasets ($p < 0.05$; Table 6 indicated by *). GMYC also delimited similar number of species using the single threshold models of the Yule and coalescent constant population priors in all datasets except mtSSU (Tabel 6).

In the ITS phylogeny, GMYC single threshold (GMYC^s) was unable to distinguish between species from *A. pullulans* to *A. mangrovei* and from *A. planticola* to *A. essambei*. GMYC multiple threshold (GMYC^m) grouped sequences from *A. pullulans* to *A. musti* as a single species*, A. mahoniae* and *A. bupleuri* as conspecific, *A. caulivorum*, *A. tremulum,* and an unidentified species (*Aureobasidium.* sp.1, CBS 114.84, originally identified as *A. microstictum*)

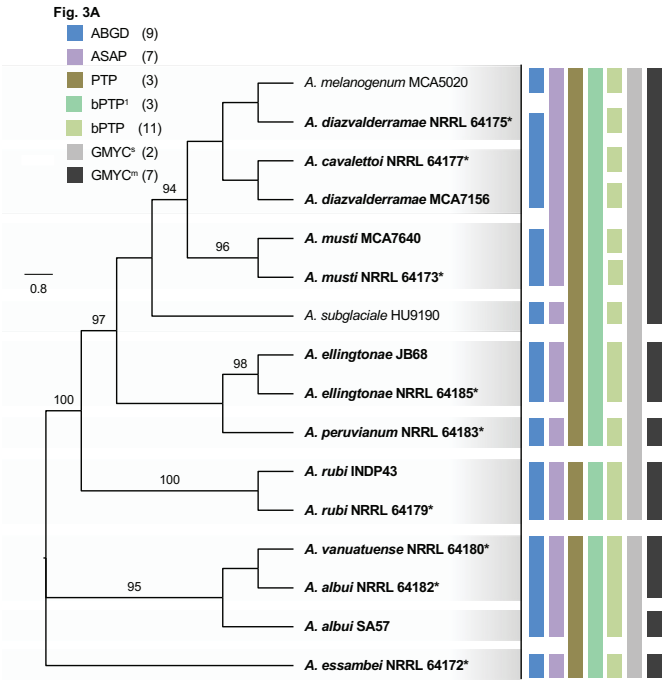

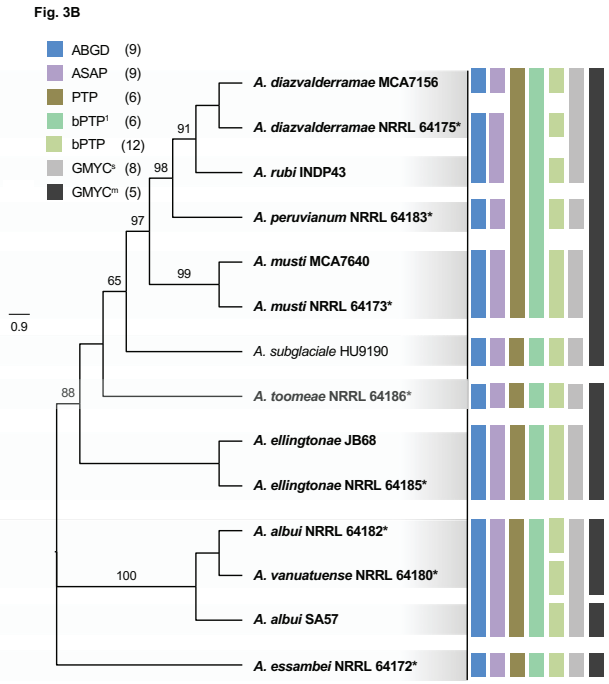

Fig. 3. Phylogenetic trees inferred by maximum parsimony (MP) analyses, trees showing species detection by different recognition criteria. Single locus analyses of all sequences used in the concatenated analyses of: **A.** mtLSU sequences of 16 *Aureobasidium* isolates, and **B.** mtSSU sequences of 14 isolates. The bootstrap percentages of the MP ≥ 70 % are presented at the nodes. Scale bar = the number of nucleotide substitutions per site. The tree is midpoint rooted. Sequences from ex-types are indicated with an asterisk (*). Bold names = new species, combinations, or names from this study. Colored vertical blocks represent the species detected by: blue = Automatic Barcode Gap Delimitation (ABGD); lavender = Assemble Species by Automatic Partitioning (ASAP); khaki = Poisson Tree Processes (PTP); green = Bayesian PTP maximum likelihood (bPTP1); yellow-green = Bayesian PTP (bPTP); grey = General Mixed Yule Coalescent by single threshold (GMYC^s); black = General Mixed Yule Coalescent by multiple threshold (GMYC^m). Numbers in parentheses in key refer to total number of species delimited by that method.

as a species, *A. iranianum, A. peruvianum, A. faidherbiae,* and *A. welwitschiae* as conspecific, and finally from *A. albui* to *A. essambei* as a single species (Fig. 2A). GMYC^{s} and GMYC^{m} delimited the same species in the 28S phylogeny as observed for PTP except that GMYC^{m} separated the group from *A. pullulans* to *A. toomeae* into three species and also separated *A. essambei* from *A. microtermitis* (Fig. 2B). Both models also grouped *A. albui, A. castaneae, A. thailandense,* and *A. vanuatuense* as conspecific. In the mtLSU, GMYC^{s} grouped all sequences from *A. melanogenum* to *A. rubi* as a single species and from *A. vanuatuense* to *A. essambei* as another species. While GMYC^{m} grouped sequences from *A. melanogenum* to *A. subglaciale* as conspecific, and *A. vanuatuense* and one sequence of *A. albui* as a species (Fig. 3A), GMYC^{s} grouped *A. diazvalderramae* and *A. rubi* as conspecific and *A. vanuatuense* and one sequence of *A. albui* as a species in mtSSU. In the same gene tree, GMYC^{m} delimited *A. diazvalderramae*, *A. rubi*, *A. peruvianum*, *A.*

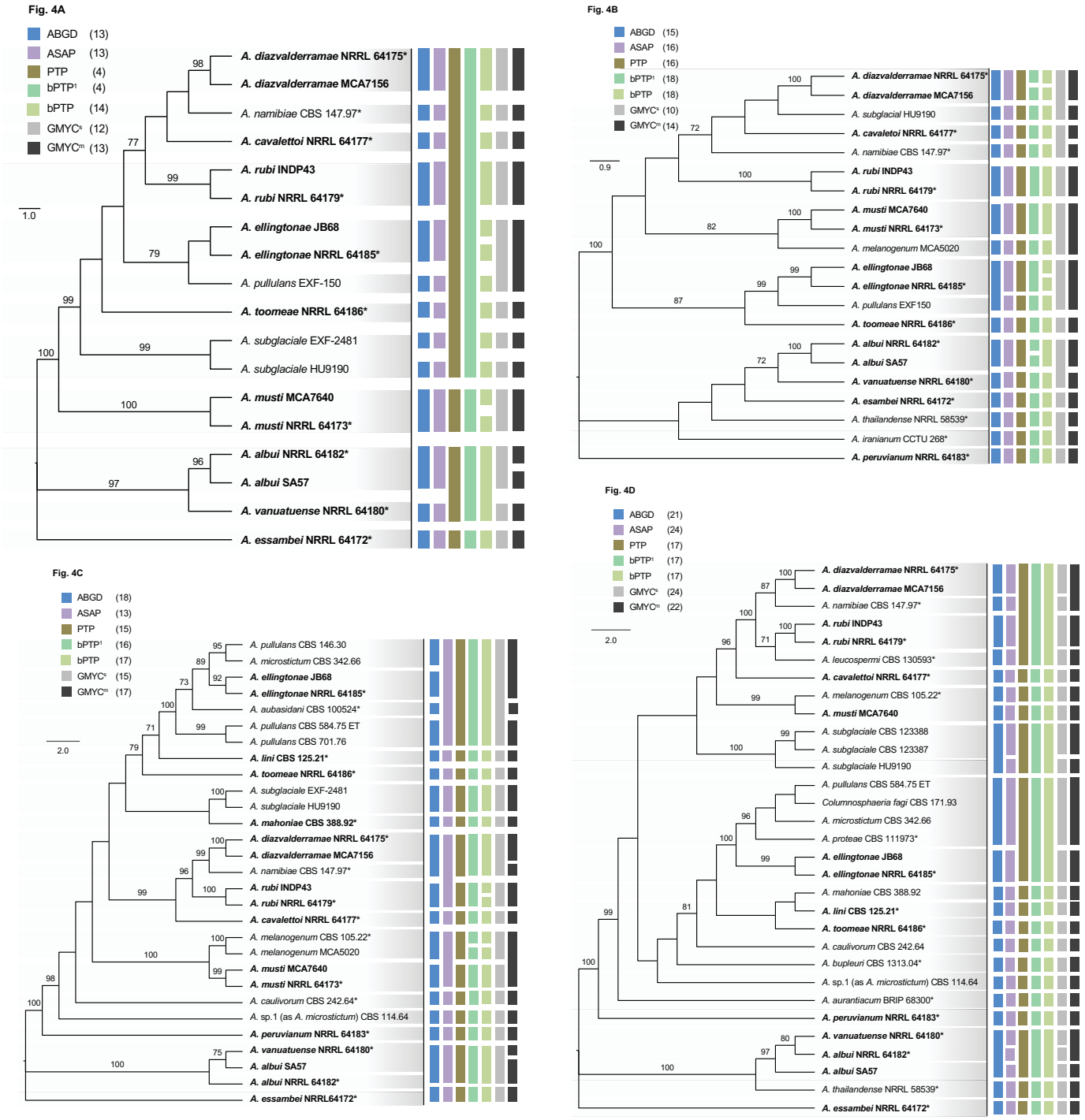

Fig. 4. Phylogenetic trees inferred by maximum parsimony (MP) analyses, trees showing species detection by different recognition criteria. Single locus analyses of all sequences used in the concatenated analyses of: **A.** *BTUB* sequences of 18 *Aureobasidium* isolates. **B.** *EF1a* sequences of 21 isolates. **C.** *ELO2* sequences of 29 isolates. **D.** *RPB2* sequences of 31 isolates. The bootstrap percentages of the MP ≥ 70 % are presented at the nodes. Scale bar = the number of nucleotide substitutions per site. The tree is midpoint rooted. Sequences from ex-types are indicated with an asterisk (*). Bold names = new species, combinations, or names from this study. Colored vertical blocks represent the species detected by: blue = Automatic Barcode Gap Delimitation (ABGD); lavender = Assemble Species by Automatic Partitioning (ASAP); khaki = Poisson Tree Processes (PTP); green = Bayesian PTP maximum likelihood (bPTP1); yellow-green = Bayesian PTP (bPTP); grey = General Mixed Yule Coalescent by single threshold (GMYCs); black = General Mixed Yule Coalescent by multiple threshold (GMYCm). Numbers in parentheses in key refer to total number of species delimited by that method.

Fig. 5. Phylogenetic trees inferred by maximum parsimony (MP) analyses trees showing species detection by different recognition criteria. Multilocus analyses of: **A.** 8-LDS (ITS, 28S, mtLSU, mtSSU, *BTUB*, *EF1a*, *ELO2*, and *RPB2*) of *Aureobasidium* sequences. **B.** 6-LDS (ITS, mtSSU, *BTUB*, *EF1a*, *ELO2*, and *RPB2*) of *Aureobasidium pullulans* PullG complex. The bootstrap percentages of the MP ≥ 70 % are presented at the nodes. Scale bar = the number of nucleotide substitutions per site. The tree is midpoint rooted. Sequences from ex-types are indicated with an asterisk (*). Bold names = new species, combinations, or names from this study. The red star in 5A indicates the node containing PullG, the *A. pullulans* species complex. Colored vertical blocks represent the species detected by: blue = Automatic Barcode Gap Delimitation (ABGD); lavender = Assemble Species by Automatic Partitioning (ASAP); khaki = Poisson Tree Processes (PTP); green = Bayesian PTP maximum likelihood (bPTP¹); yellow-green = Bayesian PTP (bPTP); grey = General Mixed Yule Coalescent by single threshold (GMYCˢ); black = General Mixed Yule Coalescent by multiple threshold (GMYCᵐ). Numbers in parentheses in key refer to total number of species delimited by that method.

musti, and *A. subglaciale* as conspecific, *A. toomeae* and *A. ellingtonae* as one species and *A. vanuatuense* and one sequence of *A. albui* as a species (Fig. 3B).

GMYC delimited species better in the four protein-coding genes and MLT datasets. In *BTUB*, *EF1a*, and *ELO2* datasets, *A. ellingtonae* and the ApC were grouped as conspecific (Fig. 4A–C) while these were separated into different species in the *RPB2* dataset (Fig. 4D). In the *BTUB* dataset, GMYC^{s} and GMYC^{m} delimited similar species except that the latter separated *A. albui* into two individual species (Fig. 4A). GMYC^{s} and GMYC^{m} also delineated similar species in the *EF1a* dataset except that the former grouped *A. diazvalderramae* and *A. subglaciale* as conspecific as well as *A. cavalettoi* and *A. namibiae*. Both models also delineated *A. melanogenum* and *A. musti* as a single species (Fig. 4B). Apart from *A. toomeae* and *A. lini*, *A. ellingtonae* was delimited as part of the ApC by GMYC^{s} in the *ELO2* phylogeny. *Aureobasidium diazvalderramae* and *A. namibiae* were also grouped as a species while *A. albui* and *A. vanuatuense* were delimited as one species by GMYC^{s}. In contrast, GMYC^{m} delineated *A. aubasidani* as a separate species from the ApC, *A. diazvalderramae* and *A. namibiae* as separate species, grouped *A. melanogenum* and *A. musti* as a species and separated *A. albui* and *A. vanuatuense* (Fig. 4C). In the *RPB2* dataset, both GMYC^{s} and GMYC^{m} delimited similar species except that the latter grouped *A. diazvalderramae* and *A. namibiae* as a single species and *A. vanuatuense* and one sequence of *A. albui* as conspecific. GMYC^{s} delimited these groups as separate species. However, both models separated *A. subglaciale* (HU9190) from the other two *A. subglaciale* sequences (Fig. 4D).

In the concatenated dataset, both the GMYC^{s} and GMYC^{m} models delineated the same species from *A. essambei* to *A. welwitschiae, Aureobasidium* sp.1 to *A. lini*, *A. bupleuri*, *A. aerium* to *A. uvarum*, *A. motuoense*, *A. musti*, and *A. intercalariosporum* to *A. rubi* (Fig. 5A). However, GMYC^{s} recovered *A. cavalettoi* and *A. insectorum* as conspecific and the GMYC^{m} recovered *A. aurantiacum* and a second undescribed species (*Aureobasidium* sp.2, represented by sequences from two isolates originally identified as *A. zeae*) as conspecifics. GMYC^{s} also grouped *A. ellingtonae* as part of the ApC (indicated by the red star), but GMYC^{m} delineated *A. ellingtonae* as conspecific with *A. aubasidani* and *A. pullulans* (CBS 109810). While GMYC^{s} grouped *A. melanogenum* (CBS 105.22 and MCA5020), and *A. acericola* as one species, GMYC^{m} separated the latter from

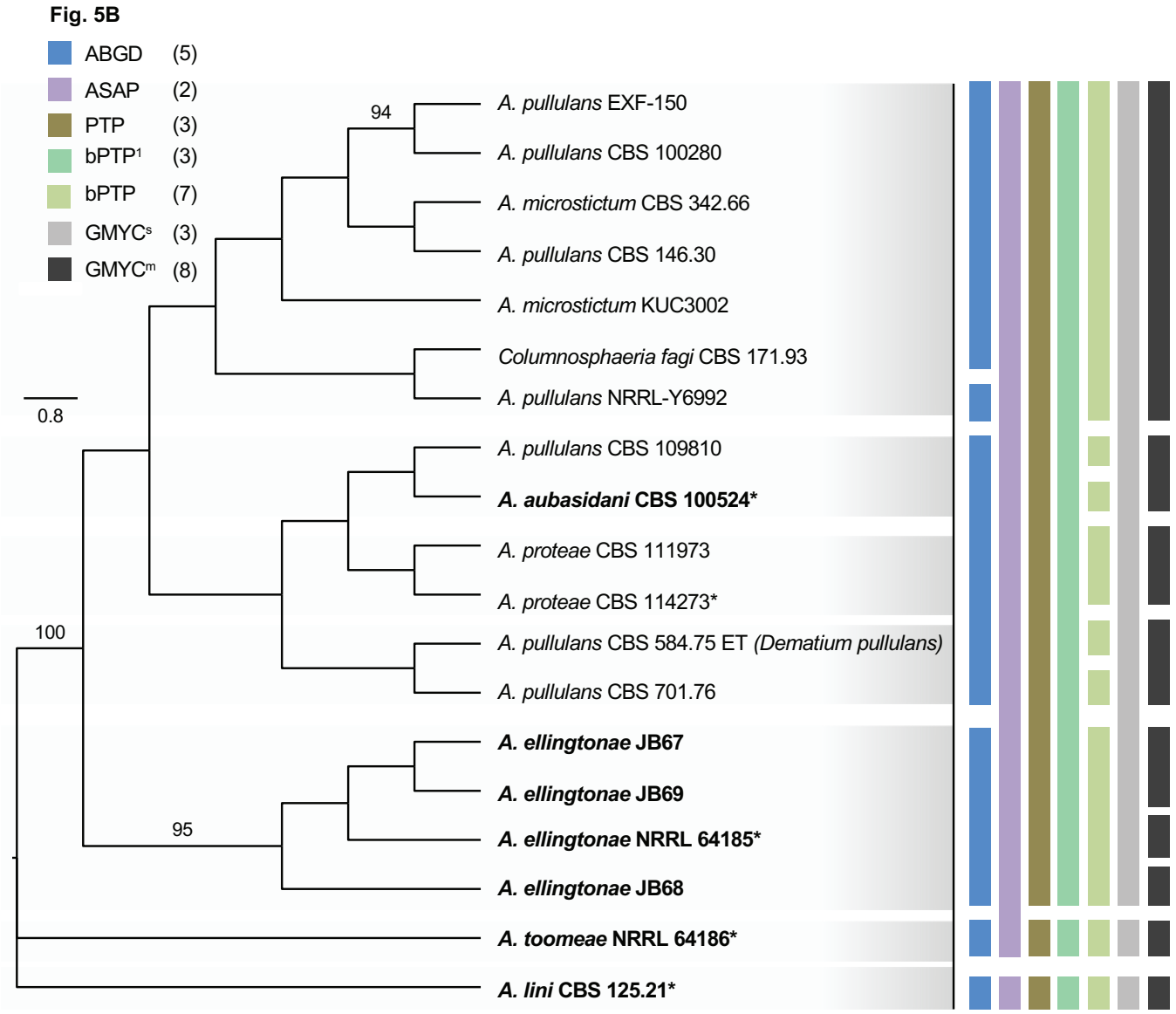

Fig. 5. (Continued).

the other two sequences (Fig. 5A). GMYC^{s} grouped all four sequences representing *A. subglaciale* as one species but GMYC^{m} delineated *A. subglaciale* isolates CBS 123388 and HU9190 as separate from EXF-2481 and CBS 123387. Similarly, GMYC^{s} grouped the two sequences representing *A. iranianum* as a species while GMYC^{m} separated them as two individual species. In the *A. pullulans* complex dataset, GMYC^{s} found three species including *A. lini*, *A. toomeae,* and the rest of the sequences as a third species (Fig. 5B). However, GMYC^{m} recovered eight species including *A. aubasidani*, *A. ellingtonae* (as three separate species), *A. lini, A. pullulans* s. s. (CBS 584.75 and CBS 701.76), *A. toomeae*, and *A. microstictum*, *A. proteae* and the sequences from *Columnosphaeria fagi* as one species.

Altogether, the different in silico methods for species delimitation estimated the total number of *Aurobasidium* species with available sequence data in the 8-LDS to be between eight and 49 (Table 6, Fig. 5A, B); estimates for PullG which includes the ApC ranged from 1–18 (Table 6). GCPSR resolved the number of *Aurobasidium* species with sequence data at 43 (Fig. 1A) with seven species resolved in PullG (Fig. 1B), and was the species delimitation method that most closely reflects prior studies on the genus, and, as it evaluates evidence for potential recombination appears to be a better predictor of biological species. Applying the GCPSR, 43 *Aureobasidium* species are resolved, of which nine are described herein as new, and two are undescribed and denoted as *Aureobasidium* sp.1 (sequences of CBS 114.64, identified as *A. microstictum*, van Nieuwenhuijzen *et al*. 2016) and *Aureobasidium* sp.2 (sequences from two strains identified as *A. zeae*, Sun & Xue 2014). We were able to resolve five species (*A. aubasidani*, *A. ellingtonae*,

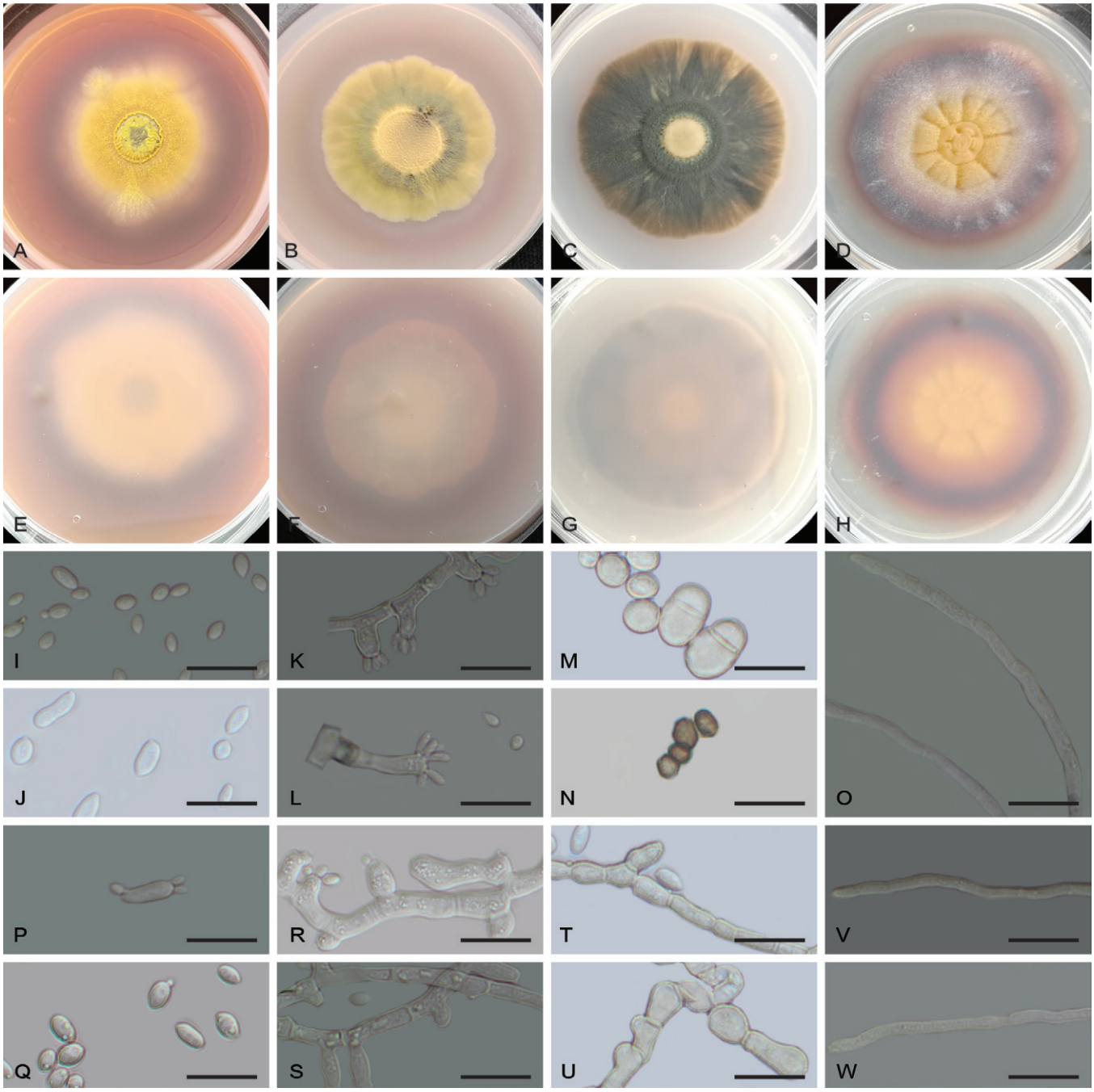

Fig. 6. Morphological characters of *Aureobasidium albui* (ex-holotype, NRRL 64182). **A–D.** Colonies at 7 dpi on MEA, MEA at 30 °C, PDA, and M40Y, respectively. **E–H.** Colony reverse on MEA, MEA at 30 °C, PDA, and M40Y, respectively. **I, J, P, Q.** Primary and secondary conidia. **K, L, R, S.** Conidiogenous hyphae. **M, N, T, U.** Chlamydospores. **O, V, W.** Vegetative hyphae. Scale bars = 20 µm.

A. microstictum, *A. proteae*, and *A. pullulans* s. s.) in the *A. pullulans* complex, although support of *A. microstictum* is still lacking in some analyses.

TAXONOMY

Aureobasidium Viala & G. Boyer, *Rev. Gén. Bot*. **3**: 371. 1891.
Synonym: *Kabatiella* Bubák, *Hedwigia* **46**: 297. 1907.
Additional synonyms in MycoBank

Description: Hermanides-Nijhof (1977).

Type species: *Aureobasidium vitis* Viala & G. Boyer

Notes: *Kabatiella* (based on *K. microsticta* Bubák, from living leaves of *Convallaria majalis*: Czech Republic; Bubák & Kabát 1907), has traditionally been seen as a genus of plant pathogens, in contrast to *Aureobasidium*, which was seen as a morphologically similar genus containing epiphytes and saprobes. However, Hermanides-Nijhof (1977) regarded the two genera as synonymous, and as shown in this study, various species of *Aureobasidium* are plant pathogenic. Furthermore, a reference strain of *K. microsticta* (CBS 342.66, specimen CBS H-13724, from a dying leaf of *Convallaria majalis*, Germany, Jul. 1966, coll. *W. Gams*, isol. *J.A. von Arx*), clusters within the genus *Aureobasidium*, thus providing further support for this synonymy.

Aureobasidium albui Jumbam & Aime, ***sp. nov.*** MycoBank MB 848255. Fig. 6.

Etymology: Named for Sebastian Albu who isolated the type.

Diagnosis: Morphologically similar to *Aureobasidium vanuatuense* but differing in the robust growth at 30 °C (vs limited yeasty growth in *A. vanuatuense*). Additionally, *A. vanuatuense* growth is almost entirely melanised on PDA, vs the limited melanisation of *A. vanuatuense* on this medium (Figs 6, 7, 16).

Typus: **USA**, Louisiana, East Baton Rouge Parish, Baton Rouge, Louisiana State University campus, on phylloplane of unidentified leaf, 27 Oct. 2010, *S. Albu*, SA46 (**holotype** PUL F29026 preserved as a dried inert culture), ex-type culture SA46 (PUL culture collection) = NRRL 64182 = CBS 149008.

Barcodes: ITS = OK376936; 28S = OK353650; mtLSU = OK376709; mtSSU = OL504989; *ELO2* = OK485106; *EF1a* = OK413253; *RPB2* = OK485130; *BTUB* = OK485072.

Culture characteristics (Fig. 6A–H): Colonies reaching diameters of 20, 20, and 21 mm on MEA, PDA, and M40Y

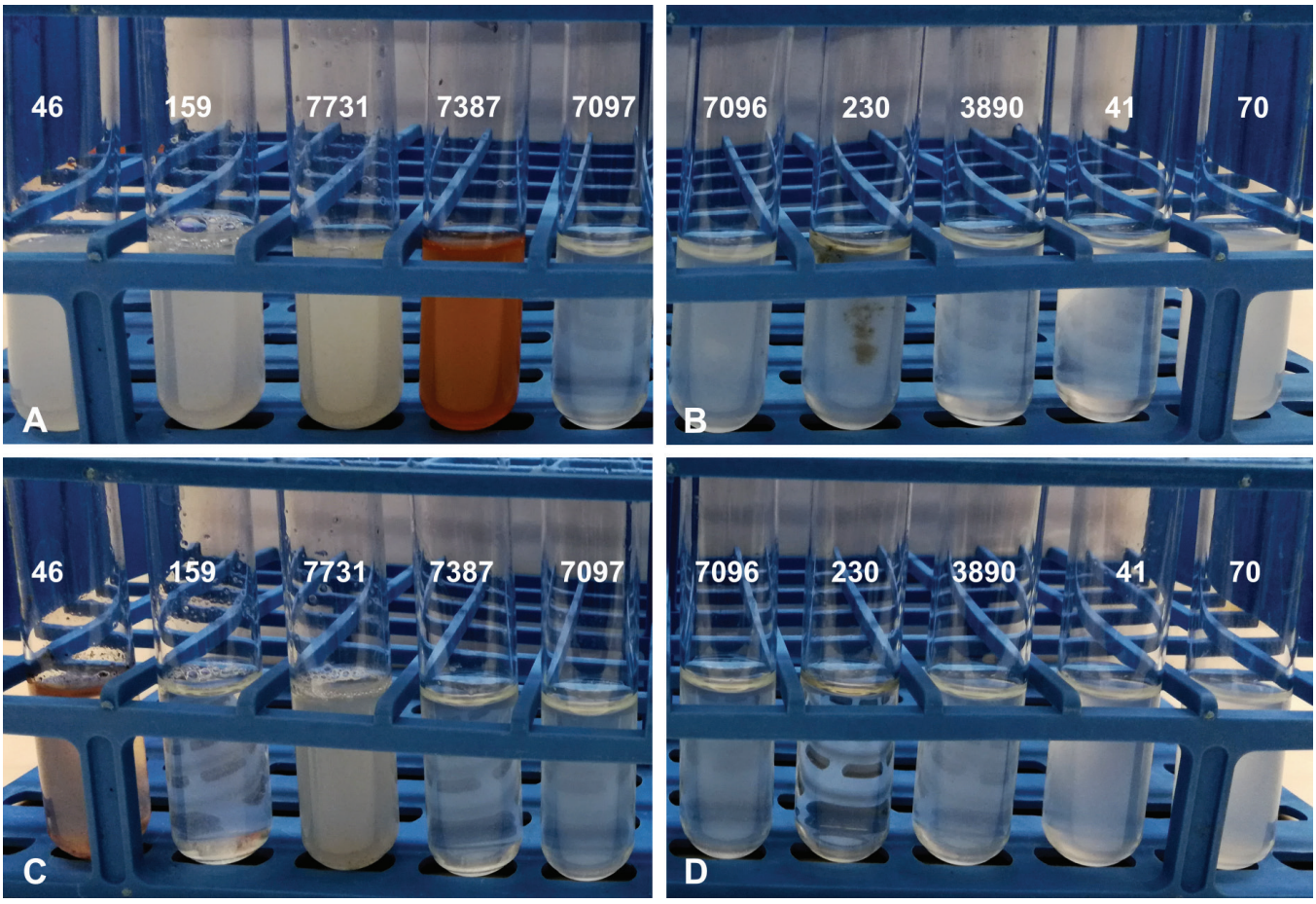

Fig. 7. Assimilation 10 *Aureobasidium* isolates. **A, B.** Assimilation of D-quinic acid, from left to right: *A. albui* (SA46, ex-type), *A. toomeae* (MT159, ex-type), *A. essambei* (MCA7731, ex-type), *A. vanuatuense* (MCA7387, ex-type), *A. peruvianum* (MCA7097, ex-type), *A. diazvalderramae* (MCA7096, ex-type), *A. mustum* (TAR230), *A. rubi* (MCA3890, ex-type), *A. cavalettoi* (INDP41, ex-type), and *A. ellingtonae* (JB70, ex-type). **C, D.** Assimilation of L-sorbose, from left to right: *A. albui* (SA46, ex-type), *A. toomeae* (MT159, ex-type), *A. essambei* (MCA7731, ex-type), *A. vanuatuense* (MCA7387, ex-type), *A. peruvianum* (MCA7097, ex-type), *A. diazvalderramae* (MCA7096, ex-type), *A. mustum* (TAR230), *A. rubi* (MCA3890, ex-type), *A. cavalettoi* (INDP41, ex-type), and *A. ellingtonae* (JB70, ex-type).

respectively at 25 °C, 7 dpi (Table 3). On MEA, melanisation beginning at 3 dpi, greenish brown (oac744–745) at first with a thick yellow (oac856) margin. On PDA, growth is pale yellow (oac851) and yeast-like in the centre, becoming brownish (oac681) at the margins. On M40Y, centre pale yellow (oac851), then pink to black to brick red toward margin and farinaceous. On PDA, colonies pale pink and dull. Hyphae are produced in all media. Similar on the reverse.

Microscopic characteristics: *Vegetative hyphae* smooth, thin walled, 6.1–16.0 µm wide, septate (Fig. 6O, V, W). *Conidiogenous hyphae* hyaline, synchronously producing abundant conidia both terminally and laterally (Fig. 6K, L, R, S). *Conidia* hyaline, 5.4–14.0 × 2.6–6.8 µm, smooth walled, ovoid to ellipsoidal or occasionally elongate, cells multiplying by polar budding (Fig. 6I, J, P, Q). *Chlamydospores* ovoid (1-celled) to subglobose, pale brown, produced as intercalary arthrospores (oac730–731), 1–2-celled, rarely 3-celled, constricted at the septum (Fig. 6M, N); 1-celled chlamydospores measuring 5.4–19.5 × 4.3–18.0 µm, 2-celled chlamydospores 11.8–15.7 × 5.8–16.1 µm (Fig. 6T, U).

Assimilation profiles: Carbon compounds strongly assimilated were D-glucose, L-arabinose, sodium succinate dibasic hexahydrate, and D-quinic acid (Table 5). Assimilation of galactitol and gluconic acid sodium salt was moderate while that of L-sorbose, gluconic acid lactone, and D-mannitol was weak. A pinkish (oac578) pigmentation was produced while assimilating L-sorbose. At 21 dpi a light pink pigmentation is produced in D-mannitol, light orange in gluconic acid lactone and purple in erythritol. Fermentation of sucrose and melibiose was weak (Table 5). *A. albui* strongly utilizes

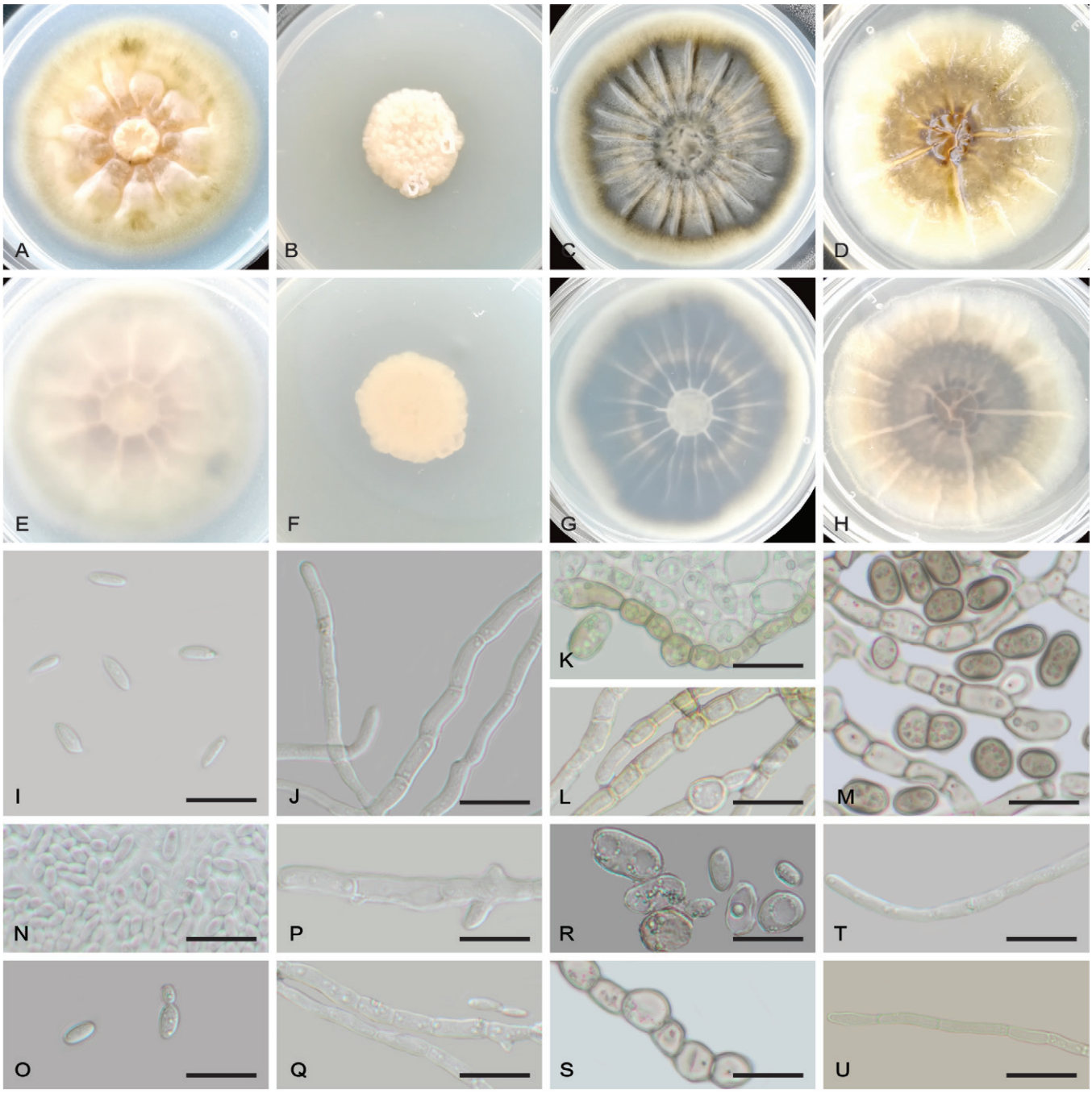

Fig. 8. Morphological characters of *Aureobasidium cavalettoi* (ex-holotype, NRRL 64177). **A–D.** Colonies at 7 dpi on MEA, MEA at 30 °C, PDA, and M40Y, respectively. **E–H.** Colony reverse on MEA, MEA at 30 °C, PDA, and M40Y, respectively. **I, N, O.** Primary and secondary conidia. **J, P, Q.** Conidiogenous hyphae. **K, L, R, S.** Chlamydospores. **M, T, U.** Vegetative hyphae. Scale bars = 20 µm.

potassium nitrate, potassium nitrite, ethylamine hydrochloric acid, L-lysine, and D-glucosamine, and weakly assimilates cadaverine hydrochloric acid, as the sole source of nitrogen (Table 5).

Growth temperature and salt tolerance (Tables 3, 4): Growth positive between 4–30 °C, with optimal growth at 28 °C. Growth positive on 10 % NaCl but not 15 %. At 14 dpi, growth on osmotic media very slow, yellow (oac814) with pale brown (oac797) melanised regions; media is not discoloured.

Known distribution: Known from various plant phylloplanes in East Baton Rouge, Louisiana.

Additional materials examined: **USA**, Louisiana, East Baton Rouge Parish, Baton Rouge, Louisiana State University campus, on phylloplane of *Nephrolepis exaltata*, 28 Oct. 2010, *S. Albu*, SA57 (dried voucher PUL F29043; culture PUL SA57); on leaf phylloplane of *Cyrtomium falcatum*, 16 Oct. 2011, *S. Albu*, SA688 (culture PUL SA688); on leaf phylloplane of *Cyrtomium falcatum*, 16 Oct. 2011, *S. Albu*, SA689 (culture PUL SA689).

Aureobasidium aubasidani (Yurlova) Jumbam & Aime, ***comb. nov.*** MycoBank MB 848279.
Basionym: *Aureobasidium pullulans* var. *aubasidani* Yurlova, *Antonie van Leeuwenhoek* **72**: 146. 1997. MB 442903.

Typus: **Russia**, Leningrad region, from birch sap, 1959, *J.M. Voznjakovskaja* (**holotype** VKPM F-448; ex-type culture CBS 100524).

Description: See Yurlova & de Hoog (1997).

Barcodes: ITS = FJ150905; 28S = FJ150952; *ELO2* = FJ039839.

Notes: *Aureobasidium pullulans* var. *aubasidani* CBS 100524 and one other sequence (CBS 109810, as *A. pullulans* var. *pullulans*) resolve as sister to the ex-type of *A. ellingtonae* and *A. proteae* (Fig. 1A, B). The branch carrying *A. pullulans* var. *aubasidani* is well supported (100/96) in the 8-LDS (Fig. 1A) and in the 6-LDS (73/98) of PullG (Fig. 1B). ITS sequences of *A. aubasidani* differed from the ex-type of *A. ellingtonae* in 1/486 bp but not from the ex-types of *A. proteae* and *A. pullulans*. The 28S sequence differed from *A. proteae* and *A. ellingtonae* in 1/566 and 1/489 bp, respectively. Sequences of the *ELO2,* shown to have better resolving power in *Aureobasidium* (Zalar *et al.* 2008), differed from *A. pullulans* at 12/699 base pairs and from *A. ellingtonae* at 10/692 bp. These and the physiological differences, including the production of aubasidan-like EPS, rather than the pullulan-type of EPS produced by *A. pullulans* (Yurlova & Hoog 1997), differentiate this species.

Aureobasidium cavalettoi Jumbam & Aime, ***sp. nov.*** MycoBank MB 848256. Fig. 8.

Etymology: Named for John Cavaletto, laboratory coordinator for the Department of Botany and Plant Pathology, Purdue University, who isolated the type.

Diagnosis: Closely related to *A. insectorum*, differing in the slower growth rate (23 mm vs 34 mm for *A. insectorum*, on PDA, 7 dpi at 25 °C), and larger conidia (6.5–22.6 × 3.0–7.3 µm vs 4.2–7.4 × 1.7–3.5 µm).

Typus: **USA**, Indiana, Tippecanoe, West Lafayette, Purdue University campus, on phylloplane of *Salix* sp., 12 Jan. 2015, *J. Cavaletto*, INDP41 (**holotype** PUL F29023 preserved as a dried inert culture), ex-type culture INDP41 (PUL culture collection) = NRRL 64177 = CBS 148906.

Barcodes: ITS = OK376877; 28S = OK353610; mtLSU = OK376681; mtSSU = NA; *ELO2* = OK485078; *EF1a* = OK413225; *RPB2* = OK485112; *BTUB* = OK485046.

Culture characteristics (Fig. 8A–H): Colonies reaching a diameter of 23 mm on each of MEA, PDA, and M40Y at 25 °C, 7 dpi (Table 3). On MEA, pink (oac676) with darker areas in the centre, glistening; margins become greenish (oac833) at 14 dpi. On PDA, colonies are white (oac909) developing dark portions at the centre, dull and unchanging at 14 dpi. On M40Y, colonies with greenish (oac832) centre, outer 1/2 cream, glistening, no changes observed at 14 dpi. On MEA, PDA, and M40Y, hyphae formed at margins and colony surface ridged with lighter radial bands, giving the colony a starburst-like appearance; colony reverse the same but paler. Aerial hyphae not produced on any of the media.

Microscopic characteristics: *Vegetative hyphae* smooth, thin walled, 3.6–5.7 µm wide, septate (Fig. 8T, U). *Conidiogenous hyphae* undifferentiated, hyaline, synchronously producing conidia both terminally and laterally (Fig. 8J, P, Q). *Conidia* hyaline, 4–15.6 × 2.5–6.7 µm, smooth, mostly ellipsoidal; cells multiplying by polar and bipolar budding (Fig. 8I, N, O). *Chlamydospores* frequent, formed as intercalary arthrospores, ellipsoidal to subglobose, hyaline becoming dark brown at maturity 1–3-celled (Fig. 8K–M, R, S); 1-celled chlamydospores measuring 8–17.6 × 4.3–13.4 µm (Fig. 8M, R), 2-celled chlamydospores 13.1–19.8 × 7.8–13.6 µm (Fig. 8M), 3-celled chlamydospores rare, measuring 21.7–28.3 × 5.1–6.6 µm.

Assimilation profiles: Gluconic acid sodium salt (strongly) and D-glucose (moderately) are assimilated; assimilation of L-sorbose, L-arabinose, D-salicin, ribitol, D-mannitol, and sodium succinate dibasic hexahydrate was weak (Table 5). D-quinic acid is not assimilated and no pigmentation observed while assimilating the above carbon compounds. Fermentation was negative for all tested carbon compounds (Table 5). Potassium nitrate and L-lysine hydrochloric acid are strongly assimilated as sole nitrogen sources. The assimilation of cadaverine hydrochloric acid, D-glucosamine, and D-tryptophan was weak (Table 5).

Growth temperature and salt tolerance (Tables 3, 4): Growth positive between 4–30 °C, with optimal growth at 28 °C. Growth positive on 15 % NaCl but not 20 %; colonies pale pink (oac794) with net-like radiations from reverse view, no hyphae or melanisation, in osmotic media at 14 dpi.

Known distribution: United States, isolated from weeping willow leaves on the campus of Purdue University in three successive years. Three publicly available sequences (GenBank KT693715, KT693676, and KT693690, van Nieuwenhuizen *et al.* 2016) appear conspecific; if so this would extending the known range to South Africa and Norway.

Additional materials examined: **USA**, Indiana, Tippecanoe, West Lafayette, Purdue University campus, on phylloplane of *Salix* sp., Spring 2014, *J. Cavaletto*, INDP001 (PUL culture collection); ibid., Spring 2016, *J. Cavaletto*, INDP0086 (PUL culture collection).

Aureobasidium diazvalderramae Jumbam & Aime, ***sp. nov.*** MycoBank MB 848257. Fig. 9.

Etymology: Named for Jorge R. Díaz-Valderrama who isolated the ex-type strain.

Diagnosis: Similar to *A. namibiae* (Zalar *et al.* 2008), differing in having longer (4.1–18.2 µm vs 7–17 µm for *A. namibiae*) and slenderer (2.7–6.5 µm vs 3.5–7 µm) conidia and larger 1-celled chlamydospores (5.5–17.0 × 5.1–11.4 µm vs 8–13 × 5–9 µm).

Typus: **Peru**, Cajamarca Dept., San Ignacio Prov., Huarango District, Jaen Provence, Bellavista, Cielo Ramos Farm, -5.651782, -78.709666, 491 m a.s.l., isolated from air on 50 % glucose amended PDA, 28 Sep. 2016, *J.R. Díaz-Valderrama & M.C. Aime*, MCA7096 (**holotype** PUL F29022 preserved as a dried inert culture), ex-type culture MCA7096 (PUL culture collection) = NRRL 64175 = CBS 148905.

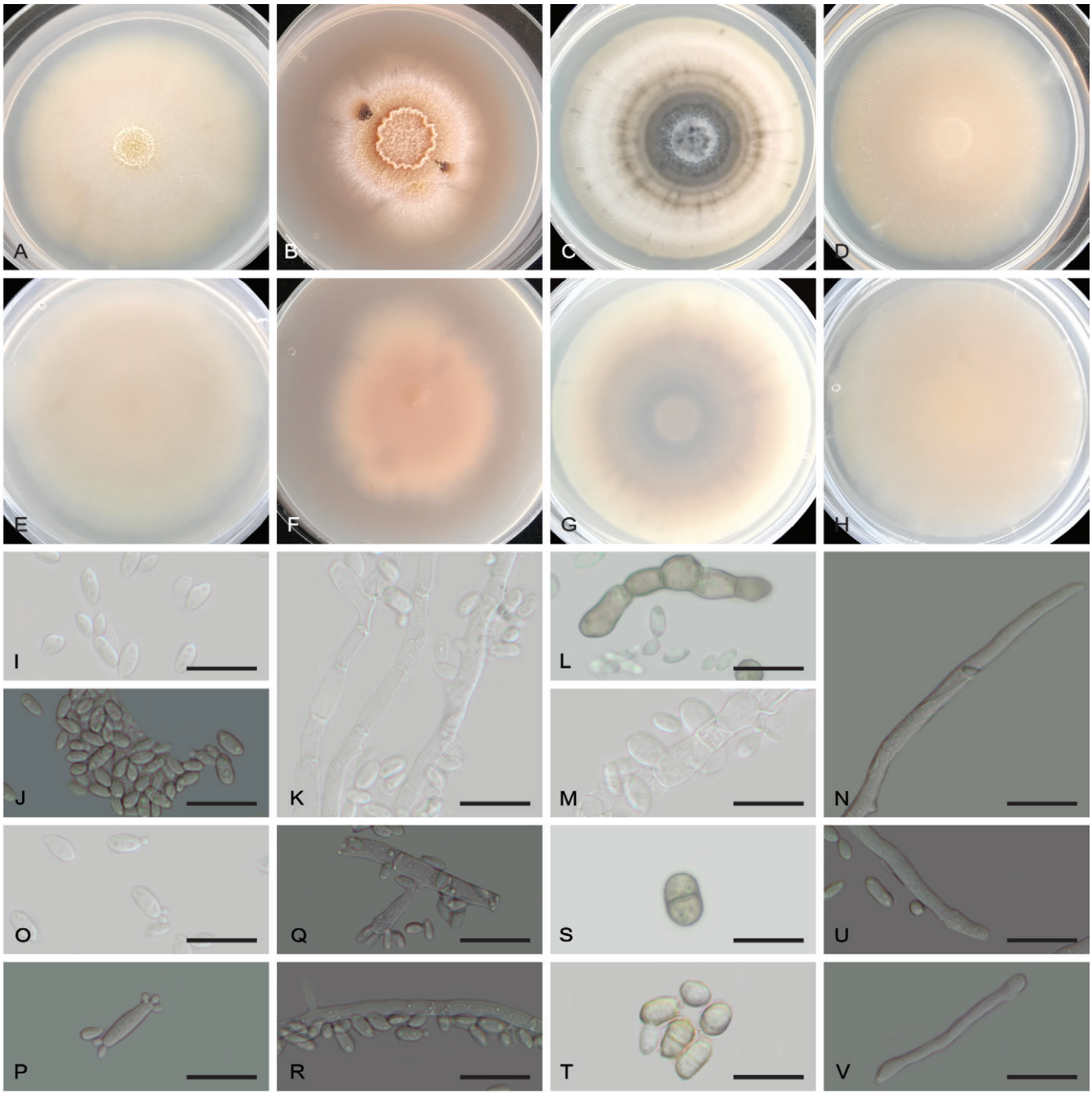

Fig. 9. Morphological characters of *Aureobasidium diazvalderramae* (ex-holotype, NRRL 64175). **A–D.** Colonies at 7 dpi on MEA, MEA at 30 °C, PDA, and M40Y, respectively. **E–H.** Colony reverse on MEA, MEA at 30 °C, PDA, and M40Y, respectively. **I, J, O, P.** Primary and secondary conidia. **K, Q, R.** Conidiogenous hyphae. **L, M, S, T.** Chlamydospores. **N, U, V.** Vegetative hyphae. Scale bars = 20 µm.

Barcodes: ITS = OK376904; 28S = OK353629; mtLSU = OK376694; mtSSU = OL504986; *ELO2* = OK485092; *EF1a* = OK413237; *RPB2* = OK485121; *BTUB* = OK485059.

Culture characteristics (Fig. 9A–H): Colonies attained a diameter of 26, 28, and 27 mm on MEA, PDA, and M40Y, respectively, at 25 °C, 7 dpi (Table 3). On MEA and M40Y there was no melaninization, colony surface dull, pink (oac676) on MEA and cream on M40Y. Colonies on PDA melanised, white (oac909) in centre, then forming a dark brown ring surrounded by thin bands of cream and brown, outer 1/2 to margin white with scattered brownish spots, glistening. Hyphae formed at margins in all media; colonies in reverse similar to the top. Aerial hyphae not observed on any tested media.

Microscopic characteristics: *Vegetative hyphae* smooth, thin walled, 2.3–11.4 µm wide, septate (Fig. 9N, U, V). *Conidiogenous hyphae* undifferentiated, hyaline, synchronously producing conidia mostly terminally (Fig. 9K, Q, R). *Conidia* hyaline, 4.1–18.2 × 2.7–6.5 µm, smooth, mostly ellipsoidal, cells multiplying by polar and bipolar budding (Fig. 9I, J, O, P). *Chlamydospores* frequently formed, produced as intercalary arthrospores, 1–2-celled, ellipsoidal to subglobose, light brown at maturity (Fig. 9L, M, S, T); 1-celled chlamydospores 5.5–17.0 × 5.2–10.1 µm (Fig. 9M, T), 2-celled chlamydospores 10.6–21.8 × 5.1–12 µm (Fig. 9S), 3-celled chlamydospores rare.

Assimilation profiles: D-glucose, L-arabinose, and sodium succinate dibasic hexahydrate were moderately assimilated

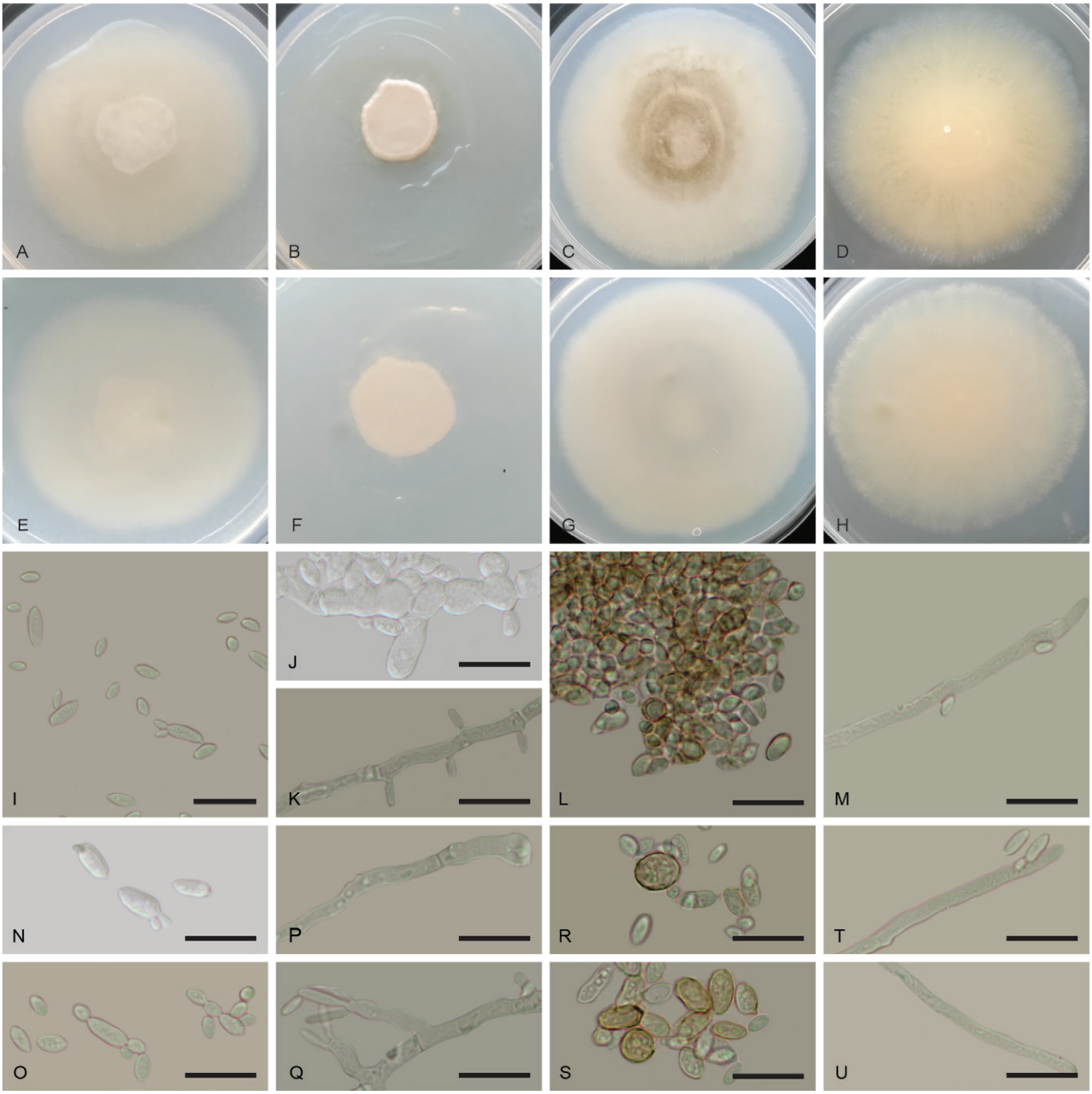

Fig. 10. Morphological characters of *Aureobasidium ellingtonae* (ex-holotype, NRRL 64185). **A–D.** Colonies at 7 dpi on MEA, MEA at 30 °C, PDA, and M40Y, respectively. **E–H.** Colony reverse on MEA, MEA at 30 °C, PDA, and M40Y, respectively. **I, N, O.** Primary and secondary conidia. **J, K, P, Q.** Conidiogenous hyphae**. L, R, S.** Chlamydospores. **M, T, U.** Vegetative hyphae. Scale bars = 20 µm.

as the sole carbon source, while α-rhamnose monohydrate, D-salicin, erythritol, D-mannitol, myo-inositol, and D-quinic acid were weakly assimilated (Table 5). No pigmentation observed during the assimilation of the above carbon compounds. Fermentation was negative for all tested carbon compounds (Table 5). Potassium nitrate, ethylamine hydrochloric acid, L-lysine hydrochloric acid, and cadaverine hydrochloric acid are assimilated as sole nitrogen sources (Table 5).

Growth temperature and salt tolerance (Tables 3, 4): Growth positive between 4–30 °C, with optimal growth at 28 °C. Growth positive on 10 % NaCl but not 15 %; growth on osmotic media white (oac909), dull, not producing melanin or hyphae at 14 dpi.

Known distribution: Peru, isolated from air in Cajamarca Department.

Additional material examined: **Peru**, Cajamarca Dept., Cajamarca Prov., Cajamarca Dist., near El Pongo, -7.175009, -78.958154, 1153 m a.s.l., isolated from air on 50 % glucose amended PDA, 28 Sep. 2016, *J.R. Diaz-Valderrama & M.C. Aime*, MCA7156 (PUL F29041 dried voucher; PUL culture collection MCA7156).

Aureobasidium ellingtonae Jumbam, Zasada & Aime, ***sp. nov.*** MycoBank MB 848258. Fig. 10.

Etymology: Refers to *Globodera ellingtonae*, the potato cyst nematode species from which this species was isolated.

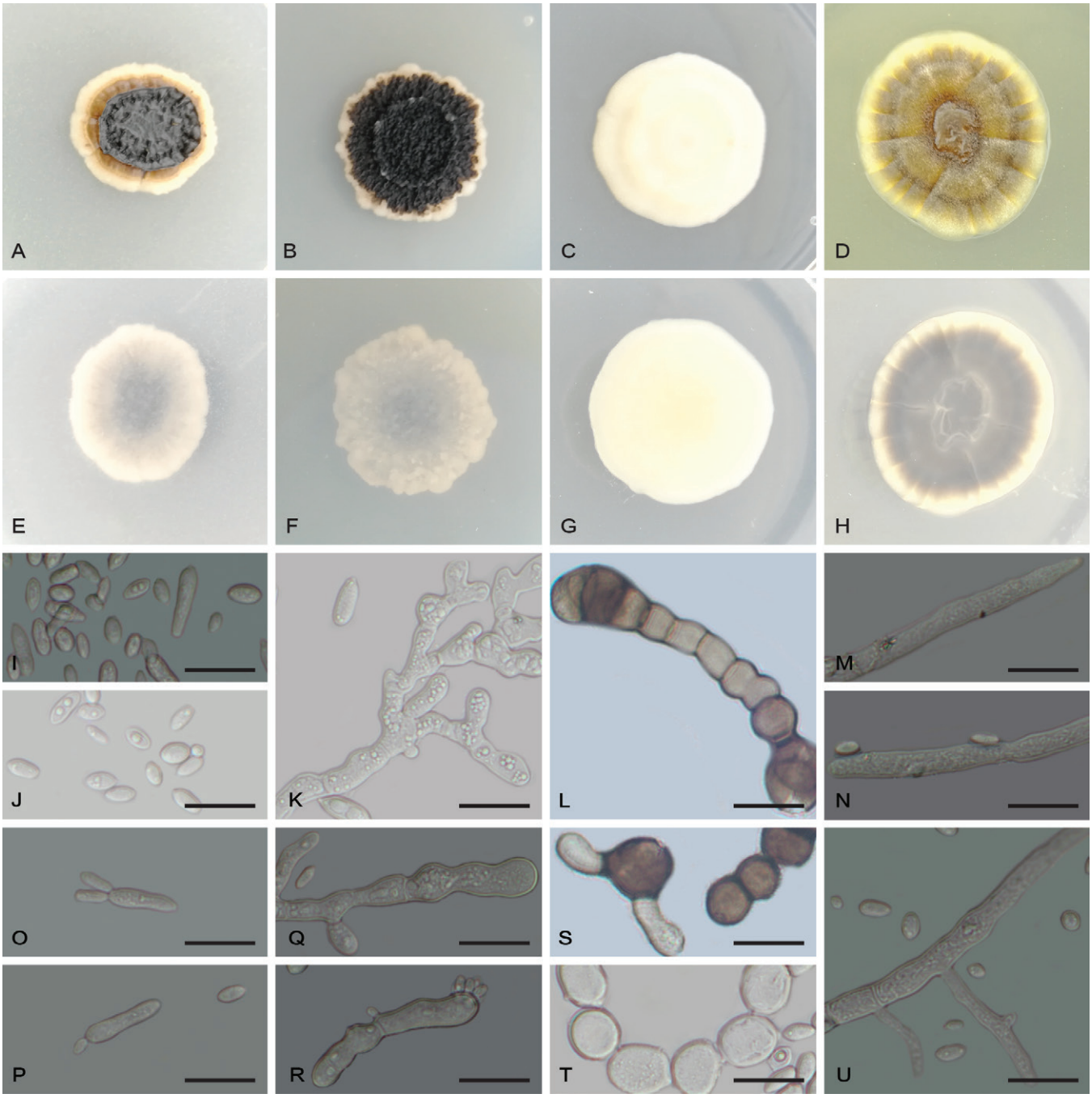

Fig. 11. Morphological characters of *Aureobasidium essambei* (ex-holotype, NRRL 64172). **A–D.** Colonies at 7 dpi on MEA, MEA at 30 °C, PDA, and M40Y, respectively. **E–H.** Colony reverse on MEA, MEA at 30 °C, PDA, and M40Y, respectively. **I, J, O, P.** Primary and secondary conidia. **K, Q, R.** Conidiogenous hyphae. **L, S, T.** Chlamydospores. **M, N, U.** Vegetative hyphae. Scale bars = 20 µm.

Diagnosis: Similar to *A. pullulans*, differing in shorter (4.4–14.6 µm vs 7.5–16 µm for *A. pullulans*) and narrower (2.4–5.4 µm vs 3.5–7 µm) conidia (Zalar *et al.* 2008) and the absence of two-celled chlamydospores.

Typus: **USA**, Oregon, Powell Butte, isolated from cysts of the potato cyst nematode (*Globodera ellingtonae*), Oct. 2018, coll.*I. Zasada,* isol.*B. Jumbam*, JB70 (**holotype** PUL F29029 preserved as a dried inert culture), ex-type culture JB70 (PUL culture collection) = NRRL 64185 = CBS 148908.

Barcodes: ITS = OK376885; 28S = OK353615; mtLSU = OK376685; mtSSU = OK360973; *ELO2* = OK485082; *EF1a* = OK413230; *RPB2* = OK485116; *BTUB* = OK485051.

Culture characteristics (Fig. 10A–H): Colonies reached diameters of 43, 32, and 37 mm on MEA, PDA, and M40Y, respectively, at 25 °C, 7 dpi (Table 3). Colonies pink (oac548/676), not melanised at 14 dpi on any of the three media, glistening, margins smooth, hyphae produced at margins. Colony reverse whitish with vein-like radiations from centre. Aerial hyphae observed on MEA.

Microscopic characteristics: *Vegetative hyphae* smooth, thin walled, 2–6 µm wide, septate (Fig. 10M, Y–U). *Conidiogenous hyphae* undifferentiated, hyaline, synchronously producing conidia both terminally and laterally (Fig. 10J, K, P, Q). *Conidia* hyaline, 4.4–14.6 × 2.4–5.4 µm, smooth, ovoid to ellipsoid, or rarely subfusiform, multiplying by polar and bipolar budding (Fig. 10I, N, O). *Chlamydospores* rarely formed, ellipsoidal to subglobose, hyaline, mostly 1-celled (Fig. 10L, R, S), measuring 6.9–16.6 × 4.4–9.8 µm.

Assimilation profiles: Carbon compound assimilation was moderate for D-glucose and weak for L-arabinose and gluconic acid sodium salt. No assimilation was observed for sodium succinate dibasic hexahydrate, D-quinic acid, L-sorbose, D-salicin, glycerol, erythritol, ribitol (adonitol), xylitol, D-mannitol, and gluconic acid lactone (Table 5). No pigmentation observed while assimilating these carbon compounds. Fermentation was negative for all the carbon compounds (Table 5). The following nitrogen compounds were strongly assimilated: potassium nitrite, ethylamine hydrochloric acid, and L-lysine hydrochloric acid. Potassium nitrate and cadaverine hydrochloric acid were moderately assimilated while the assimilation of D-glucosamine and D-tryptophan was weak (Table 5).

Growth temperature and salt tolerance (Tables 3, 4): Growth positive between 4–37 °C, with optimal growth at 25 °C. Growth positive on 15 % NaCl but not 20 % and remains pink (oac696) with pink reverse and without production of hyphae or melanisation at 14 dpi in osmotic media.

Known distribution: United States, isolated from the interior of cysts of the potato cyst nematode in potato fields in Oregon and from plant phylloplanes in Indiana.

Additional materials examined: **USA**, Oregon, Powell Butte, isolated from cysts of the potato cyst nematode (*Globodera ellingtonae*), Oct. 2018, coll. *I. Zasada*, isol. *B. Jumbam*, JB68 (PUL culture collection, PUL F29028 voucher); ibid., JB67 (PUL culture collection); ibid., JB69 (PUL culture collection); Indiana, Tippecanoe Co., West Lafayette, from phylloplane of unidentified plant, 9 Oct. 2015, *P.P. Parra*, PPP33 (PUL culture collection).

Aureobasidium essambei Jumbam & Aime, ***sp. nov.*** MycoBank MB 848259. Fig. 11.

Etymology: In honour of Baka Chief Jean-Pierre Essambe (a.k.a. Papa Chef) of the Somalomo region of the Dja Biosphere, Cameroon, for his enormous contributions to field expeditions in the Dja Biosphere Reserve.

Diagnosis: Similar to *A. microtermitis* but differing in melanisation, becoming completely melanised within 3 d of growth on MEA vs *A. microtermitis* that only showed a few dark brown spots after 10 d (Crous *et al.* 2021). Additionally, *A. essambei* has a slower growth rate, measuring 13 mm on PDA 7 d vs 23 mm in *A. microtermitis*.

Typus: **Cameroon**, East Region, Somalomo Subdivision, Dja Biosphere Reserve, on phylloplane of unidentified plant, Sep. 2017, *M.C. Aime*, MCA7731 (**holotype** PUL F29027 preserved as a dried inert culture), ex-type culture MCA7731 (PUL culture collection) = NRRL 64172 = CBS 149006.

Barcodes: ITS = OK376911; 28S = OK353636; mtLSU = OK376700; mtSSU = OK360982; *ELO2* = OK485097; *EF1a* = OK413243; *RPB2* = OM321982; *BTUB* = OK485064.

Culture characteristics (Fig. 11A–H): Colonies on MEA, PDA, and M40Y showed diameters of 12, 13, and 16 mm respectively at 25 °C, 7 dpi (Table 3). On MEA at 1 wk turning completely black (oac908), margins whitish and producing hyphae. On PDA at 1 wk cream (oac909), smooth, glistening, without hyphae. On M40Y, greenish brown (oac736), dull, surface reticulate with whitish margins, producing hyphae at margins. Reverse similar but paler, except appearing more melanised on M40Y.

Microscopic characteristics: *Vegetative hyphae* smooth, thin walled, 6.8–14.6 µm wide, septate (Fig. 11M, N, U). *Conidiogenous hyphae* hyaline, produced terminally and laterally (Fig. 11K, Q, R), *conidia* occasionally subapical (Fig. 11O, P). Conidia hyaline, 5.1–16 × 2.3–8.4 µm, smooth, mostly ellipsoid, occasionally ovoid or fusiform, cells proliferating by polar budding (Fig. 11I, J). *Chlamydospores* produced as intercalary arthrospores (Fig. 11L, S, T), deep brown (oac636–638) 1–2-celled, rarely 3-celled, constricted at the septum; 1-celled chlamydospores 6.6–22.5 × 4.8–18.7 µm, two-celled chlamydospores 15.9–31.4 × 6.9–16.2 µm.

Assimilation profiles: The following carbon compounds were assimilated: D-glucose, L-sorbose, L-Arabinose, gluconic acid sodium salt and D-quinic acid (Table 5). Fermentation of D-glucose, sucrose, melezitose and raffinose was weak (Table 5). The following nitrogen compounds were assimilated as the sole nitrogen source: potassium nitrate, ethylamine

hydrochloric acid, L-lysine hydrochloric acid, cadaverine hydrochloride, and D-glucosamine while the assimilation of D-tryptophan was weak (Table 5).

Growth temperature and salt tolerance (Tables 3, 4): Growth positive between 4–30 °C, with optimal growth at 28 °C. Growth on 15 % NaCl scant, slow, becoming greyish black with melanised white margins at 14 dpi; no growth on 20 % NaCl.

Known distribution: Cameroon, known only from the type isolate.

Aureobasidium fermentans (Wynne & Gott), Jumbam & Aime, ***comb. nov.*** MycoBank MB 848272.

Basionym: *Pullularia fermentans* Wynne & Got, *J. Gen. Microbiol*. **14**: 516. 1956. MB 304824.

Description and illustrations: See Wynne & Gott (1956).

Typus: USA, Texas, clinical specimen from the lymph node of a boy with Hodgkin's granuloma, isol. *E.S. Wynne & C.L. Gott* in 1964 (ex-type culture ATCC 12535 = IMI 062456 = CBS 298.56).

Barcodes: ITS = MH857648; 28S = MH869192.

Notes: *Aureobasidium fermentans* var. *fermentans* has been regarded as a synonym of *A. pullulans* (e.g., Zalar *et al.* 2008). However, we resolve sequences from the ex-

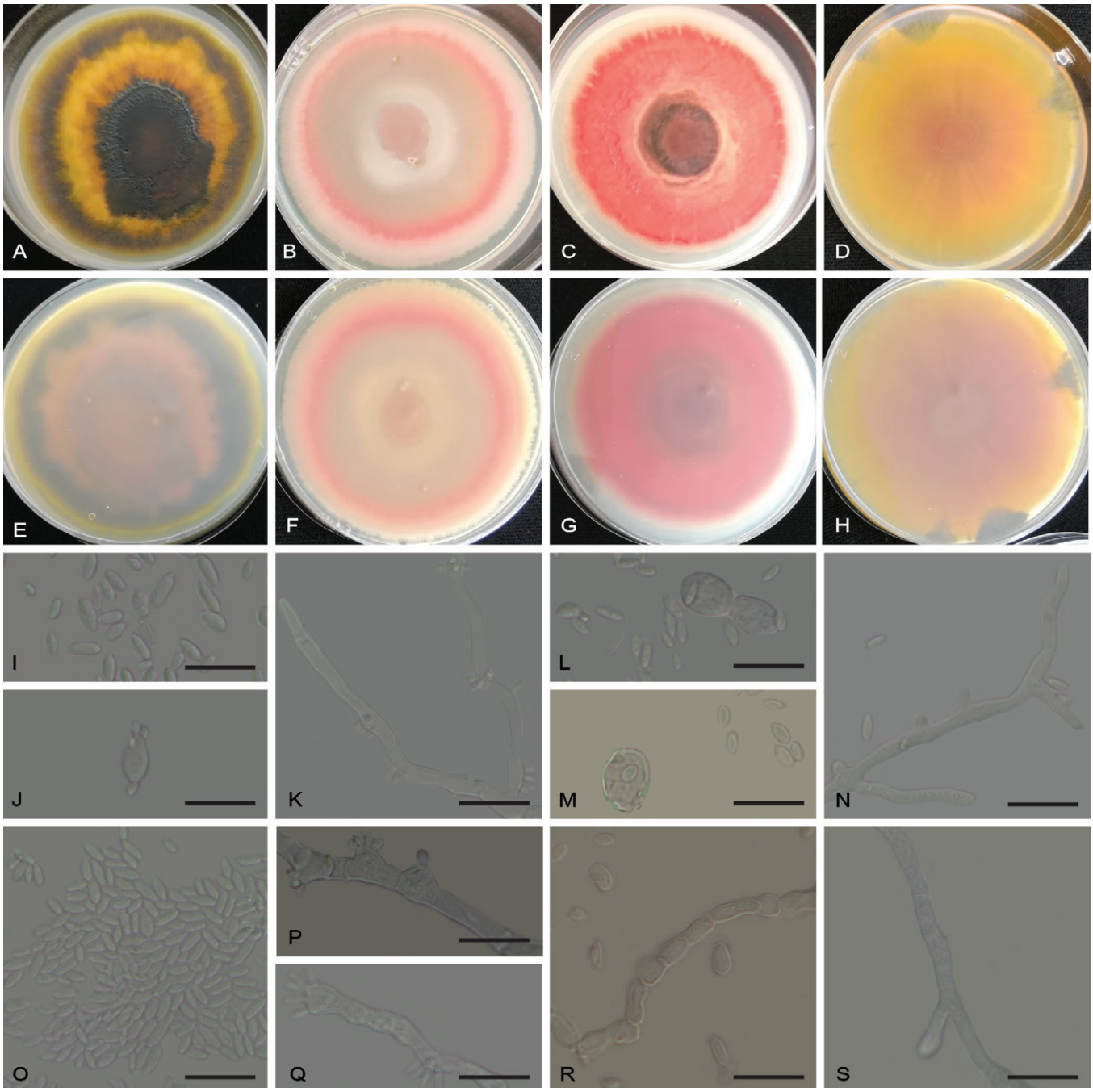

Fig. 12. Morphological characters of *Aureobasidium mustum* (NRRL 64173). **A–D.** Colonies at 7 dpi on MEA, MEA at 30 °C, PDA, and M40Y, respectively. **E–H.** Colony reverse on MEA, MEA at 30 °C, PDA, and M40Y, respectively. **I, J, O.** Primary and secondary conidia. **K, P, Q.** Conidiogenous hyphae. **L, M, R.** Chlamydospores. **N, S.** Vegetative hyphae. Scale bars = 20 µm.

type culture, CBS 298.56 (Vu *et al.* 2019), within NamiG as a distinct species. *Aureobasidium fermentans* differs from other *Aureobasidium* species in PullG by its ability to ferment glucose, mannose, sucrose, fructose, and raffinose (Wynne & Gott 1956). In contrast, the epitype of *A. pullulans* (CBS 584.75), does not ferment (de Hoog & Yurlova 1994).

Aureobasidium fermentans is related to *A. xishuangbannaense* and *A. pini* (Fig. 1A). *Aureobasidium fermentans* and *A. xishuangbannaense* (KUMCC 21-0703, ex-type) differ at 5/891 bp (28S), and 1/506 bp (ITS); *A. fermentans* and *A. pini* (CFCC 52778, ex-type) differ at 1/588 bp (28S) but share 100 % identity at the ITS. Morphologically, however, these are readily distinguished. *Aureobasidium fermentans* differs from *A. xishuangbannaense* by its longer and narrower conidia (10.0–14.0 × 5.0–7.0 µm vs 4.3–10.6 × 2.3–10.3 µm), the production of chlamydospores (13–15 µm in *A. fermentans* vs absent in *A. xishuangbannaense*), and the absence of aerial mycelium (produced in *A. xishuangbannaense*) (Wynne & Gott 1956, Hyde *et al.* 2023). *Aureobasidium fermentans* differs from *A. pini* by the larger conidia (10.0–14.0 × 5.0–7.0 µm vs 6.2–8.5 × 3.6–4.2 µm) (Jiang *et al.* 2019).

Aureobasidium mahoniae (A.W. Ramaley) Jumbam & Aime, ***comb. nov.*** MycoBank MB 848273.
Basionym: *Selenophoma mahoniae* A.W. Ramaley, *Mycotaxon* **43**: 448. 1992. MB 355521.

Description and illustrations: See Ramaley (1992).

Typus: **USA**, Colorado, ca 12.8 miles from the boundary of San Juan National forest, ca 1 mile from Junction Creek Road, La Plate Co., from leaves of *Mahonia repens*, 27 Jul. 1990, *A.W. Ramaley* (**holotype** BPI 1107357)

Notes: Ramaley (1992) placed this fungus in *Selenophoma* based on similarity in conidiomata, while recognizing that it produced an aureobasidium-like synasexual morph. Sequences from the presumed ex-type culture of *Selenophoma mahoniae* (CBS 388.92, Zalar *et al.* 2008, van Nieuwenhuijzen *et al.* 2016) resolve it in *Aureobasidium* (Fig. 1A), consistent with other molecular phylogenetic studies (Thambugala *et al.* 2014, van Nieuwenhuijzen *et al.* 2016). It differs from other *Selenophoma* species in having smaller conidia (11–17 × 4–6 µm: Fig. 14F), more conidiogenous apertures per conidiogenous cell (Fig. 14A), larger conidiogenous cells, and generally larger conidiomata (Sutton 1980).

Aureobasidium musti C. Onetto, S. Schmidt, M. Roach & A. Borneman ex Jumbam & Aime, MycoBank MB 858478. Fig. 12.
Synonym: *Aureobasidium mustum* C. Onetto *et al*., *FEMS Yeast Res.* **20**(6): foaa052 [4]. 2020. nom. inval. Arts 38.1, 40.8 (Shenzhen Code, Turland *et al.* 2018).

Typus: **Australia**, South Australia, Adelaide Hills, Mt. Barker, isolated from Shiraz grape juice, 2017, *unknown collector*, AWRI 4233 [**holotype** AWRI 4233, maintained in a metabolically inactive (cryopreservation beads at -80 ℃) state at the Australian Wine Research Institute (AWRI) Wine Microorganism Culture Collection].

Diagnosis: Similar to *A. melanogenum* and *A. motuoense*, but differing morphologically from the former in being orange to purple to deep red in culture, reaching diameters of 47 and 38 mm respectively on MEA and PDA vs 25 mm for *A. melanogenum* on both media at 7 dpi. *Aureobasidium musti* differs from *A. motuoense* in that it only reaches a diameter of 36 and 27 mm in M40Y and M60Y, respectively, vs to 43 and 40 mm on the same media for *A. motuoense*.

Culture characteristics (Fig. 12A–H): The following description refers to isolate NRRL 64173 (Louisiana, USA). Colonies reached diameters of 47, 38, and 36 mm on MEA, PDA, and M40Y respectively, at 25 °C and 7 dpi (Table 3). On MEA, colonies orange (oac671–672) in the centre, followed by a yellow (oac852) zone, dark brown and glistening at the margin; at 14 dpi, orange centre turns black, yellow zone persists, and the colony reverse is pale brown in the centre, then light orange (oac695), followed by grey then pale-yellow margins. On PDA, the centre is purple (oac670–671), followed by a light brown (oac717–718) zone, and dull; the centre darkens at 14 dpi, followed by a red zone (oac614–615) with a thin white margin. On M40Y, the centre is orange (oac813–815), followed by a moist glistening zone and whitish margin that becomes darkened at 14 dpi. Margins in all media are smooth and regular with hyphae; aerial hyphae not observed in any of the media.

Microscopic characteristics: *Vegetative hyphae* smooth, thin walled, 1–2.4 µm wide, septate (Fig. 12N, S). *Conidiogenous hyphae* undifferentiated, hyaline, synchronously producing conidia mostly terminally (Fig. 12K, P, Q). *Conidia* hyaline, 1.1–4.3 × 0.5–2.2 µm, smooth, ovoid to ellipsoidal, with hilum; cells multiplying mostly by synchronous polar and bipolar budding (Fig. 12I, J, O). *Chlamydospore* production intercalary (Fig. 12L, M, R), these 1–2-celled, ellipsoidal to subglobose to irregular in shape, hyaline; 1-celled chlamydospores, 3.3–8.7 × 2.2–5 µm (Fig. 12M), 2-celled chlamydospores rare, 7–8.8 × 3.5–3.8 µm (Fig. 12L), 3-celled chlamydospores not observed.

Assimilation profiles: The following carbon sources are assimilated: Gluconic acid sodium salt strongly assimilated; D-glucose and L-arabinose moderately assimilated; sodium succinate dibasic hexahydrate and D-quinic acid weakly assimilated (Table 5). Melanisation was absent while assimilating the above carbon compounds. Fermentation was negative for all tested carbon compounds (Table 5). Assimilation of L-lysine hydrochloric acid as a sole nitrogen source was moderate, while that of potassium nitrate, potassium nitrite, ethylamine hydrochloric acid, cadaverine hydrochloric acid, D-glucosamine, and D-tryptophan was weak (Table 5).

Growth temperature and salt tolerance (Tables 3, 4): Cultures grew at 4–37 °C, optimally at 25 °C. Growth was present on 10 % NaCl but not 15 % and was whitish, without melaninization or pigmentation, dull, without hyphae, and with a white reverse in osmotic media at 14 dpi.

Known distribution: In tropical and subtropical regions of North America (Louisiana) and the South Pacific (Vanuatu, Australia) from a variety of host plant leaf surfaces.

Materials examined: **USA**, Louisiana, East Baton Rouge Parish, Baton Rouge, on phylloplane of *Oryza sativa*, Feb. 2011, *T. Rush*, TAR230 [PUL F29044 voucher; culture TAR230 (PUL culture collection) = NRRL 64173 = CBS 148904]; isolated from a bird feather, 21 Nov. 2010, *S. Albu*, SA12 (PUL culture collection); isolated from *Lygodium japonicum* phylloplane, *S. Albu*, SA338 (PUL culture collection); isolated from a diseased shrub leaf, Nov. 2007, *J. Kosamund*, JLK12 (PUL culture collection); isolated from *Cyrtomium falcatum* phylloplane, 15 Feb. 2011, *S. Albu*, SA234 (PUL culture collection); isolated from unidentified phylloplane, Nov. 2009, *M.C. Aime*, MCA3872 (PUL culture collection). **Vanuatu**, Aneityum Island, Aneghowhat Village, -20.225879, 169.791631, 24 m a.s.l., as endophyte from pine needles, 2 Aug. 2017, *M.C. Aime*, MCA 7640 (PUL culture collection); ibid., *M.C. Aime*, MCA 7652 (PUL culture collection).

Notes: The type of *A. musti* (AWRI4233) was isolated from grape juice used in the wine industry in Australia but described without a description or diagnosis (Onetto *et al.* 2020b). We provide a description and physiological data for this species from new isolates made from a rice phylloplane in Louisiana (NRRL 64173) that is shown to be conspecific with *A. musti* (Fig. 1A).

Aureobasidium peruvianum Jumbam & Aime, ***sp. nov.*** MycoBank MB 848261. Fig. 13.

Etymology: Named for Peru, the country from which this species was isolated.

Diagnosis: Similar to *A. vanuatuense* but differing in the smaller (4.4–12.0 × 2.6–4.7 µm vs 5.1–16 × 2.3–8.4 µm

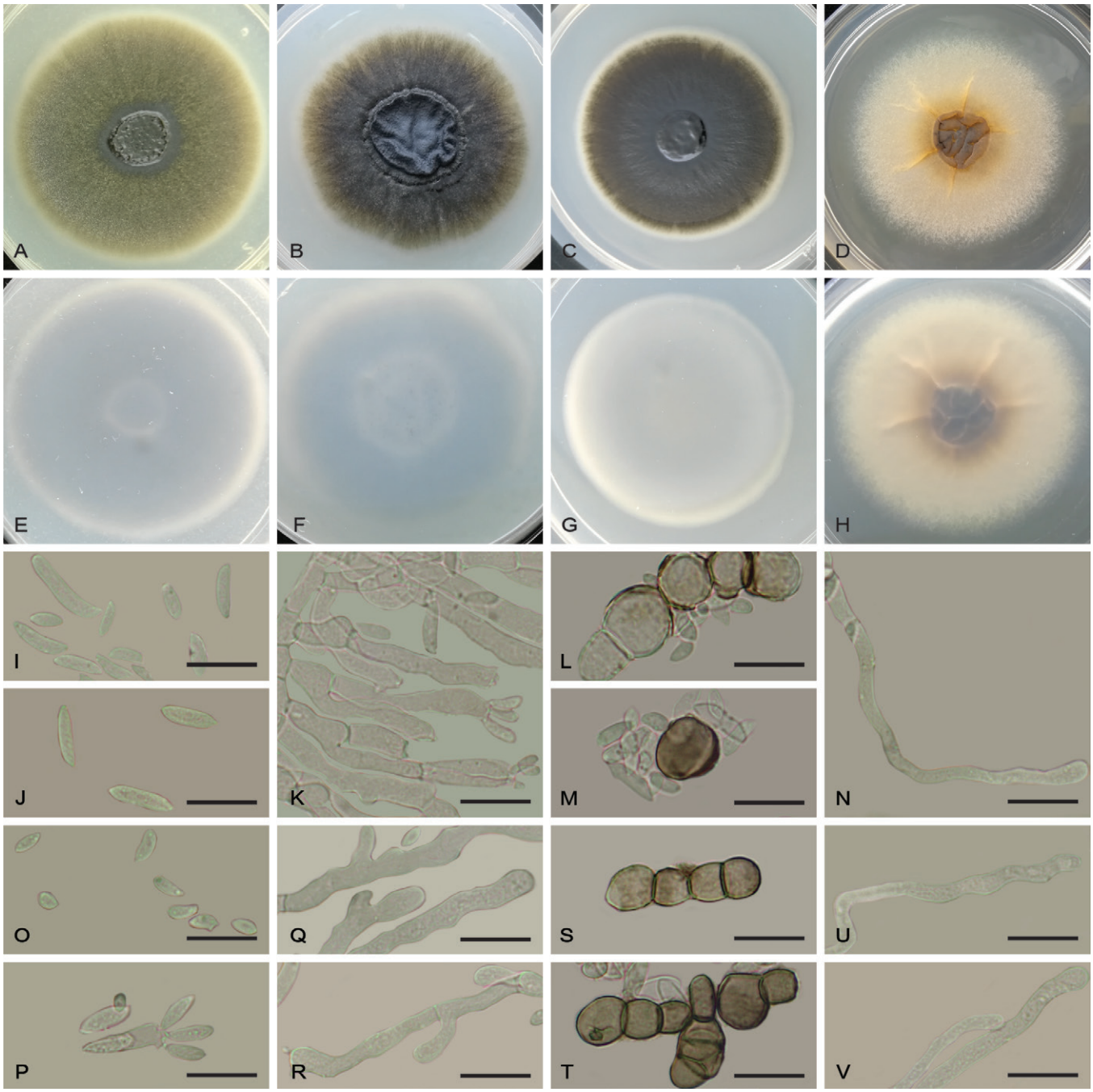

Fig. 13. Morphological characters of *Aureobasidium peruvianum* (ex-holotype, NRRL 64183). **A–D.** Colonies at 7 dpi on MEA, MEA at 30 °C, PDA, and M40Y, respectively. **E–H.** Colony reverse on MEA, MEA at 30 °C, PDA, and M40Y, respectively. **I, J, O, P.** Primary and secondary conidia. **K, Q, R.** Conidiogenous hyphae. **L, M, S, T.** Chlamydospores. **N, U, V.** Vegetative hyphae. Scale bars = 20 µm.

in *A. vanuatuense*) and curved to bean-shaped conidia vs uncurved, ellipsoidal conidia in *A. vanuatuense*.

Typus: **Peru**, Piura Dept., Huancabamba Prov., farm near Barrios, isolated from air on 50 % glucose medium, 5 Oct. 2016, *M.C. Aime*, MCA7097 (**holotype** PUL F29025, preserved as a dried inert culture); ex-type culture MCA7097 (PUL culture collection) = NRRL 64183 = CBS 149009.

Barcodes: ITS: OK376905; 28S = OK353630; mtLSU = OK376695; mtSSU = OK360978; *ELO2* = OL505736; *EF1a* = OL505731; *RPB2* = OM321980; *BTUB* = not available.

Culture characteristics (Fig. 13A–H): Colonies diameters 38, 34, and 36 mm on MEA, PDA, and M40Y, respectively at 25 °C, 7 dpi (Table 3). At 7 dpi, colonies white to cream (oac909), glistening to dull, margins smooth with hyphae produced; colony reverse is white. Colours unchanged at 14 dpi on MEA and M40Y; at 14 dpi on PDA, colony centre white, outer zone melanised and brown margin whitish; colony reverse the same but paler on PDA.

Microscopic characteristics: *Vegetative hyphae* smooth, thin walled, 2.6–19.8 µm wide, septate (Fig. 13N, U, V). *Conidiogenous hyphae* hyaline, synchronously producing conidia both terminally and laterally (Fig. 13K, Q–R). *Conidia* hyaline, 4.0–30.3 × 2.6–6.4 µm, smooth, curved to bean-shaped, cells multiplying by polar budding (Fig. 13I, J, O, P). *Chlamydospores* ovoid to ellipsoid to subglobose, production intercalary (Fig. 13L, M, S, T); chlamydospores pale brown (oac730–731), 1–2-celled, rarely 3-celled; 1-celled chlamydospores 8.1–22.6 × 5.8–17.8 µm, 2-celled

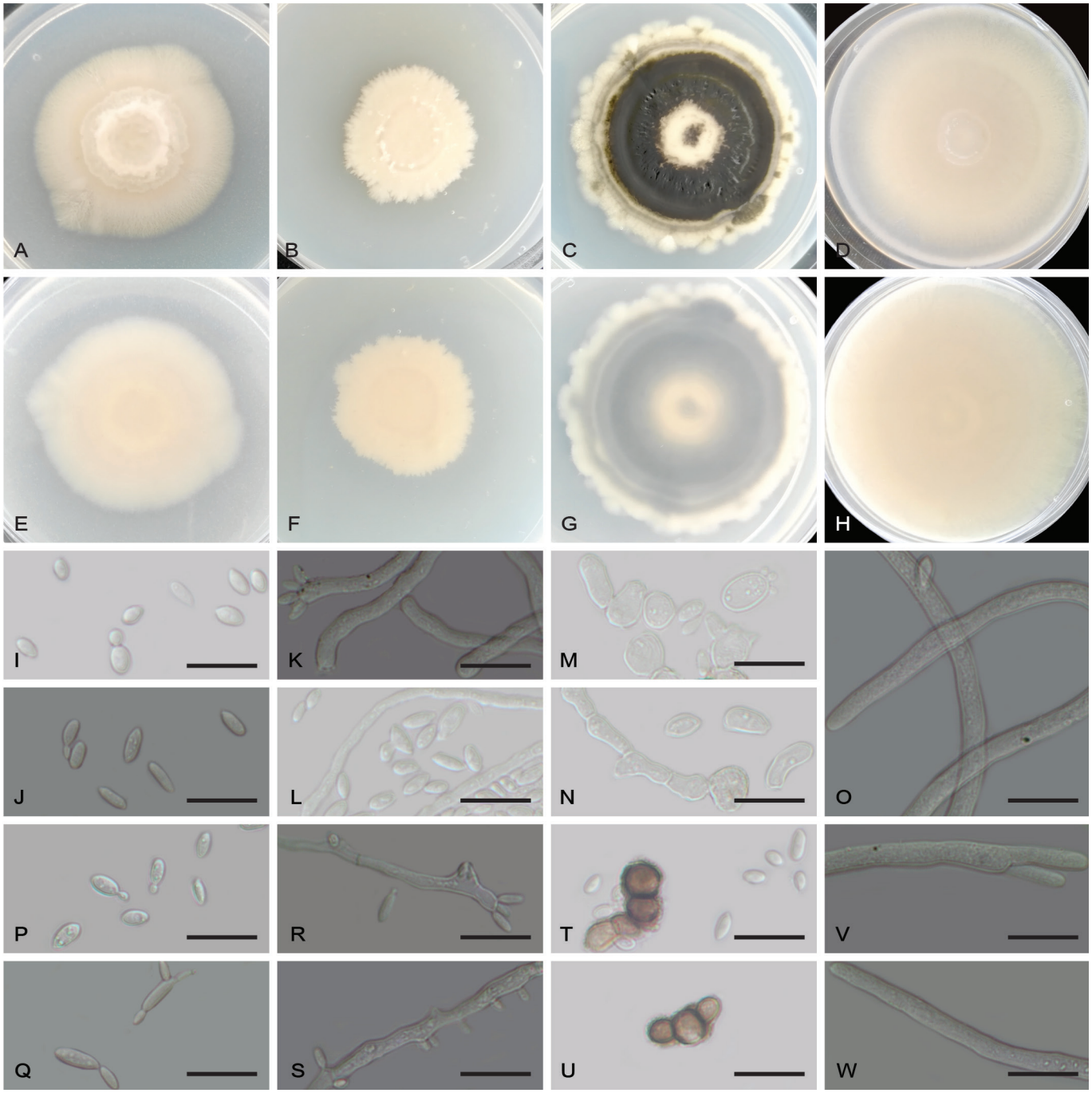

Fig. 14. Morphological characters of *Aureobasidium rubi* (ex-holotype, NRRL 64179). **A–D.** Colonies at 7 dpi on MEA, MEA at 30 °C, PDA, and M40Y, respectively. **E–H.** Colony reverse on MEA, MEA at 30 °C, PDA, and M40Y, respectively. **I, J, P, Q.** Primary and secondary conidia. **K, L, R, S.** Conidiogenous hyphae. **M, N, T, U.** Chlamydospores. **O, V, W.** Vegetative hyphae. Scale bars = 20 µm.

chlamydospores 9.6–33.2 × 7.3–19.2 µm, constricted at the septum (Fig. 13L, S, T).

Assimilation profiles: Carbon assimilation was weak for D-glucose, L-arabinose, a-rhamnose monobasic, D-salicin, erythritol, xylitol, D-mannitol, galactitol, gluconic acid lactone, gluconic acid sodium salt, and propane-1,2-diol. L-sorbose, D-glucosamine, D-arabinose, soluble starch, glycerol, ribitol, myo-inositol, sodium succinate dibasic hexahydrate, ethanol, and D-quinic acid were not assimilated (Table 5). For the carbon compounds assimilated, no pigmentation was produced. Fermentation of melibiose was strong while that of D-glucose, maltose, sucrose, trehalose, cellobiose, melezitose and raffinose was moderate, and fermentation of inulin was weak (Table 5). Assimilation of potassium nitrate, L-lysine hydrochloric acid, D-glucosamine, and D-tryptophan as the sole source of nitrogen was strong. Sodium nitrite was moderately assimilated while the assimilation of cadaverine hydrochloric acid was weak. Ethylamine hydrochloric acid, creatinine, creatine, and imidazole were not assimilated (Table 5).

Growth temperature and salt tolerance (Tables 3, 4): Colonies grew between 4–37 °C with optimal growth at 28 °C. Growth on 10 % NaCl but not 15 %; colonies white (oac909), surface dull, regular margin and without production of hyphae, melanin, or pigmentation in osmotic media.

Known distribution: Peru, Piura Department, known only from the type locale.

Aureobasidium pullulans (de Bary) G. Arnaud, *Les Astérinées*: 39. 1918.
Basionym: *Dematium pullulans* de Bary, *Morph. Physiol. Pilze*: 182, fig. 73. 1866.

Typus: *Dematium pullulans* de Bary, Morph. Physiol. Pilze: 183, fig. 73. 1866, selected as **lectotype** here MBT 10025624. **France**, Beaujolais, Beaujeu, from grapes of *Vitis vinifera*, 1974, *E.J. Hermanides-Nijhof* (**epitype** of *Dematium pullulans* designated here MBT 10025625, CBS 584.75, preserved as metabolically inactive epitype specimen), ex-epitype culture CBS 584.75.

Hermanides-Nijhof (1977) designated a neotype for *Dematium pullulans*. This typification was however not Code compliant, as a line drawing is available, which is designated here as lectotype, with the same culture of Hermanides-Nijhof (1977) thus designated as the epitype.

Aureobasidium rubi Jumbam & Aime, ***sp. nov.*** MycoBank MB 848262. Fig. 14.

Etymology: Referring to the host genus (*Rubus* sp.) from which the type was isolated.

Diagnosis: Similar to *A. intercalariosporum* (Wu *et al.* 2023), differing in the slower growth rate (colony diameter 18 mm vs 34 mm for *A. intercalariosporum*, on PDA 7 dpi at 25 °C), shorter conidia (up to 14.7 µm long vs up to 17.0 µm in *A. intercalariosporum*), and smaller 1-celled chlamydospores (9.6–16.6 × 5–13.2 µm vs 10.5–17.1 × 10.5–12.9 µm for *A. intercalariosporum*).

Typus: **USA**, Louisiana, East Baton Rouge Parish, Baton Rouge, Highland Lakes, on phylloplane of *Rubus* sp. infected with *Gymnoconia interstitialis*, 10 Apr. 2010, *M.C. Aime*, MCA3890 (**holotype** PUL F29019 preserved as a dried inert culture), ex-type culture MCA3890 (PUL culture collection) = NRRL 64179 = CBS 148907.

Barcodes: ITS: OK376892; 28S = OK353620; mtLSU = OK376688; mtSSU = not available; *ELO2* = OK485086; *EF1a* = OK413232; *RPB2* = OM321979; *BTUB* = OK485054.

Culture characteristics (Fig. 14A–H): Colonies attained a diameter of 18, 24, 30 mm on MEA, PDA, and M40Y respectively at 25 °C, 7 dpi (Table 3). On all three media, colonies pink (oac548/676), glistening, margins smooth, hyphae production at the margins, aerial hyphae not observed; colony reverse pale pink. At 14 dpi, culture on PDA has white yeast-like centre surrounded by a completely black melanised zone, margin whitish with brown speckling, edge irregular; colony reverse similar but paler.

Microscopic characteristics: *Vegetative hyphae* smooth, thin-walled, 2.5–9.9 µm wide, septate (Fig. 14O, V, W). *Conidiogenous hyphae* undifferentiated, hyaline, conidia produced synchronously, mostly terminal (Fig. 14K, L, R, S). *Conidia* hyaline, 4.2–14.7 × 2.6–7.2 µm, smooth, mostly ovoid to ellipsoidal, sometimes subfusiform; cells multiply mostly by synchronous polar budding (Fig. 14I, J, P, Q). *Chlamydospores* intercalary (Fig. 14M, N, T, U), 1–2(–3)-celled, ellipsoidal to subglobose, brown (Fig. 14M, T, U); 1-celled chlamydospores 9.6–16.6 × 5–13.2 µm, 2-celled chlamydospores 11.2–20.7 × 5.2–13.4 µm, and 3-celled chlamydospores 13.1–24.7 × 7–11.6 µm (Fig. 14U).

Assimilation profiles: D-glucose, L-arabinose, D-mannitol, and gluconic acid sodium salt were moderately assimilated as the sole source of carbon, while D-salicin was only weakly assimilated (Table 5). Assimilation of D-quinic acid was negative. No pigmentation was produced during the assimilation of the above carbon compounds. Fermentation was negative for all tested carbon compounds (Table 5). Assimilation of potassium nitrate and L-lysine hydrochloric acid as the sole source of nitrogen was strong, while that for ethylamine hydrochloric acid and cadaverine hydrochloric acid was weak (Table 5).

Growth temperature and salt tolerance (Tables 3, 4): Colonies grew between 4–30 °C; optimal growth at 28 °C. Growth positive on 10 % and 15 % NaCl but not on 20 %; growth on osmotic media at 14 dpi pinkish (oac696), without melanisation, dull, and without hyphal production.

Known distribution: United States and Europe, primarily from plant phylloplanes, also isolated from air on 20 % glucose media.

Additional material examined: **Netherlands**, Amsterdam, isolated from air on 20 % glucose medium, 10 Apr. 2012, *M.C. Aime*, MCA4717 (PUL culture collection). **UK**, Scotland, Edinburgh, Dawyck Botanic Gardens, on phylloplane of unidentified fern, 1 Aug. 2010, *M.C. Aime*, MCA4187 (PUL culture collection). **USA**, Indiana, Tippecanoe Co., West Lafayette, Purdue University campus, isolated from *Pinus*

strobus phylloplane, Feb. 2015, *J. Cavaletto*, INDP43 [PUL F29042, voucher; culture INDP43 (PUL culture collection)]; Louisiana, East Baton Rouge Parish, Baton Rouge, Louisiana State University campus, isolated from *Citrus trifoliata* phylloplane, 18 Jun. 2012, *S. Albu*, SA817 (PUL culture collection).

Aureobasidium toomeae Jumbam & Aime, ***sp. nov.*** MycoBank MB 848263. Fig. 15.

Etymology: In honour of Merje Toome who isolated the ex-type strain.

Diagnosis: Similar to *A. lini*, differing in the shorter and more narrow conidia (1.6–10 × 0.8–2.2 µm vs 11–16 × 4–5.5 µm in *A. lini*) (Hermanides-Nijhof 1977). Additionally, *A. toomeae* produces greenish brown colonies and bottle-shaped conidia on MEA vs the whitish grey colonies with curved conidia in *A. lini*.

Typus: **USA**, California, Contra Costa Co., Walnut Creek, from bark of *Betula* sp., May 2012, *M. Toome*, MT159 (**holotype** PUL F29020 preserved as a dried inert culture), ex-type culture MT159 (PUL culture collection) = NRRL 64186 = CBS 149010.

Barcodes: ITS: OK376912; 28S = OK353638; mtLSU = not available; mtSSU = OL504988; *ELO2* = OK485098; *EF1a* = OL505732; *RPB2* = OK485125; *BTUB* = OK485065.

Culture characteristics (Fig. 15A–H): Colony diameters 23 mm on MEA, PDA, and M40Y at 25 °C, 7 dpi (Table 3). Colonies on MEA at 7 dpi with melanised greenish brown

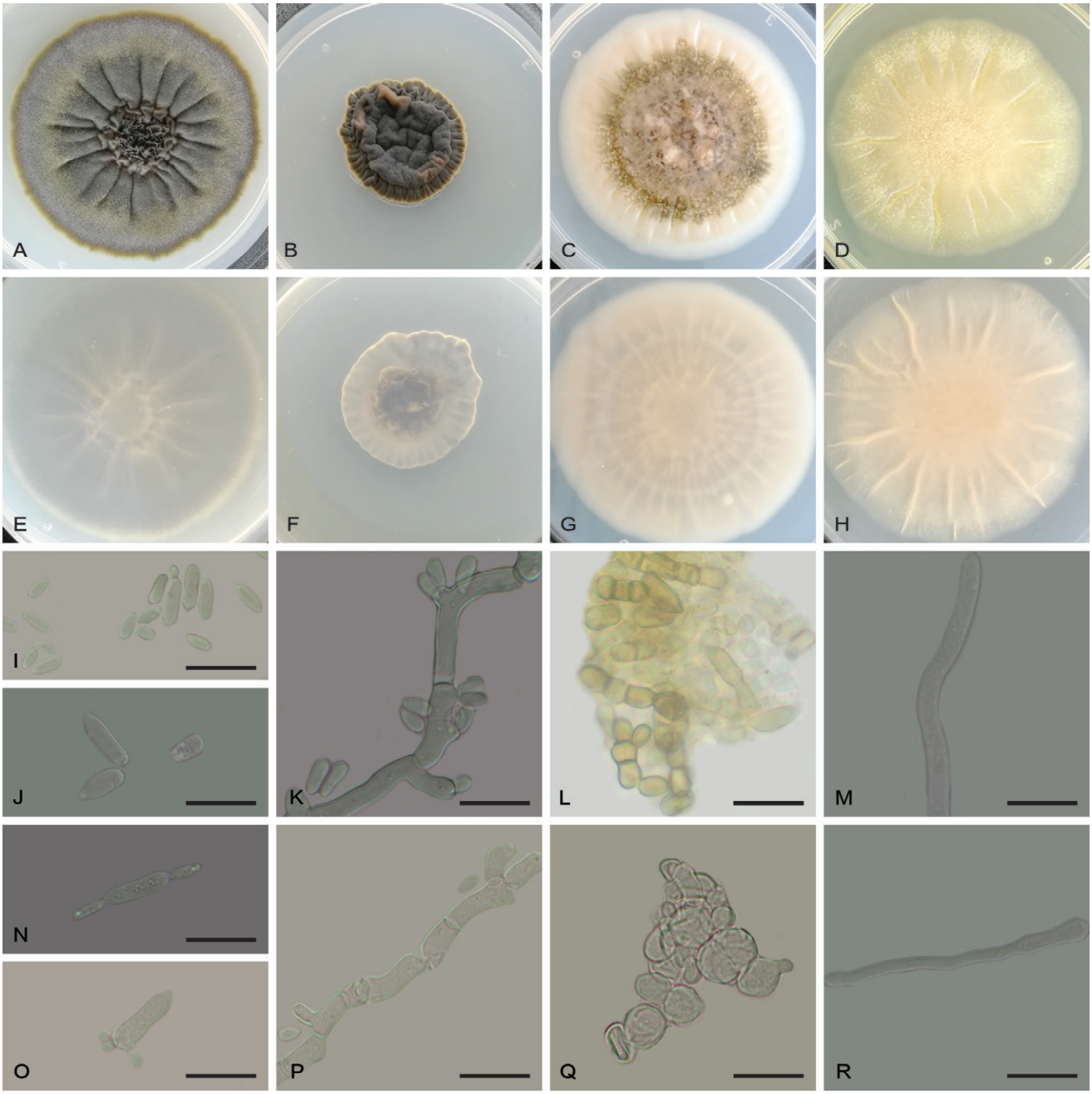

Fig. 15. Morphological characters of *Aureobasidium toomeae* (ex-holotype, NRRL 64186). **A–D.** Colonies at 7 dpi on MEA, MEA at 30 °C, PDA, and M40Y, respectively. **E–H.** Colony reverse on MEA, MEA at 30 °C, PDA, and M40Y, respectively. **I, J, N, O.** Primary and secondary conidia. **K, P.** Conidiogenous hyphae. **L, Q.** Chlamydospores. **M, R.** Vegetative hyphae. Scale bars = 20 µm.

centre (oac831), white margins with hyphae produced; reverse similar but paler; completely black at 14 dpi with furrows radiating from centre, margins greenish brown and smooth. On PDA at 7 dpi, colonies not melanised, dry creamy and yeast-like in the centre, whitish outer zone, margin with hyphae, vein-like radiations emanating from centre, reverse pale white. At 14 dpi on PDA, centre melanised, dark green (oac869), outer 1/3 to margin cream, with vein-like radiations; reverse pale. On M40Y at 7 dpi, dry, whitish without melaninization, no hyphae produced, reverse similar; at 14 dpi, pinkish (oac697), not melanised, pale white on reverse.

Microscopic characteristics: *Vegetative hyphae* smooth, thin-walled, 0.9–2.4 µm wide, septate (Fig. 15M, R). *Conidiogenous hyphae* hyaline, synchronously producing conidia both terminally and laterally (Fig. 15K, P). *Conidia* hyaline, 1.6–10.0 × 0.8–2.2 µm, smooth, ellipsoid, fusiform, or bottle-shaped, cells multiply by polar and bipolar budding (Fig. 15I, J, N, O). *Chlamydospores* subglobose to ellipsoid, produced as intercalary arthrospores (Fig. 15L, Q), brownish (oac730–731), 1–3-celled; 1-celled chlamydospores 6.8–19.7 × 3.8–9 µm, 2-celled chlamydospores 10–20.9 × 4.1–7.5 µm, 3-celled chlamydospores 21.7–28.3 × 5.1–6.6 µm (Fig. 15I, Q); 2- and 3-celled chlamydospores constricted at septa, constriction occasionally eccentric (Fig. 15L).

Assimilation profiles: Carbon compounds moderately assimilated are gluconic acid sodium salt and D-quinic acid; D-glucose, L-arabinose, erythritol and D-mannitol are weakly assimilated (Table 5). Cloudiness observed in all isolates as they assimilate carbon compounds, but pigmentation was not produced. Fermentation was negative for all tested

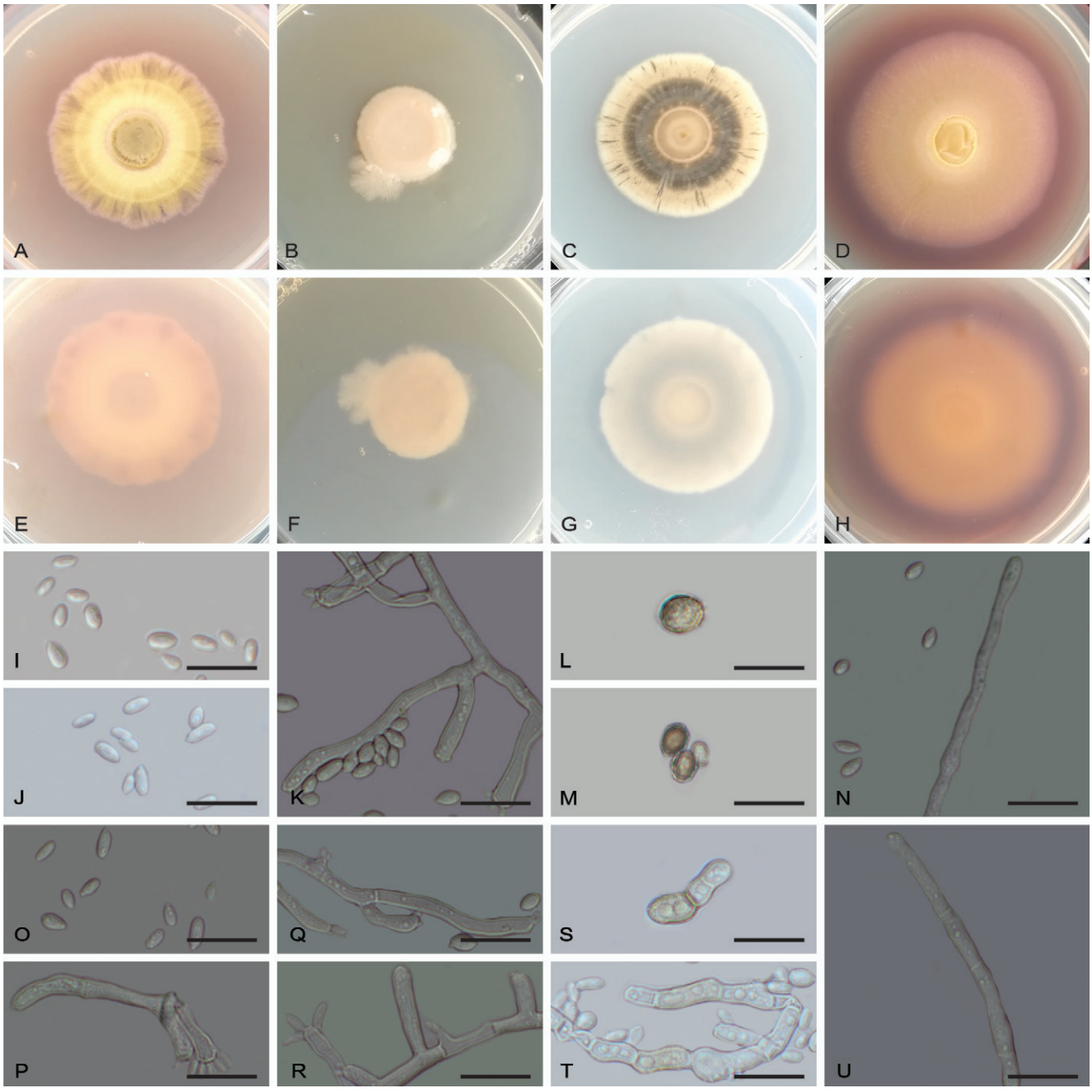

Fig. 16. Morphological characters of *Aureobasidium vanuatuense* (ex-holotype, NRRL 64180). **A–D.** Colonies at 7 dpi on MEA, MEA at 30 °C, PDA, M40Y. **E–H.** Colony reverse on MEA, MEA at 30 °C, PDA, and M40Y, respectively. **I, J, O, P.** Primary and secondary conidia. **K, Q, R.** Conidiogenous hyphae. **L, M, S, T.** Chlamydospores. **N, U.** Vegetative hyphae. Scale bars = 20 µm.

carbon compounds (Table 5). Cadaverine hydrochloric acid is moderately assimilated as the sole nitrogen source, ethylamine hydrochloric acid, and L-lysine hydrochloric acid are weakly assimilated (Table 5).

Growth temperature and salt tolerance (Tables 3, 4): Colonies grew between 4–37 °C; optimal growth is at 25 °C. Growth positive on 10 % NaCl but not 15 %; growth on osmotic media was pale brown (oac743–744) with a white margin, melanised at centre, without hyphae, with similar but paler reverse.

Known distribution: United States, California, known only from the type.

Aureobasidium uvarum C. Onetto, S. Schmidt, M. Roach & A. Borneman ex Jumbam & Aime, MycoBank MB 858477. Fig. 12.
Synonyms: *Aureobasidium uvarum* C. Onetto *et al*., *FEMS Yeast Res.* **20**: foaa052 [4]. 2020. nom. inval. Arts 38.1, 40.8 (Shenzhen Code, Turland *et al.* 2018).
Aureobasidium vineae C. Onetto, S. Schmidt, M. Roach & A. Borneman, *FEMS Yeast Res.* **20**: foaa052 [4]. 2020. nom. inval. Arts 38.1, 40.8 (Shenzhen Code, Turland *et al.* 2018).

Typus: **Australia**, South Australia, McLaren Vale, Shiraz grape juice sample from a winery, 2018, *unknown collector*, AWRI 4620 [**holotype** AWRI 4620 preserved in a metabolically inactive state (cryopreservation beads at -80 ℃) at the Australian Wine Research Institute (AWRI) Wine Microorganism Culture Collection].

Diagnosis: Similar to *A. insectorum* (Wu *et al.* 2023) but differing in the larger conidia (~8–10 × 3–5 µm vs 4.2–7.4 × 1.7–3.5 µm in *A. insectorum*) and absence of melanisation at 1 mo (vs *A. insectorum* which is almost completely melanised on four tested standard media)

Description: The following description is derived from fig. S2 in Onetto *et al.* (2020b). Colonies on YPD at 1 mo medium to slow growing, pale-yellow, not melanised, rough, dry, 3 cm diam., with irregular margins. At 1 wk in YPD, conidia ovoid to ellipsoid, hyaline, thin-walled, budding terminal, ca 8–10 × 3–5 µm.

Notes: Onetto *et al.* (2020) proposed two species, *A. uvarum* (type AWRI4620) and *A. vineae* (type AWRI4619), based on a comparative genomic analysis, but without diagnoses or descriptions. Our eight locus analyses resolved AWRI4620 and AWRI461, as conspecific and closely related to *A. cavalettoi* and *A. insectorum* (Fig. 1A). ITS sequence data of AWRI4620 and *A. insectorum* share 521/527 bp; AWRI4619 shares 520/527 bp with *A. insectorum*. AWRI4620 and *A. cavalettoi* differed at eight positions (seven substitutions and one indel) sharing 510/518 bp; AWRI4619 differed at nine positions (seven substitutions and two indels) sharing 509/518 bp. Figures of this species can be found in Onetto *et al.* (2020b) supplementary materials.

Additional strains: **Australia**, South Australia, McLaren Vale, Shiraz grape juice sample from a winery, 2018, *unknown collector*, AWRI 4619.

Aureobasidium vanuatuense Jumbam & Aime, ***sp. nov.*** MycoBank MB 848260. Fig. 16.

Etymology: Referring to the Melanesian country of Vanuatu from where the type was isolated.

Diagnosis: Similar to *A. castaneae* and *A. albui*, but differs from the first in the slower growth rate (19 mm vs 40 mm in *A. castanea* at 7 dpi on PDA) and from *A. albui* by the production of orange pigmentation on PDA and in D-quinic acid assimilation media, the lack of melanisation on M40Y, and the limited yeast-like growth at 30 °C (Figs 6, 7A, 16).

Typus: **Vanuatu**, Aneityum Island, Aneghowhat Village, -20.214487, 169.795337, 134 m a.s.l., isolated from phylloplane of an unidentified *Apocynaceae*, 27 July 2017, *M.C. Aime*, MCA7387 (**holotype** PUL F29024 preserved as a dried inert culture), ex-type culture MCA7387 (PUL culture collection) = NRRL 64180 = CBS 149007.

Barcodes: ITS: OK376908; 28S = OK353633; mtLSU = OK376698; mtSSU = OK360980; *ELO2* = OK485095; *EF1a* = OK413240; *RPB2* = OK485124; *BTUB* = OK485062.

Culture characteristics: On MEA, PDA, and M40Y, colony diameter 18, 19, and 21 mm, respectively, at 25 °C, 7 dpi (Table 3). On MEA, melanisation begins at 3 dpi, turning greenish brown (oac736) at centre, pale yellow (oac815) outer zone, and greenish brown speckling at the margin, hyphae at margin pinkish. On PDA, creamy orange (oac681) yeast-like centre and margin, intermediate zone greenish (oac833) and melanised, hyphae produced at margin. On M40Y, purplish (oac611) without melanisation, hyphae at margin reddish. Colonies similar in reverse with paler melanised regions (Fig. 16A–H).

Microscopic characteristics: *Vegetative hyphae* smooth, thin walled, 5.7–12.8 µm wide, becoming septate (Fig. 16N, U). *Conidiogenous hyphae* hyaline or slightly purple pigmented, producing conidia mostly laterally (Fig. 16K, R, R). *Conidia* hyaline, 4.4–12.0 × 2.6–4.7 µm, smooth, ellipsoidal, rarely pyriform, cells proliferate by polar budding (Fig. 16I, J, O, P). *Chlamydospores* ellipsoidal to subglobose, intercalary (Fig. 16L, M, S, T), deep brown (oac636-638), 1–2-celled; 1-celled chlamydospores 5.3–13.7 × 4.8–12.2 µm (Fig. 16L, M), 2-celled chlamydospores 13.9–27 × 6.3–12.9 µm, constricted at the septum (Fig. 16S). Three-celled chlamydospores are rarely seen.

Assimilation profiles: Carbon compounds strongly assimilated were D-glucose, L-arabinose, gluconic acid sodium salt, sodium succinate dibasic hexahydrate, and D-quinic acid (Table 5). Assimilation of erythritol and D-mannitol was weak. An orange pigmentation was produced at 14 dpi while assimilating D-quinic acid. At 21 dpi, colonies produced a light orange pigmentation in L-arabinose and sodium succinate dibasic hexahydrate, and pinkish pigment in erythritol. Fermentation of D-glucose, sucrose, melezitose and raffinose was weak (Table 5). The following nitrogen compounds were assimilated: potassium nitrate, ethylamine hydrochloric acid, and L-lysine hydrochloric acid; sodium nitrite, cadaverine hydrochloride, D-glucosamine, and D-tryptophan were weakly assimilated (Table 5).

Growth temperature and salt tolerance (Tables 3, 4): Growth positive between 4–30 °C, with optimal growth at 28 °C. Growth positive on 15 % NaCl but not at 20 %. Growth slow, becoming pale brown (oac817–818) at 14 dpi on osmotic media.

Known distribution: Oceania (Vanuatu). Known only from the type.

DISCUSSION

In this study, we analysed sequence data from eight loci for 208 isolates of *Aureobasidium*, including from 128 newly isolated cultures generated for this study, and environmental sequence data (Table S1, Fig. S1A). We also collected and analysed a combination of growth, macro- and micromorphological, and physiological data for 10 species of *Aureobasidium*. Our analyses included representative sequences from ex-type strains of all previously described *Aureobasidium* species for which these data were available or could be generated. Sequences from strains identified as *A. zeae* (van Nieuwenhuijzen *et al.* 2016, Vu *et al.* 2019) were excluded from analyses as they were determined to belong to other lineages and did not originate from ex-type strains. In total, we were able to resolve 43 well supported species, including two, *Aureobasidium* sp.1 and sp.2, that were analysed only from publicly available sequence data but appear to represent two additional new species (Fig. 1A, B). An additional nine new species were described from newly collected strains of *Aureobasidium*, and three new combinations were made. Together with *A. zeae* and 12 other accepted species for which there were no sequence data brings the total number of described *Aureobasidium* species to 54. We also document several new distribution records (Table S1). For example, *A. melanogenum* (MCA5020) was isolated in Guyana, *A. namibiae* was isolated from the USA, and *A. pini*, previously only known from China (Jiang *et al.* 2019) was isolated from the USA (also see Fig. S1A, Supplementary data).

In addition to phylogenetic methods, other approaches to delimit and establish well-supported species boundaries are recommended (Aime *et al.* 2021). DNA-based species recognition methods have been used to circumscribe species in other fungal groups such as *Beauveria*, *Colletotrichum*, *Bipolaris*, and *Diaporthe* (Liu *et al.* 2016, Bustamante *et al.* 2019, Bhunjun *et al.* 2020, 2021, Hilário *et al.* 2021). Here we tested six DNA-based in silico species recognition criteria methods (GCPSR, ABGD, ASAP, PTP, bPTP, and GMYC) and found the genealogical concordance phylogenetic species recognition (GCPSR) proposed by Taylor *et al.* (2000) to be most accurate and consistent at delimiting previously described species. We then applied a polyphasic approach that included GCPSR, phenotypic (micro- and macromorphological), and physiological data to delimit species in *Aureobasidium*.

Of the species recognition methods tested, ASAP showed a high level of incongruence with the multi-locus phylogeny in the single locus ITS, 28S, mtLSU, *ELO2*, and the 6-LDS *A. pullulans* species complex (ApC) datasets. However, ABGD and ASAP showed results somewhat similar to the multi-locus phylogeny in the other single-locus phylogenies. These two models delimited *A. ellingtonae*, *A. aubasidani*, *A. toomeae,* and the rest of sequences in the *A. pullulans* complex as a single species (Fig. 5A). *Aureobasidium ellingtonae* and *A. toomeae* were delimited as separate species from the complex by ABGD in the other gene trees including *BTUB*, *ELO2*, and *RPB2*. A similar scenario was observed for *A. albui* and *A. vanuatuense* as well as *A. diazvalderramae* and *A. namibiae* that were grouped into one species by these distance-based methods in some gene trees. Results from coalescent-based methods (PTP, bPTP, and GMYC) were similar to those from the distance-based methods.

Aureobasidium pullulans s. l. has long been recognized as a species complex that has been particularly recalcitrant to resolution (e.g., Cooke 1962, Yurlova *et al.* 1999, Zalar *et al.* 2008, Gostinčar *et al.* 2014). Zalar and colleagues (2008) analysed five individual loci (ITS, 28S, *BTUB*, *EF1a,* and *ELO2*) in combination with growth data to delineate varieties of *A. pullulans*. The resulting four varieties (*A. pullulans* var. *pullulans*, *A. pullulans* var. *melanogenum*, *A. pullulans* var. *namibiae*, and *A. pullulans* var. *subglaciale*) from their study are now considered species (*A. pullulans*, *A. melanogenum*, *A. namibiae*, and *A. subglaciale*) after a comparative genomic analysis by Gostinčar *et al.* (2014). Other studies have placed *A. lini* within the *A. pullulans* complex (e.g., Crous *et al.* 2019, 2021, Jiang *et al.* 2021, Wang *et al.* 2022); our data, however, resolve *A. lini* as a sister to the *A. pullulans* complex. Nonetheless, the core species in the complex, especially *A. pullulans*, *A. proteae*, and *A. microstictum* have received little support in phylogenetic reconstructions (e.g., Yurlova *et al.* 1997, 1999, Manitchotpisit *et al.*2009, Wu *et al.* 2023). In the present study, we used a combination of six loci (ITS, *BTUB*, *EF1a*, *ELO2*, mtSSU, and *RPB2*) to resolve most of the species of the ApC – *A. aubasidani*, *A. proteae*, *A. ellingtonae*, and *A. pullulans* s. s., and *A. microstictum* – although support for *A. microstictum* remains low (Figs 1A, B, 5A, B). Interestingly, although sequences representing *Columnosphaeria fagi* CBS 171.93 have previously been resolved as conspecific with either *A. lini* or *A. pullulans* (Yurlova *et al.* 1999, Zalar *et al.* 2008), our data resolve these as conspecific with *A. microstictum* (Fig. 1B).

The type of *A. microstictum* was collected on leaves of *Convallaria majalis* by J.E. Kabat in the Czech Republic, September 1905 and described the same year by Bubák as *Kabatiella microsticta* (Bubák & Kabát 1907). This taxon is represented by sequences from two cultures: CBS 114.64 and CBS 342.66, that are not, however, conspecific in our analyses (Fig. 1A). The former was isolated by G.L. Boerema from *Hemerocallis* sp. in Wageningen, Netherlands, while the latter was isolated from the type host, *Convallaria majalis* in Germany by von Arx and identified by Walter Gams, effectively rendering *Kabatiella* to synonymy under *Aureobasidium* in this study based on phylogeny, as proposed by Hermanides-Nijhof (1977) based on morphology. CBS 114.64 appears to represent an undescribed *Aureobasidium* species (sp.1) (Fig. 1A). Sequences of *A. harposporum* from F121513 and CBS 122914 (Bills *et al.* 2012, van Nieuwenhuijzen *et al.* 2016), are not congeneric with *Aureobasidium* (Fig. 1A) and are allied instead in *Selenophoma* (not shown). However, we tentatively retain *A. harposporum* in *Aureobasidium* pending examination of type material.

Aureobasidium species display differing colony morphologies on different growth media (de Hoog &

Yurlova 1994) as can be seen in Tables 3 and 4. The growth characteristics of the isolates on various media were important in delineating the species. All species described in this study grew on MEA supplemented with 10 % (w/v) NaCl. *Aureobasidium cavalettoi*, *A. ellingtonae*, *A. essambei*, *A. rubi*, and *A. vanuatuense* also tolerated 15 % (w/v) NaCl concentrations. This capacity to tolerate salinity indicates that these species could be good colonizers of osmotic environments such as salt marshes, halophytes, intertidal zones, and even certain indoor environments (Manitchotpisit *et al.* 2009). For instance, *A. pullulans* has been isolated from bathroom cement walls and latex-painted surfaces in some geographic regions (Prasongsuk *et al.* 2005) and can also be found in food and animal feed (Samson *et al.* 2004). In our study, all species showed luxuriant growth and formed hyphae on MEA supplemented with 5 % (w/v) NaCl, and the high sugar media M40Y, although growth rates declined on M40Y compared to PDA (Table 3). The best overall average growth for all species was recorded on MEA (26.8 mm) at 25 °C. These results agree with Peterson *et al.* (2013), whose data showed that the best overall growth was on MEA when comparing the growth of *A. pullulans* and two strains of *A. thailandense*.

Previous studies by de Hoog & Yurlova (1994) reported two strains of *A. pullulans* capable of growing at 37 °C. Three of our newly described *Aureobasidium* species – *A. ellingtonae*, *A. peruvianum,* and *A. toomeae* – as well as *A. musti*, are also capable of growth at 37 °C (Table 3). Koppang *et al.* (1991) identified *A. pullulans* in an infected mandible after a tooth removal. The species is known to cause fungemia in patients suffering from AIDS (Mittal *et al.* 2018), cancer (Kaczmarski *et al.* 1986) and other disease conditions that compromise the immune system. Pikazis *et al.* (2009) reported an extended skin infection by *A. pullulans* in an aging immunosuppressed woman in Europe. Interestingly, two of our *A. pullulans* strains (RFL 168, RFL 292) were isolated from decaying pig carcasses used in controlled forensics experiments at Purdue University (Table S1).

Aureobasidium species are generally poor fermenters (de Hoog & Yurlova 1994). While *A. essambei*, *A. vanuatuense,* and *A. albui* fermented sucrose, only the latter was able to ferment melibiose. The former two species also fermented D-glucose, melezitose, and raffinose, but fermentation in all cases was weak. *Aureobasidium peruviana* is an exception in that it is able to ferment a variety of sugars including melibiose, D-glucose, maltose, sucrose, trehalose, cellobiose, melezitose, and raffinose and weakly ferment inulin (Table 5). Given their poor fermentation of sugars, one would expect a low abundance of members of the genus in wine production. Contrary to this expectation, *Aureobasidium* spp. have been reported among the most predominant yeast species of the grape microflora and have been isolated from the precursors to wine (e.g., Onetto *et al.* 2020a). Potentially these species may be useful as biocontrol in that industry (Pinto *et al.* 2018). For instance, a strain of *A. pullulans* was employed as a biocontrol agent against the grapevine trunk disease pathogen *Diplodia seriata* (Pinto *et al.* 2018). Another *A. pullulans* strain was also used as a biocontrol agent for the management of grey mould caused by *Botrytis cinerea* in grapes (Parafati *et al.* 2015, Wang *et al.* 2018).

Potassium nitrate, potassium nitrite, ethylamine hydrochloric acid, L-lysine hydrochloric acid, cadaverine hydrochloric acid, D-glucosamine, and D-tryptophan were regularly assimilated by most isolates tested, while creatine, creatinine, and imidazole were not assimilated by any. These results are similar to those of de Hoog & Yurlova (1994), although the ability of species to assimilate imidazole was not tested in that work. *Aureobasidium toomeae* (NRRL 64186) only assimilated ethylamine, lysine, and cadaverine of the carbon sources we tested which might indicate a narrower ecological niche for that fungus. Apart from *A. ellingtonae, A. peruvianum,* and *A. diazvalderramae*, the rest of the new species described in this study were isolated via the spore drop culture method, as described in Toome *et al.* (2013), from various plant phylloplanes. Mowll & Gadd (1985) reported the dominance of *A. pullulans* on plant surfaces after heavy metal pollution. *Aureobasidium pullulans* strain FE13 isolated from industrial waste was shown by dos Santos *et al.* (2009) to degrade phenols. Cazarolli *et al.* (2020) also demonstrated the ability of *A. pullulans* to degrade certain ultra-low-sulphur diesels.

Pigment production during assimilation of carbon compounds could be an important diagnostic feature for delineating species of *Aureobasidium*. Some of the carbon compounds in which pigmentation was observed include D-quinic acid, L-sorbose, D-mannitol, gluconic acid lactone, erythritol, L-arabinose, and sodium succinate dibasic hexahydrate. We also found that increasing the incubation period during assimilation profile assessment of carbon compounds would be helpful for feature studies of this genus since some species take longer than 14 d (up to 21 d and beyond) to show evidence of pigment production. The use of a polyphasic approach that incorporates phenotypic, physiological, phylogenetic, and DNA-based species recognition criteria greatly facilitated our resolution of *Aureobasidium*. Additionally, in accordance with recommendations from previous studies (Zalar *et al.* 2008, Manitchotpisit *et al.* 2009, Peterson *et al.* 2013, Gostinčar *et al.* 2014), the four protein-coding genes (*BTUB*, *EF1a*, *ELO2*, and *RPB2*) and the two mitochondrial genes (mtLSU and mtSSU), rather than ITS and 28S, are better loci for phylogenetic resolution, and may be better barcodes for identifying species in the *Aureobasidium*. The use of these loci would therefore be invaluable in future studies of this genus.

Names of additional *Aureobasidium* species not studied

We provide notes on the remaining *Aureobasidium* species names for which there are no publicly available sequence data, to aid in future studies of the genus.

Aureobasidium aleuritis (Vassiljevsky) Herm.-Nijh., *Stud. Mycol*. **15**: 146. 1977. MB 309377.
Basionym: *Kabatiella aleuritis* Vassiljevski [as '*aleuritidis*'], *Bot. Mater. Gerb. bot. Inst. V. A. Komarova* **5**: 15. 1940.
Synonym: *Microstroma aleuritis* (Vassiljevski) W.B. Cooke [as '*aleuritidis*'], *Mycopathol. Mycol. Appl*. **17**: 15. 1962.

Type material: **Russia**, Batun, from leaves of *Aleurites fordii*, unknown collection date and *collector* [**holotype** a herbarium specimen in LE sensu Hermanides-Nijhof (1977)].

Notes: The following description is modified from Cooke (1962). Members are plant parasites on the leaves of *Aleurites*

fordii. Leaf spots large, irregular, dark reddish brown on adaxial surface, pale reddish brown on abaxial side. Acervuli hypophyllous, pallid to pale brown, minute, 50–100 µm diam. Conidiogenous cells erect, clavate to subcylindrical, densely packed, 15–30 × 5–7 µm. Conidia 1-celled, smooth, hyaline, fusiform to subcylindric with straight or slightly curved sides, 6–8(–10.5) × 2.5–3.5(–4.0) µm, rarely 2-celled, these measuring 8.5–11.4 × 4–5 µm. Conidia are produced simultaneously only at the apex of conidiogenous cells on a small denticle.

Aureobasidium apocryptum (Ellis & Everh.) Herm.-Nijh., *Stud. Mycol*. **15**: 147. 1977. MB 309378.
Basionym: *Gloeosporium apocryptum* Ellis & Everh., *J. Mycol*. **4**: 52. 1888.
Synonyms: *Kabatiella apocrypta* (Ellis & Everh.) Arx, *Verh. Kon. Ned. Akad. Wetensch., Afd. Natuurk., Ser*. 2, **51**: 59. 1957.
Microstroma apocryptum (Ellis & Everh.) W.B. Cooke, *Mycopathol. Mycol. Appl*. **17**: 17. 1962.

Type material: **USA**, Wisconsin, Racine, on leaves of *Acer negundo*, Jul. 1887, unknown collection date and *collector* [**type** specimen ex herb. JJ Davis (NY)].

Notes: The following description is adapted from Hermanides-Nijhof (1977). Parasitic on the leaves of *Acer* plant species; leaf spots irregular, often confluent, dark brown. Acervuli mostly hypophyllous, minute, 40–70 µm diam., with pale brown stromata of globose cells, 5–9 µm diam. Conidiogenous cells densely packed, erect, clavate to subcylindrical, 14–20 × 5.5–7.5 µm. Conidia smooth, hyaline, ellipsoidal, 1-celled, rarely slightly curved, 7–12 × 2.5–4.5 µm, formed simultaneously at apex of conidiogenous cell.

Aureobasidium australiense (as *australiensis*) McAlpine, in Viala, *Rev. Vitio*. **6**: 588. 1896. MB 501787. nom. inval. Art. 38.1 (Shenzhen Code, Turland *et al.* 2018).

Notes: The first reference to this name (as *A. australiensis*) is in a note by Viala (1896), after communications with McAlpine, but without a diagnosis or description. McAlpine himself later considered this taxon to represent a new variety, *A. vitis* var. *tuberculatum*, rather than a new species (McAlpine 1898) and *A. australiense* was not a name that was used by McAlpine. Cooke (1962) considers *A. australiense* as conspecific with *A. pullulans,* citing the protologue as McAlpine in Viala, Rev. Vitio. 5: 588. 1896. Hermanides-Nijhof (1977), citing Cooke, considers *A. australiense* a doubtful species. As the name was never validly published and it cannot be diagnosed against *A. pullulans*, we treat *A. australiense*, as well as *A. vitis* var. *tuberculatum* as synonyms of *A. pullulans*.

Aureobasidium dalgeri (M. Morelet) Herm.-Nijh., *Stud. Mycol*. **15**: 146. 1977 MB 309379.
Basionym: *Kabatiella dalgeri* M. Morelet [as '*dalgerii*'], *Ann. Soc. Sci. Nat. Archéol. Toulon & Var*. **20**: 104. 1968.

Type material: **Tunisia**, Saroula, Banzart, on leaves of *Eucalyptus* cf. *gomphocephala*, Feb. 1967, *M. Delatour* (**type** specimen ex pers. coll. M. Morelet no. 515).

Notes: The following description is adapted from Hermanides-Nijhof (1977). *Aureobasidium dalgeri* is similar to *A. aleuritis* but differs in producing larger acervuli, occasionally intercalary conidiogenous cells, and in the shape of the tips of the conidiogenous cells. Leaf spots large, irregular, pale brown with a purplish margin. Acervuli hypophyllous, circular or elliptical, colourless, 100–150 µm diam. Conidiogenous cells erect, terminal or occasionally intercalary, subcylindrical to clavate, densely packed, 6–22 × 5–9 µm; terminally produced conidiogenous cells with inflated apex. Conidia 1-celled, smooth, hyaline, straight or very slightly curved, ellipsoidal, 5.5–8(–11) × 2–4 µm.

Aureobasidium indicum A. Pande & Ghate, *Biovigyanam* **11**: 113. 1985. MB 103074.

Note: Doubtful species. The type is from India, Maharashtra, from paper factory effluent. However, neither material for examination nor the protologue (to ascertain type deposition) could be acquired, as also remarked in Yurlova *et al.* (1996).

Aureobasidium lilii Crişan & Hodişan, *Contr. Bot. Univ. Cluj-Napoca Gradina Botanica* p.85. 1964. MB 326819.

Note: The type was isolated from a plant (*fide* Rensink *et al.* 2024). We were unable to locate a copy of the protologue as cited to ascertain additional type details.

Aureobasidium prunicola (Ellis & Everh.) Herm.-Nijh., *Stud. Mycol*. **15**: 157. 1977. MB 309382.
Basionym: *Gloeosporium prunicola* Ellis & Everh., *J. Mycol*. **3**: 129. 1887.
Synonyms: *Kabatiella prunicola* (Ellis & Everh.) Arx, *Verh. Kon. Ned. Akad. Wetensch., Afd. Natuurk.*, Ser. 2, **51**: 124. 1957.
Microstroma prunicola (Ellis & Everh.) W.B. Cooke, *Mycopathol. Mycol. Appl.* **17**: 22. 1962.

Type material: **USA**, Wisconsin, Racine, on leaves of *Prunus virginiana*, Jul. 1887, unknown *collector* [**type** specimen ex herb. JJ Davis (NY)].

Notes: The following description is adapted from Hermanides-Nijhof (1977). *Aureobasidium prunicola* is a plant parasite on leaves of *Prunus virginiana.* Leaf spots scattered, irregular, necrotic, dark rusty brown with lighter margins, 3–9 mm. Acervuli minute, inconspicuous, mostly hypophyllous, rarely hypophyllous, 40–60 µm diam. Stromata hyaline, hyphae thin-walled, growing in parallel, 3–5 µm wide. Conidiogenous cells clavate to broadly ellipsoidal, erect, densely packed, 10–20 × 7–9 µm. Conidia hyaline, 1-celled, smooth, ellipsoidal, straight or occasionally slightly curved, 4.5–9.5 × 2.5–4 µm, formed simultaneously at the apex of the conidiogenous cells.

Aureobasidium ribis (Vassiljevsky) Herm.-Nijh., *Stud. Mycol*. **15**: 161. 1977. MB 309384.
Basionym: *Kabatiella ribis* Vassiljevski, *Morbi plant. Leningrad*: 10. 1923.
Synonym: *Microstroma ribis* (Vassiljevski) W.B. Cooke, *Mycopathol. Mycol. Appl.* **17**: 23. 1962.

Type material: Information on type locality not accessible, from leaves of *Ribes nigrum*, unknown collection date and *collector* [**holotype** a herbarium specimen in LE sensu Hermanides-Nijhof (1977)].

Notes: The following description is adapted from Hermanides-Nijhof (1977). Parasitic on *Ribes nigrum*. Leaf spots irregular, greyish brown with dark brown margins, usually arranged on leaf margin. Acervuli minute, pallid, hypophyllous, subepidermal, 20–40 µm diam. Stromata hyphae hyaline, flexuose, sinuose, thin-walled, 7–10 µm wide. Conidiogenous cells densely packed, ascending or erect, clavate to subcylindrical, rounded tips, 20–30 × 6–15 µm, often branched. Conidia 1-celled, hyaline, ellipsoidal, straight, smooth, 6.5–9 × 3–4 µm, formed simultaneously at the apical portion of the conidiogenous cells.

Aureobasidium sanguinariae (Ellis & Everh.) Herm.-Nijh., *Stud. Mycol*. **15**: 163. 1977. MB 309386.
Basionym: *Gloeosporium sanguinariae* Ellis & Everh., *Proc. Acad. Nat. Sci. Philadelphia* **46**: 371. 1894.
Synonyms: *Kabatiella sanguinariae* (Ellis & Everh.) Arx, *Verh. Kon. Ned. Akad. Wetensch., Afd. Natuurk*., Ser. 2, **51**: 132. 1957.
Microstroma sanguinariae (Ellis & Everh.) W.B. Cooke, *Mycopathol. Mycol. Appl*. **17**: 23. 1962.

Type material: **USA**, Virginia, Nuttalburg, from leaves of *Sanguinaria canadensis*, unknown collection date and *collector* [**type** specimen ex herb. LW Nuttal (NY) Nr. 555 sensu Hermanides-Nijhof (1977)].

Notes: The following description is adapted from Hermanides-Nijhof (1977). *Aureobasidium sanguinariae* is parasitic on *Sanguinaria canadensis*. Leaf spots irregular, yellowish brown with darker margins, 3–6 mm diam. Acervuli hypophyllous, inconspicuous, subepidermal, commonly near the leaf margin, 40–90 µm diam. Stromata of hyaline, thin-walled hyphae arranged in a parallel manner, 3.5–6 µm wide. Conidiogenous cells erect, broadly ellipsoidal, densely packed, clavate or subcylindrical, often branched, 20–35 × 9–12 µm. Conidia hyaline, 1-celled, smooth, reniform to sickle-shaped, sometimes cylindrical with obtuse ends, 10–15 × 3–4.5 µm, formed simultaneously at the apex of the conidiogenous cells (Hermanides-Nijhof 1977).

Aureobasidium thujae-plicatae M. Morelet, *Bull. Soc. Sci. Nat. Archéol. Toulon & Var.* **34**: 15. 1978. MB 309387.

Notes: The type is from France, on branches of *Thuja plicata*. We were unable to locate a copy of the protologue as cited for additional type or descriptive details.

Aureobasidium umbellulariae (J.M. Harv.) Herm.-Nijh., *Stud. Mycol*. **15**: 163. 1977. MB 309388.
Basionym: *Kabatiella phoradendri f. umbellulariae* J.M. Harv., *Madroño* **11**: 170. 1951.
Microstroma umbellulariae (J.M. Harv.) W.B. Cooke, *Mycopathol. Mycol. Appl*. **17**: 23. 1962.

Type material: **USA**, California, Sonoma Co., north side of Russian River near Monte Rio, on leaves of *Umbellularia californica*, 15 Nov. 1949, *J.M. Harvey* (**type** Herb. Univ. CA no. 924306).

Notes: The following description is adapted from Hermanides-Nijhof (1977) and Harvey (1951). Parasitic on leaves of *Umbellularia californica*. Leaf spots irregular, primarily on abaxial surface, appearing as brown, necrotic patches with black margins, eventually extending over the entire leaf. Acervuli usually hypophyllous, erumpent, 150–250 µm diam. Stromata thin-walled, hyaline, cells globose, 8–12 µm diam., merged with hyaline, smooth, 3–6 µm wide hyphae. Conidiogenous cells densely packed, erect, clavate to cylindrical, 20–60 × 7–12 µm. Conidia are 1-celled, smooth, allantoid, often with a visible denticle, 20–29 × 3–4 µm, simultaneously formed at the apex.

Aureobasidium vaccinii Richiţ. & Teodoru, Rev. Roumaine Biol., Sér. Biol. Vég. 34: **94**. 1989. MB 126507.

Type material: **Romania**, from leaf of *Vaccinium* cv. Pemberton x Bluecrop, 1989, unknown *collector* (**holotype** BUCM 94373).

Notes: *Aureobasidium vaccinii* was described as a *Kabatiella*-like species on living leaves of blueberries (*Vaccinium* spp.). It produces acervuli and conidia in a synchronous manner (Yurlova *et al.* 1996). Yurlova *et al.* (1996) were unable to obtain material of *Aureobasidium vaccinii* for additional study.

ACKNOWLEDGEMENTS

We are grateful to the following for assisting in field work. In Cameroon: Conservator of the Dja Biosphere Reserve, Mr. Ndinga Hilaire, and his staff, the staff of the Congo Basin Institute in Bastos, Yaoundé, for logistical support, Olivier Séné for assistance with permitting, and to Chief Essambe, Alamane Gabriel (a.k.a. Sikiro), Bryn Dentinger, Noah Siegel, Constantin Engoulou, Carolyn Delevich, Rachel Koch, and Jessie Uehling for assistance in the field. Permits were granted by the Ministry of Forestry and Wildlife and the Ministry of Scientific Research and Innovation. In Vanuatu: Brian Perry, Anthony Amend, and the NY Botanical Garden Team are thanked for arranging logistics. Permits were granted by the Department of Forests, Port Vila. In Guyana: Dillon Husbands, Rachel Koch, and local parataxonomists Seigo Edmund, Luciano Edmund, Chris Andrew, and Valentino Joseph assisted with field work; we are also grateful to the staff of the University of Guyana for assistance with specimen processing for permits. Permits were granted by the Guyana Environmental Protection Agency. In Peru: Jorge Díaz-Valderrama was instrumental in arranging logistics, field work, and permitting. Permits were granted by the Direccion General de Gestion Sostenbile del Patrimonio Forestal y de Fauna Silvestre. We thank Anthony Borneman at the Australian Wine Research Institute for providing the ITS sequences of, and to staff at AWRI for responding to inquiries about, the types for *A. musti, A. vineae*, and *A. uvarum*. We thank Tom May for providing details regarding the protologue and typification of *A. australiense.* Finally, we are grateful to Lucy Liu for prepping samples for Sanger sequencing and to the entire Aime Lab for proofreading earlier versions

of manuscript, and especially to all former and current lab members who have enriched the PUL culture collection, especially Sebastian Albu, Jorge Díaz-Valderrama, Tomas Rush, Pedro Pablo Parra, R. Fanni Lakatos, and Merje Toome who cultured *Aureobasidium* isolates used in this study. This research was funded in part by a US Department of Agriculture USDA-ARS cooperative agreement 2072-12220-004-00D and 2072-22000-043-00-D (MCA and IZ) and USDA NIFA Hatch project 1010662 (MCA); isolate collection was supported in part by funding to MCA from the US National Science Foundation NSF DEB-0732968, NSF DEB-1556412, and NSF DEB-2127290.

Declaration on conflict of interest The authors declare that there is no conflict of interest.

REFERENCES

Adobe Inc (2019). *Adobe Illustrator*. Retrieved from https://adobe.com/products/illustrator

Aime MC, Miller A, Aoki T, *et al*. (2021). How to publish a new fungal species, or name, version 3.0. *IMA Fungus* **12**: 11. https://doi.org/10.1186/s43008-021-00063-1

Al-Araimi SH, Al-Hatmi AMS, Elshafie AE, *et al*. (2019). New record of *Aureobasidium mangrovei* from plant debris in the Sultanate of Oman. *Czech Mycology* **71**(2): 219–229. https://doi.org/10.33585/cmy.71207

Al-Araimi SH, Elshafie AE, Al-bhary SN, *et al*. (2021). Biopolymer production by *Aureobasidium mangrovei* SARA-138H and its potential for oil recovery enhancement. *Applied Microbiology and Biotechnology* **105**(1): 105–117. https://doi.org/10.1007/s00253-020-11015-x

Arnaud G (1910). Contribution à l'étude des Fumagines. *Annales Mycologici* **8**: 470–476.

Arzanlou M, Khodaei S (2012). *Aureobasidium iranianum*, a new species on bamboo from Iran. *Mycosphere* **3**(4): 404–408. https://doi.org/10.5943/mycosphere/3/4/2

Bakonyi T, Derakhshifar I, Grabensteiner E, *et al*. (2003). Development and evaluation of PCR assays for the detection of *Paenibacillus* larvae in honey samples: comparison with isolation and biochemical characterization. *Applied and Environmental Microbiology* **69**(3): 1504–1510. https://doi.org/10.1128/AEM.69.3.1504-1510.2003

Bettencourt S, Miranda C, Pozdniakova TA, *et al*. (2020). Single cell oil production by oleaginous yeasts grown in synthetic and waste-derived volatile fatty acids. *Microorganisms* **8**(11): 1–18. https://doi.org/10.3390/MICROORGANISMS8111809

Bhunjun CS, Dong Y, Jayawardena RS, *et al*. (2020). A polyphasic approach to delineate species in *Bipolaris*. *Fungal Diversity* **102**(1): 225–256. https://doi.org/10.1007/s13225-020-00446-6

Bhunjun CS, Phukhamsakda C, Jayawardena RS, *et al*. (2021). Investigating species boundaries in *Colletotrichum*. *Fungal Diversity* **107**: 107–127. https://doi.org/10.1007/s13225-021-00471-z

Bills GF, Menéndez VG, Platas G (2012). *Kabatiella bupleuri sp. nov*. (*Dothideales*), a pleomorphic epiphyte and endophyte of the mediterranean plant *Bupleurum gibraltarium* (*Apiaceae*). *Mycologia* **104**: 962–973. https://doi.org/10.3852/12-003

Bouckaert R, Heled J, Kühnert D, *et al*. (2014). BEAST 2: A software platform for Bayesian evolutionary analysis. *PLoS Computational Biology* **10**(4): e1003537. https://doi.org/10.1371/journal.pcbi.1003537

Bubák F, Kabát JE (1907). Mykologische Beiträge. IV. *Hedwigia*. **46**: 288–298.

Bustamante DE, Oliva M, Leiva S, *et al*. (2019). Phylogeny and species delimitations in the entomopathogenic genus *Beauveria* (*Hypocreales*, *Ascomycota*), including the description of *B. peruviensis sp. nov*. *MycoKeys* **58**: 47–68. https://doi.org/10.3897/mycokeys.58.35764

Castoria R, De Curtis F, Lima G, *et al*. (2001). *Aureobasidium pullulans* (LS-30) an antagonist of postharvest pathogens of fruits: study on its modes of action. *Postharvest Biology and Technology* **22**(1): 7–17. https://doi.org/10.1016/S0925-5214(00)00186-1

Cazarolli JC, Silva TL, Ribas C da RK, *et al*. (2020). Deterioration potential of *Aureobasidium pullulans* on biodiesel, diesel, and B20 blend. *International Biodeterioration & Biodegradation* **147**: 104839. https://doi.org/10.1016/J.IBIOD.2019.104839

Chi Z, Wang F, Chi Z, *et al*. (2009). Bioproducts from *Aureobasidium pullulans*, a biotechnologically important yeast. *Applied Microbiology and Biotechnology* **82**(5): 793–804. https://doi.org/10.1128/AEM.69.3.1504-1510.2003

Clements FE, Shear CL (1931). *The Genera of Fungi*. The H.W. Wilson Company, New York.

Cooke WB (1959). An ecological life history of *Aureobasidium pullulans* (de Bary) Arnaud. *Mycopathologia et Mycologia Applicata* **12**(1): 1–45. https://doi.org/10.1007/BF02118435

Cooke WB (1962). A taxonomic study in the "black yeasts". *Mycopathologia et Mycologia Applicata* **10**: 17: 1–43. https://doi.org/10.1007/BF02279261

Crous PW, Carnegie AJ, Wingfield MJ, *et al.* (2019). Fungal Planet description sheets: 868–950. *Persoonia* **42**: 291–473. https://doi.org/10.3767/PERSOONIA.2019.42.11

Crous PW, Groenewald JZ. 2016. They seldom occur alone. *Fungal Biology* **120**(11): 1392–1415. https://doi.org/10.1016/J.FUNBIO.2016.05.009

Crous PW, Osieck ER, Jurjevi Ž, *et al.* 2021. Fungal Planet description sheets: 1284–1382. *Persoonia* **47**(1): 178–374. https://doi.org/10.3767/PERSOONIA.2021.47.06

Crous PW, Osieck ER, Shivas RG, *et al.* (2023). Fungal Planet description sheets: 1478–1549. *Persoonia* **50**: 158–310. https://doi.org/10.3767/persoonia.2023.50.05

Crous PW, Summerell BA, Swart L, *et al.* (2011). Fungal pathogens of *Proteaceae*. *Persoonia* **27**: 20–45. https://doi.org/10.3767/003158511X606239

de Hoog GS, Guarro J, Gené J, *et al.* (2000). *Atlas of Clinical Fungi.* Centraalbureau voor Schimmelcultures/Universitat Rovira I Virgili, Utrecht, the Netherlands.

de Hoog GS, Yurlova NA (1994). Conidiogenesis, nutritional physiology and taxonomy of *Aureobasidium* and *Hormonema*. *Antonie van Leeuwenhoek* **65**(1): 41–54. https://doi.org/10.1007/BF00878278

de Jong H, Reglinski T, Elmer PAG, *et al*. (2019). Integrated use of *Aureobasidium pullulans* strain CG163 and acibenzolar-s-methyl for management of bacterial canker in kiwifruit. *Plants* **8**(8): plants8080287. https://doi.org/10.3390/PLANTS8080287

Díaz-Valderrama JR, Nguyen HDT, Aime MC (2017). *Wallemia peruviensis sp. nov*., a new xerophilic fungus from an agricultural setting in South America. *Extremophiles* **21**: 1017–1025. https://doi.org/10.1007/s00792-017-0960-0

di Francesco A, di Foggia M, Baraldi E (2020). *Aureobasidium pullulans* volatile organic compounds as alternative postharvest method to control brown rot of stone fruits. *Food Microbiology* **87**: 103395. https://doi.org/10.1016/J.FM.2019.103395.

Diguță CF, Proca IG, Jurcoane S, *et al*. (2019). Molecular characterization by PCR-RFLP of indigenous fungal isolates from hypersaline stream water in Romania. *Folia Microbiologica* **64**(3): 407–414. https://doi.org/10.1007/s12223-018-0664-6.

dos Santos VL, Monteiro A de S, Braga DT, *et al*. (2009). Phenol degradation by *Aureobasidium pullulans* FE13 isolated from industrial effluents. *Journal of Hazardous Materials* **161**(2–3): 1413–1420. https://doi.org/10.1016/J.JHAZMAT.2008.04.112

Drummond AJ, Suchard MA, Xie D, *et al*. (2012). Bayesian phylogenetics with BEAUti and the BEAST 1.7. *Molecular Biology and Evolution* **29**(8): 1969–1973. https://doi.org/10.1093/molbev/mss075

Edgar RC (2004). MUSCLE: Multiple sequence alignment with high accuracy and high throughput. *Nucleic Acids Research* **32**(5): 1792–1797. https://doi.org/10.1093/NAR/GKH340

Flett BC, Nowell DC (1995). First report of maize eyespot caused by *Aureobasidium zeae* in South Africa. *African Plant Protection* **1**: 49–50. https://journals.co.za/doi/pdf/10.10520/AJA10233121_296

Friend RJ (1965). A study of sooty mould on lime trees (*Tilia* × *Vulgaris*). *Transactions of the British Mycological Society* **48**: 367–370.

Fujisawa T, Barraclough TG (2013). Delimiting species using single-locus data and the generalized mixed Yule coalescent approach: A revised method and evaluation on simulated data sets. *Systematic Biology* **62**(5): 707–24. https://doi.org/10.1093/sysbio/syt033

Gardes M Bruns TD (1993). ITS primers with enhanced specificity for *Basidiomycetes*-application to the identification of mycorrhizae and rusts. *Molecular Ecology* **2**(2): 113–118. https://doi.org/10.1111/J.1365-294X.1993.TB00005.X

Gaur R, Singh R, Gupta M, *et al*. (2010). *Aureobasidium pullulans*, an economically important polymorphic yeast with special reference to pullulan. *African Journal of Biotechnology* **9**(47): 7989–7997. https://doi.org/10.5897/AJB10.948

Glass NL, Donaldson GC (1995). Development of primer sets designed for use with the PCR to amplify conserved genes from filamentous ascomycetes. *Applied and Environmental Microbiology* **61**(4): 1323–1330. https://doi.org/10.1128/AEM.61.4.1323-1330.1995

Gostinčar C, Ohm RA, Kogej T, *et al.* (2014). Genome sequencing of four *Aureobasidium pullulans* varieties: biotechnological potential, stress tolerance, and description of new species. *BMC Genomics* **15**(1): 549. https://doi.org/10.1007/s12223-018-0664-6

Haelewaters D, Urbina H, Brown S, *et al*. (2021). Isolation and molecular characterization of the romaine lettuce phylloplane mycobiome. *Journal of Fungi* **7**(4): 277. https://doi.org/10.3390/JOF7040277/S1

Hall TA (1999). BioEdit. A user-friendly biological sequence alignment editor and analysis program for Windows 95 98 and NT. *Nucleic Acids Symposium Series* **41**: 95–98. Retrieved March 11, 2025, from https://www.scirp.org/reference/ReferencesPapers?ReferenceID=1383440.

Harvey JM (1951). An anthracnose disease of *Umbellularia californica*. *Madroño* **11**(4): 162–171. https://www.jstor.org/stable/41422723

Hermanides-Nijhof EJ (1977). *Aureobasidium* and allied genera. *Studies in Mycology* **15**: 1–222.

Hilário S, Santos L, Alves A (2021). *Diaporthe amygdali*, a species complex or a complex species? *Fungal Biology* **125**(7): 505–518. https://doi.org/10.1016/j.funbio.2021.01.006

Hoang DT, Chernomor O, von Haeseler A, *et al.* (2018). UFBoot2: Improving the ultrafast bootstrap approximation. molecular biology and evolution. *Molecular Biology and Evolution* **35**(2): 518–522. https://doi.org/10.1093/MOLBEV/MSX281

Hogg BM, Hudson HJ (1966). Micro-fungi on leaves of *Fagus sylvatica*. *Transactions of the British Mycological Society* **49**(2): 185–192. https://doi.org/10.1016/S0007-1536(66)80052-9

Hongsanan S, Hyde KD, Phookamsak R, *et al.* (2020). Refined families of *Dothideomycetes: Dothideomycetidae* and *Pleosporomycetidae*. *Mycosphere* **11**: 1553–2107. https://doi.org/10.5943/mycosphere/11/1/13

Humphries Z, Seifert KA, Hirooka Y, *et al.* (2017). A new family and genus in *Dothideales* for Aureobasidium-like species isolated from house dust. *IMA Fungus* **8**(2): 299–315. https://doi.org/10.5598/imafungus.2017.08.02.05

Huson DH (1998). SplitsTree: Analyzing and visualizing evolutionary data. *Bioinformatics* **14**(1): 68–73. https://doi.org/10.1093/bioinformatics/14.1.68

Huson DH, Bryant D (2006). Application of phylogenetic networks in evolutionary studies. *Molecular Biology and Evolution* **23**(2): 254–267. https://doi.org/10.1093/molbev/msj030

Hyde KD, Norphanphoun C, Ma J, *et al.* (2023). Mycosphere notes 387–412 – novel species of fungal taxa from around the world. *Mycosphere* **14**(1): 663–744. https://doi.org/10.5943/mycosphere/14/1/8

Ippolito A, El Ghaouth A, Wilson CL, *et al.* (2000). Control of postharvest decay of apple fruit by *Aureobasidium pullulans* and induction of defense responses. *Postharvest Biology and Technology* **19**(3): 265–272. https://doi.org/10.1016/S0925-5214(00)00104-6

Jiang N, Xinlei F, Chengming T (2021). Identification and characterization of leaf-inhabiting fungi from *Castanea* plantations in China. *Journal of Fungi* **7**(1): 1–59. https://doi.org/10.3390/JOF7010064

Jiang N, Liang YM, Tian CM (2019). *Aureobasidium pini sp. nov*. from pine needle in China. *Phytotaxa* **402**(4): 199–206. https://doi.org/10.11646/PHYTOTAXA.402.4.3

Jumbam B, Haelewaters D, Kock RA, *et al.* (2019). A new and unusual species of *Hericium* (*Basidiomycota*: *Russulales*, *Hericiaceae*) from the Dja Biosphere Reserve, Cameroon. *Mycological Progress* **18**(10): 1253–1262. https://doi.org/10.1007/S11557-019-01530-1/METRICS

Kaczmarski EB, Yint JAL, Tooth JA, *et al.* (1986). Systemic infection with *Aureobasidium pullulans* in a leukaemic patient. *Journal of Infection* **13**(3): 289–291. https://doi.org/10.1016/S0163-4453(86)91388-5

Kalyaanamoorthy S, Minh BQ, Wong TKF, *et al.* (2017). ModelFinder: Fast model selection for accurate phylogenetic estimates. *Nature Methods* **14**(6): 587–589. https://doi.org/10.1038/nmeth.4285

Kekkonen M, Mutanen M, Kaila L, *et al.* (2015). Delineating species with DNA barcodes: A case of taxon dependent method performance in moths." *PLoS ONE* **10**(4): e0122481. https://doi.org/10.1371/journal.pone.0122481

Kim JS, Lee IK, Yun BS (2015). A novel biosurfactant produced by *Aureobasidium pullulans* L3-GPY from a tiger lily wildflower, *Lilium lancifolium* Thunb. *PLoS ONE* **10**(4): e0122917. https://doi.org/10.1371/JOURNAL.PONE.0122917

Koppang HS, Olsen I, Stuge U, *et al.* (1991). *Aureobasidium* infection of the jaw. *Journal of Oral Pathology & Medicine* **20**(4): 191–195. https://doi.org/10.1111/J.1600-0714.1991.TB00920.X

Kramer LA (2004). *The Online Auction Color Chart*. Online Auction Color Chart Company, Stanford, 1–12.

Kutleša M, Emilija MM, Lóránt H, *et al.* (2012). Chronic fungal

meningitis caused by *Aureobasidium proteae*. *Diagnostic Microbiology and Infectious Disease* **73**(3): 271–272. https://doi.org/10.1016/J.DIAGMICROBIO.2012.03.007

Lee DH, Cho S-E, Oh JY, *et al.* (2021). A novel species of *Aureobasidium* (*Dothioraceae*) recovered from *Acer pseudosieboldianum* in Korea. *Journal of Asia-Pacific Biodiversity* **14**(4): 657–661. https://doi.org/10.1016/J.JAPB.2021.08.005

Li ZY, Wang Y, Shen WT, *et al.* (2014). Content determination of benzyl glucosinolate and anti-cancer activity of its hydrolysis product in *Carica papaya* L. *Asian Pacific Journal of Tropical Medicine* **5**(3): 231–233. https://doi.org/10.1016/S1995-7645(12)60030-3

Lima G, Ippolito A, Nigro F, *et al.* (1997). Effectiveness of *Aureobasidium pullulans* and *Candida oleophila* against postharvest strawberry rots. *Postharvest Biology and Technology* **10**(2): 169–178. https://doi.org/10.1016/S0925-5214(96)01302-6

Liu F, Wang M, Damm U, *et al.* (2016). Species boundaries in plant pathogenic fungi: A *Colletotrichum* case study. *BMC Evolutionary Biology* **16**(1): 81. https://doi.org/10.1186/S12862-016-0649-5/TABLES/2

Liu YJ, Whelen S, Hall BD (1999). Phylogenetic relationships among ascomycetes: evidence from an RNA polymerse II subunit. *Molecular Biology and Evolution* **16**(12): 1799–1808. https://doi.org/10.1093/OXFORDJOURNALS.MOLBEV.A026092

Loncaric I, Oberlerchner JT, Heissenberger B, *et al.* (2009). Phenotypic and genotypic diversity among strains of *Aureobasidium pullulans* in comparison with related species. *Antonie van Leeuwenhoek* **95**(2): 165–178. https://doi.org/10.1007/s10482-008-9300-9

López-Moral A, Llorens E, Scalschi L, *et al.* (2018). Resistance induction in olive tree (*Olea europaea*) against *Verticillium* wilt by two beneficial microorganisms and a copper phosphite fertilizer. *Frontiers in Plant Science* **13**: 831794. https://doi.org/10.3389/fpls.2022.831794

Manitchotpisit P, Leathers TD, Peterson SW, *et al.* (2009). Multilocus phylogenetic analyses, pullulan production and xylanase activity of tropical isolates of *Aureobasidium pullulans*. *Mycological Research* **113**: 1107–1120. https://doi.org/10.1016/j.mycres.2009.07.008

Mari M, Martini C, Spadoni A, *et al.* (2012). Biocontrol of apple postharvest decay by *Aureobasidium pullulans*. *Postharvest Biology and Technology* **73**: 56–62. https://doi.org/10.1016/j.postharvbio.2012.05.014

McAlpine D (1898). *Additions to the Fungi on the Vine in Australia*. Victoria, Australia: Department of Agriculture.

Mittal J, Szymczak WA, Pirofski LA, *et al.* (2018). Fungemia caused by *Aureobasidium pullulans* in a patient with advanced aids: a case report and review of the medical literature. *JMM Case Reports* **5**(4): e005144. https://doi.org/10.1099/JMMCR.0.005144

Mowll JL, Gadd GM (1985). Effect of vehicular lead pollution on phylloplane mycoflora. *Transactions of the British Mycological Society* **84**(4): 685–689. https://doi.org/10.1016/S0007-1536(85)80124-8

Monaghan MT, Wild R, Elliot M, *et al.* (2009). Accelerated species inventory on Madagascar using coalescent-based models of species delineation. *Systematic Biology* **58**(3): 298–311. https://doi.org/10.1093/sysbio/syp027

Mulay YR, Deopurkar RL (2017). Production of amylase from indigenously isolated strain of *Aureobasidium pullulans* and its hyper producing mutant. *Journal of Microbiology, Biotechnology and Food Sciences* **7**(3): 287–293. https://doi.org/10.15414/JMBFS.2017/18.7.3.287-293

Nasr S, Mohammadimehr M, Vaghei MG, *et al.* (2018). *Aureobasidium mangrovei sp. nov*., an ascomycetous species recovered from hara protected forests in the Persian Gulf, Iran. *Antonie van Leeuwenhoek* **111**(9): 1697–1705. https://doi.org/10.1007/S10482-018-1059-Z

Onetto CA, Borneman AR, Schmidt SA (2020a). Investigating the effects of *Aureobasidium pullulans* on grape juice composition and fermentation. *Food Microbiology* **90**: 103451. https://doi.org/10.1016/J.FM.2020.103451

Onetto CA, Schmidt SA, Roach MJ, *et al.* (2020b). Comparative genome analysis proposes three new *Aureobasidium* species isolated from grape juice. *FEMS Yeast Research* **20**(6): foaa052. https://doi.org/10.1093/FEMSYR/FOAA052

Parafati L, Vitale A, Restuccia C, *et al.* (2015). Biocontrol ability and action mechanism of food-isolated yeast strains against *Botrytis cinerea* causing post-harvest bunch rot of table grape. *Food Microbiology* **47**: 85–92. https://doi.org/10.1016/J.FM.2014.11.013

Peterson SW, Manitchotpisit P, Leathers TD (2013). *Aureobasidium thailandense sp. nov*. isolated from leaves and wooden surfaces. *International Journal of Systematic and Evolutionary Microbiology* **63**(2): 790–795. https://doi.org/10.1099/ijs.0.047613-0

Pikazis D, Xynos ID, Xila V, *et al.* (2009). Extended fungal skin infection due to *Aureobasidium pullulans*. *Clinical and Experimental Dermatology* **34**(8): 892–894. https://doi.org/10.1111/J.1365-2230.2009.03663.X

Pinto C, Custódio V, Nunes M, *et al.* (2018). Understand the potential role of *Aureobasidium pullulans*, a resident microorganism from grapevine, to prevent the infection caused by *Diplodia seriata*. *Frontiers in Microbiology* **9**: 1–15. https://doi.org/10.3389/fmicb.2018.03047

Pitt JI, Hocking AD (2009). *Fungi and Food Spoilage*. 3rd edn. Springer, New York, USA.

Prabhugaonkar A, Pratibha J (2018). *Aureobasidium khasianum* (*Aureobasidiaceae*) a novel species with distinct morphology. *Phytotaxa* **374**(3): 257–262. https://doi.org/10.11646/phytotaxa.374.3.7

Prasongsuk S, Lotrakul P, Bankeeree W, *et al.* (2018). The current status of *Aureobasidium pullulans* in biotechnology. *Folia Microbiologica* **63**(2): 129–140. https://doi.org/10.1007/S12223-017-0561-4

Prasongsuk S, Sullivan RF, Kuhirun M, *et al.* (2005). Thailand habitats as sources of pullulan-producing strains of *Aureobasidium pullulans*. *World Journal of Microbiology and Biotechnology* **21**(4): 393–398. https://doi.org/10.1007/s11274-004-2237-x

Puillandre N, Brouillet S, Achaz G (2021). ASAP: Assemble Species by Automatic Partitioning. *Molecular Ecology Resources* **21**(2): 609–620. https://doi.org/10.1111/1755-0998.13281

Puillandre N, Lambert A, Brouillet S, *et al.* (2012). ABGD, Automatic Barcode Gap Discovery for primary species delimitation. *Molecular Ecology* **21**(8): 1864–1877. https://doi.org/10.1111/j.1365-294X.2011.05239.x

Quaedvlieg W, Binder M, Groenewald JZ, *et al.* (2014). Introducing the Consolidated Species Concept to resolve species in the *Teratosphaeriaceae*. *Persoonia* **33**: 1–40. https://doi.org/10.3767/003158514X681981

Ramaley AW (1992). *Tectracervulus mahoniae*, *Kabatina mahoniae* and *Selenophoma mahoniae*, three new fungi on *Mahonia repens*. *Mycotaxon* **43**: 437–452.

Rambaut A, Drummond AJ, Xie D, *et al.* (2018). Posterior summarization in Bayesian phylogenetics using Tracer 1.7. *Systematic Biology* **67**(5): 901–904. https://doi.org/10.1093/sysbio/syy032

Rehner SA, Samuels GJ (1994). Taxonomy and phylogeny of

Gliocladium analyzed from nuclear large subunit ribosomal DNA sequences. *Mycological Research* **98**(6): 625–634. https://doi.org/10.1016/S0953-7562(09)80409-7

Robiglio A, Sosa MC, Lutz MC *et al.* (2011). Yeast biocontrol of fungal spoilage of pears stored at low temperature. *International Journal of Food Microbiology* **147**(3): 211–216. https://doi.org/10.1016/J.IJFOODMICRO.2011.04.007

Ronquist F, Teslenko M, van der Mark P, *et al.* (2012). MrBayes 3.2: Efficient Bayesian phylogenetic inference and model choice across a large model space. *Systematic Biology* **61**(3): 539–542. https://doi.org/10.1093/SYSBIO/SYS029.

Samson RA, Hoekstra ES, Frisvad JC (2004). *Introduction to Food- and Airborne fungi*. Centraalbureau voor Schimmelcultures, Netherlands.

Schena L, Nigro F, Pentimone I, *et al.* (2003). Control of postharvest rots of sweet cherries and table grapes with endophytic isolates of *Aureobasidium pullulans*. *Postharvest Biology and Technology* **30**(3): 209–220. https://doi.org/10.1016/S0925-5214(03)00111-X

Schoch CL, Crous PW, Groenewald JZ, *et al.* (2009). A class-wide phylogenetic assessment of *Dothideomycetes*. *Studies in Mycology* **64**(1): 1–15. https://doi.org/10.3114/SIM.2009.64.01

Schoch CL, Shoemaker RA, Seifert KA, *et al.* (2006). A multigene phylogeny of the *Dothideomycetes* using four nuclear loci. *Mycologia* **98**(6): 1041–1052. https://doi.org/10.1080/15572536.2006.11832632

Sharma RR, Singh D, Singh R (2009). Biological control of postharvest diseases of fruits and vegetables by microbial antagonists: A review. *Biological Control* **50**(3): 205–221. https://doi.org/10.1016/J.BIOCONTROL.2009.05.001

Simon UK, Groenewald JZ, Crous PW (2009). *Cymadothea trifolii*, an obligate biotrophic leaf parasite of *Trifolium*, belongs to *Mycosphaerellaceae* as shown by nuclear ribosomal DNA analyses. *Persoonia* **22**: 49–55. https://doi.org/10.3767/003158509X425350

Singh RS, Saini GK, Kennedy JF (2008). Pullulan: microbial sources, production, and applications. *Carbohydrate Polymers* **73**(4): 515–531. https://doi.org/10.1016/J.CARBPOL.2008.01.003

Singh R, Gaur R, Biswas P, *et al.* (2015). *Aureobasidium pullulans*, an economically important black yeast. *Journal of Basic and Applied Mycology* **11**: 1–4. https://doi.org/10.5897/AJB10.948

Suh S-O, Zhang N, Nguyen N, *et al.* (2008). *Lab Manual for Yeast Study*. Louisiana State University, Baton Rouge, 38 pp. https://www.yumpu.com/en/document/view/13817398/lab-manual-for-yeast-study-mycology-at-lsu-louisiana-state

Tamura K, Stecher G, Kumar S (2021). MEGA11: Molecular Evolutionary Genetics Analysis version 11. *Molecular Biology and Evolution* **38**(7): 3022–3027. https://doi.org/10.1093/MOLBEV/MSAB120

Taylor JW, Jacobson DJ, Kroken S, *et al.* (2000). Phylogenetic species recognition and species concepts in fungi. *Fungal Genetics and Biology* **31**(1): 21–32. https://doi.org/10.1006/FGBI.2000.1228

Thambugala KM, Ariyamansa HA, Li YM, *et al.* (2014). *Dothideales*. *Fungal Diversity* **68**(1): 105–158. https://doi.org/10.1007/s13225-014-0303-8

Toome M, Roberson RW, Aime MC (2013). *Meredithblackwellia eburnea gen. et sp. nov*., *Kriegeriaceae fam. nov*. and *Kriegeriales ord. nov*. - toward resolving higher-level classification in *Microbotryomycetes*. *Mycologia* **105**(2): 486–495. https://doi.org/10.3852/12-251

Turland NJ, Wiersema JH, Barrie FR, *et al.* (eds.) (2018). *International Code of Nomenclature for algae, fungi, and plants (Shenzhen Code)*. Adopted by the Nineteenth International Botanical Congress Shenzhen, China, July 2017. Regnum Vegetabile 159. Glashütten: Koeltz Botanical Books. https://doi.org/10.12705/Code.2018

van Nieuwenhuijzen EJ, Houbraken JAMP, Meijer M, *et al.* (2016). *Aureobasidium melanogenum*: a native of dark biofinishes on oil treated wood. *Antonie van Leeuwenhoek* **109**(5): 661–683. https://doi.org/10.1007/S10482-016-0668-7

Viala P (1896). L'*Aureobasidium vitis* eu Australie. *Revue de Viticulture* **6**: 588–590.

Viala P, Boyer G (1891). Nouvelle maladie des raisins. *Revue Générale de Botanique* **3**: 369–371.

Vilgalys R, Hester M (1990). Rapid genetic identification and mapping of enzymatically amplified ribosomal DNA from several *Cryptococcus* species. *Journal of Bacteriology* **172**(8): 4238–4246. https://doi.org/10.1128/JB.172.8.4238-4246.1990

Vu D, Groenewald M, de Vries M, *et al.* (2019). Large-scale generation and analysis of filamentous fungal DNA barcodes boosts coverage for kingdom fungi and reveals thresholds for fungal species and higher taxon delimitation. *Studies in Mycology* **92**: 135–154. https://doi.org/10.1016/J.SIMYCO.2018.05.001

Wachowska U, Głowacka K (2014). Antagonistic interactions between *Aureobasidium pullulans* and *Fusarium culmorum*, a fungal pathogen of winter wheat. *BioControl* **59**(5): 635–645. https://doi.org/10.1007/s10526-014-9596-5

Wang CB, Jiang N, Tu Y, *et al.* (2022). *Aureobasidium aerium* (*Saccotheciaceae*, *Dothidiales*), a new yeast-like fungus from the air in Beijing, China. *Phytotaxa* **544**(2): 185–192. https://doi.org/10.11646/PHYTOTAXA.544.2.4

Wang G, Bai T, Miao Z, *et al.* (2018a). Simultaneous production of single cell oil and fumaric acid by a newly isolated yeast *Aureobasidium pullulans* var. *aubasidani* DH177. *Bioprocess and Biosystems Engineering* **41**(11): 1707–1716. https://doi.org/10.1007/S00449-018-1994-0

Wang M, Danesi P, James TY, *et al.* (2019). Comparative pathogenicity of opportunistic black yeasts in *Aureobasidium*. *Mycoses* **62**(9): 803–811. https://doi.org/10.1111/MYC.12931

Wang X, Glawe DA, Kramer E, *et al.* (2018b). Biological control of *Botrytis cinerea*: interactions with native vineyard yeasts from Washington State. *Phytopathology* **108**(6): 691–701. https://doi.org/10.1094/PHYTO-09-17-0306-R

White TJ, Bruns T, Lee S, *et al*. (1990). Amplification and direct sequencing of fungal ribosomal RNA genes for phylogenetics. In: *PCR protocols: a guide to methods and applications* (Innis MA, Gelfand DH, Sninsky JJ, *et al*., eds). *Academic Press, Inc*., New York, USA: 315–322. https://doi.org/10.1016/B978-0-12-372180-8.50042-1

Woudenberg JHC, Groenewald JZ, Binder M, *et al.* (2013). *Alternaria* redefined. *Studies in Mycology* **75**(1): 171–212. https://doi.org/10.3114/SIM0015

Wu F, Feng Z, Wang M, *et al.* (2023). Proposal of four new *Aureobasidium* species for exopolysaccharide production. *Journal of Fungi* **9**: 447. https://www.doi.org/10.3390/jof9040447

Wynne ES, Gott CL (1956). A proposed revision of the genus *Pullularia*. *Journal of General Microbiology* **14**(3): 512–519. https://doi.org/10.1099/00221287-14-3-512

Yurlova NA, de Hoog GS, van den Ende AHGG (1999). Taxonomy of *Aureobasidium* and allied genera. *Studies in Mycology* **43**: 63–69.

Yurlova NA, de Hoog GS (1997). A new variety of *Aureobasidium pullulans* characterized by exopolysaccharide structure, nutritional physiology and molecular features. *Antonie van Leeuwenhoek* **72**(2): 141–147. https://doi.org/10.1023/a:1000212003810

Yurlova NA, Uijthof JM, de Hoog GS (1996). Distinction of species in *Aureobasidium* and related genera by PCR-ribotyping. *Antonie van Leeuwenhoek* **69**(4): 323–329. https://doi.org/10.1007/BF00399621

Zajc J, Cernosa A, di Francesco A, *et al.* (2020). Characterization of *Aureobasidium pullulans* isolates selected as biocontrol agents against fruit decay pathogens. *Fungal Genomics & Biology* **10**(1): 1–13. https://doi.org/10.35248/2165-8056.20.10.161

Zalar P, Gostinčar C, de Hoog GS, *et al.* (2008). Redefinition of *Aureobasidium pullulans* and its varieties. *Studies in Mycology* **61**: 21–38. https://doi.org/10.3114/SIM.2008.61.02

Zeng W, Zhang B, Li M, *et al.* (2019). Development and benefit evaluation of fermentation strategies for poly (malic acid) production from malt syrup by *Aureobasidium melanogenum* GXZ-6. *Bioresource Technology* **274**: 479–487. https://doi.org/10.1016/J.BIORTECH.2018.12.027

Zhang J, Kapli P, Pavlidis P, *et al.* (2013). A general species delimitation method with applications to phylogenetic placements. *Bioinformatics* **29**(22): 2869–2876. https://doi.org/10.1093/bioinformatics/btt499

SUPPLEMENTARY MATERIAL

Fig. S1A. Phylogenetic inference of ITS sequences of 208 *Aureobasidium* isolates. The phylogram is based on Bayesian inference (BI) and maximum likelihood (ML) analyses. The bootstrap percentages of the ML ≥ 70 % and BI posterior probability values ≥ 0.90 are presented at the nodes (as ML/BI). Values < 70 % bootstrap support or < 0.90 posterior probability are indicated with a hyphen or not shown. The scale bar indicates the number of nucleotide substitutions per site. Sequences from ex-types are indicated with an asterisk (*). **Bold** = new names from this study. The red star represents the *A. pullulans* species complex sensu lato. The five groups also identified in the single locus phylogenies are indicated as PullG, NamiG, MelaG, SubgG and ThaiG (see text for explanation).

Fig. S1B. Phylogenetic inference of 28S sequences of 103 *Aureobasidium* isolates. The phylogram is based on Bayesian inference (BI) and maximum likelihood (ML) analysis. The bootstrap percentages of the ML ≥ 70 % and BI posterior probability (pp) values ≥ 0.90 are presented at the nodes (as ML/BI). Values < 70 % bootstrap support or < 0.90 posterior probability are indicated with a hyphen or not shown. Vertical bars indicate the different species groups delineated as explained in the text. The scale bar indicates the number of nucleotide substitutions per site. The ex-types are indicated with an asterisk (*).

Fig. S1C. Phylogenetic inference of *EF1a* gene sequence of 50 *Aureobasidium* isolates. The phylogram is based on Bayesian inference (BI) and maximum likelihood (ML) analysis. The bootstrap percentages of the ML ≥ 70 % and BI posterior probability values ≥ 0.90 are presented at the nodes (as ML/BI). Values < 70 % bootstrap support or < 0.90 posterior probability are indicated with a hyphen or not shown. Vertical bars indicate the different species groups delineated as explained in the text. Scale bar indicates the number of nucleotide substitutions per site. The tree is rooted with *Delphinella strobiligena* (AFTOL-ID 1257) and *Sydowia polyspora* (AFTOL-ID 1300). The ex-types are indicated with an asterisk (*).

Fig. S1D. Phylogenetic inference of *ELO2* sequence of 50 *Aureobasidium* isolates. The phylogram is based on Bayesian inference (BI) and maximum likelihood (ML) analysis. The bootstrap percentages of the ML ≥ 70 % and BI posterior probability (pp) values ≥ 0.90 are presented at the nodes (as ML/BI). Values < 70 % bootstrap support or < 0.90 posterior probability are indicated with a hyphen or not shown. Vertical bars indicate the different species groups delineated as explained in the text. Scale bar indicates the number of nucleotide substitutions per site. The tree is rooted with *Delphinella strobiligena* (AFTOL-ID 1257) and *Sydowia polyspora* (AFTOL-ID 1300). The ex-types are indicated with an asterisk (*).

Fig. S1E. Phylogeny inferred from the mtLSU gene sequence of 35 *Aureobasidium* isolates. The phylogram is based on Bayesian inference (BI) and maximum likelihood (ML) analysis. The bootstrap percentages of the ML ≥ 70 % and BI posterior probability (pp) values ≥ 0.90 are presented at the nodes (as ML/BI). Values < 70 % bootstrap support or < 0.90 posterior probability are indicated with a hyphen or not shown. Vertical bars indicate the different species groups delineated as explained in the text. The bar indicates the number of nucleotide substitutions per site. The tree is midpoint rooted. The ex-types are indicated with an asterisk (*).

Fig. S1F. Phylogeny inferred from the mtSSU gene sequence of 24 *Aureobasidium* isolates. The phylogram is based on Bayesian inference (BI) and maximum likelihood (ML) analysis. The bootstrap percentages of the ML ≥ 70 % and BI posterior probability (pp) values ≥ 0.90 are presented at the nodes (as ML/BI). Values < 70 % bootstrap support or < 0.90 posterior probability are indicated with a hyphen or not shown. Vertical bars indicate the different species groups delineated as explained in the text. The bar indicates the number of nucleotide substitutions per site. The tree is midpoint rooted. The ex-types are indicated with an asterisk (*).

Fig. S1G. Phylogeny inferred from the *RPB2* gene sequence of 82 *Aureobasidium* isolates. The phylogram is based on Bayesian inference (BI) and maximum likelihood (ML) analysis. The bootstrap percentages of the ML ≥ 70 % and BI posterior probability (pp) values ≥ 0.90 are presented at the nodes (as ML/BI). Values < 70 % bootstrap support or < 0.90 posterior probability are indicated with a hyphen or not shown. Vertical bars indicate the different species groups delineated as explained in the text. The bar indicates the number of nucleotide substitutions per site. The tree is midpoint rooted. The ex-types are indicated with an asterisk (*).

Fig. S1H. Phylogeny inferred from the TUB gene sequence of 37 *Aureobasidium* isolates. The phylogram is based on Bayesian inference (BI) and maximum likelihood (ML) analysis. The bootstrap percentages of the ML ≥ 70 % and BI posterior probability (pp) values ≥ 0.90 are presented at the nodes (as ML/BI). Values < 70 % bootstrap support or < 0.90 posterior probability are indicated with a hyphen or not shown. Vertical bars indicate the different species groups delineated as explained in the text. The bar indicates the number of nucleotide substitutions per site. The tree is rooted with *Lecythophora hoffmannii* (CBS 245.38). The ex-types are indicated with an asterisk (*).

Fig. S1I. GHOST phylogeny inferred from the concatenated dataset with linked GTR parameters. We used the GTR+FO+H4 rate substitution model with four site classes to verify the topology of the overall maximum likelihood phylogeny in Fig. 1A. The values above branches represent node ages multiplied by 100. The numbers in square brackets are the convergence frequencies of the branches.

Table S1. Sequenced strains and accession numbers of *Aureobasidium* isolates analysed in this study, including the

geographic origin and substrate from which the strains were isolated.

Table S2. Data on colony diam. (mm) and assimilation/fermentation profiles of three additional strains of new *Aureobasidium* species described. Plates for colony diam. were incubated at 25 °C unless otherwise noted.